



Engineering Nanostructures on Semiconducting Surfaces

Amir Abdulrahman Ahmad Zebari

The dissertation completed at the Department of Physics of Nanostructures and Nanotechnology of Marian Smoluchowski Institute of Physics under the supervision of prof. dr. hab. Marek Szymonski and presented to the Council of the Faculty of Physics, Astronomy, and Applied Computer Science of the Jagiellonian University in order to obtain the degree of doctor of philosophy in physics.

Krakow 2014

To:

The soul of my father

Remembrance of my mother

Patience of my wife

Loneliness of my Son

Acknowledgements

Doing a full time overseas PhD program is not an easy commitment. It is quite demanding to get used to a new environment (language, people, climate and even food). In the other hand the program offered the opportunity to work in a good scientific group that I have considered myself very lucky to do science among them.

I would like to express my utmost gratitude to my supervisor Prof. dr. hab. Marek Szymonski for offering to work in his research group and also for his excellent guidance and support.

I would like also to thank Dr. Jakub Prauzner-Behcicki for his support, cooperation and giving guidance in both scientific research and everyday life aspects. This task would not be possible without his kind staying by my side.

I thank Prof. Franciszek Krok for supervising an important part of my PhD work and for all useful scientific discussions.

I would also like to thank my colleagues Dr. Bartosz Such, Dr. Szymon Godlewski, Marek Kolmer for fruitful scientific discussions throughout my research work. Special thanks go to Mr. Piotr Piatkowski, Dr. Janusz Budzioch, Rafal Zuzak, Aleksander Polit and Piotr Olszowski for maintaining and keeping the instruments running.

Special thanks go to my home university “Salahaddin University” Erbil-Kurdistan and Mr. Ziyad Raoof the Kurdistan Ambassador to Poland, for his support and covering during my stay in Poland.

Truthful thanks go to my family especially my mother and my brothers Shaban and Burhan for their financial support and encouraging.

Finally, I would like to thank my wife, Rana, and my sweet son, Daniyar. They were very patient and they stood by me during the bad and the good times.

Abstract

In this thesis we present three different techniques that allow fabricating and manipulating nanostructures on semiconducting surfaces. The results are published as three publications in prestigious scientific journals.

In the first publication we have reported the first results revealing temperature dependent orientation of nanoripples on an ion irradiated titanium dioxide, $\text{TiO}_2(110)$ surface. Our scanning tunneling microscopy (STM) images have showed the development of a ripple structure with periodicity of $\sim 10\text{nm}$ under 2keV Ar^+ beam at 75° off-normal incident angle. The novelty of our results stems from the fact that the orientation of the nanoripples switches by 90° with changing the substrate temperature during irradiation process quite similar to same effect observed on the crystalline metal surfaces. At substrate temperatures of $T=120, 620, \text{ and } 720\text{K}$, the nanoripples develop parallel to the ion beam direction, while at room temperature $T=300\text{K}$, the nanopatterns organize along the high symmetry surface crystallographic directions. This observation suggests that the orientation switching at room temperature is due to anisotropic diffusion of adspecies along the surface high symmetry directions. Density functional theory (DFT) calculations proposed that a rather easier diffusion of oxygen assisted titanium, $\text{Ti}(\text{O})$, adspecies can be responsible for the morphology and orientation changes observed upon surface irradiation at room temperature.

In the second publication we have presented the first realization of covalent coupling of organic molecular precursors on a semiconducting surface, namely $\text{TiO}_2(011)-(2\times 1)$. So far, almost all of on-surface polymerization experiments have been carried out on metallic surfaces due to the catalytic activity of metal substrates which catalyze the homolysis process and create free radicals (split-off the halogen constituent) that consequently can initiate the polymerization reaction. We deposited 10,10'-dibromo-9,9'-bianthryl (DBBA) molecular precursors on a clean and atomically flat $\text{TiO}_2(011)-(2\times 1)$ surface in ultra high vacuum (UHV) conditions. Then through thermal activation the polymerization reaction was triggered resulting in single polymers and bunches of polymers. Possible reaction pathways are discussed basing on STM measurements and DFT calculations.

In the third publication we have shown the room temperature RT-STM/STS study of the formation of perylene-3,4,9,10-tetracarboxylic dianhydride (PTCDA) molecular nanocrystals on

a hydrogen passivated germanium, Ge(001):H surface. Upon depositing PTCDA molecules on the Ge(001):H surface very distinct molecular islands in the Volmer-Weber growth mode were formed indicating that introducing a monolayer of hydrogen atoms decouples the adsorbate molecules from the underlying surface and enhances their diffusivity so that the molecule-molecule interactions dominate the molecule-substrate interactions. Then through a tip-assisted manipulation technique, we were able to form a new top-most molecular layer on top of the islands. The new top-most layer formation might be attributed to a strain driven ascending molecular diffusion process that compensates the strain stored in the molecular nanocrystal from the substrate surface. The electric field of the tip seems to lower the ascending barriers for the molecules and its permanent existence seems to be crucial for the top-most layer formation completion.

List of Acronyms

AFM	Atomic Force Microscopy
BH	Bradly-Harper
1, 2, and 3D	One, Two, and Three Dimensions
DBBA	10,10'-dibromo-9,9'-bianthryl
DITF	Diiodoterfluorene
ES	Ehlich-Schwobel
FIB	Focused Ion Beam
Ge(001)	Germanium
Ge(001):H	Hydrogenated Germanium
GNR	Graphene Nano Ribbons
LT	Low Temperature
NC-AFM	Non-Contact Atomic Force Microscopy
PTCDA	3,4,9,10-Perylene-tetracarboxylic-dianhydride
RT	Room Temperature
STM	Scanning Tunneling Microscopy
TiO ₂	Titanium Dioxide
UHV	Ultra High Vacuum

Contents

Acknowledgements.....	v
Abstract.....	vii
List of Acronyms	ix
1. Introduction.....	15
1.1 Nanofabrication.....	16
1.1.1 Top-down techniques: low energy ion beam sputtering (IBS).....	16
1.1.2 Bottom-up techniques: Self-Assembly	19
1.2 Principles of on-surface molecular nanostructure formation in UHV conditions	20
1.2.1 3D molecular nanostructure growth on surfaces	22
1.2.2 On-surface covalent coupling	22
1.2.3 Halogen-based covalent reaction on different surfaces	24
1.2.4 Mechanism of halogen-based C-C coupling on metal surfaces.....	28
1.3 Nanostructure Engineering	29
1.3.1 Changing the orientation of ion-induced nanoripples.....	30
1.3.2 Decoupling adsorbate molecules from the underlying surface.....	31
1.3.3 STM tip-induced engineering	32
1.4 Main goals.....	33
1.5 Glossary of the enclosed publications.....	34
1.6 Statement.....	36
1.7 Outline.....	37
2. Experimental.....	41
2.1 Ultra High Vacuum (UHV) System.....	41
2.2 Scanning Tunneling Microscopy (STM)	43
2.2.1 STM microscope.....	43

2.2.2 STM Basic Principles	44
2.3 Sample Preparation and Molecule Deposition.....	46
3. Publication I: Temperature-dependent orientation of self-organized nanopatterns on ion-irradiated TiO ₂ (110).....	53
4. Publication II: Polymerization of Polyanthrylene on a Titanium Dioxide (011)-(2×1) Surface.....	65
5. Publication III: STM tip-assisted engineering of molecular nano-structures: PTCDA islands on Ge(001):H surfaces.....	71
6. Conclusions and Outlook.....	79
7. Appendices.....	83
8. Bibliography.....	87

Chapter One

Introduction

1. Introduction

Nanotechnology as a bald definition is simply engineering with molecular and atomic precision [1]. It is the technology that aims to controllably manipulate the structure of matter in the nanoscale (<100nm) to produce novel materials and devices. As it implies the most challenging goal of nanotechnology is the controlled nanofabrication, i.e., to gain the highest control in manufacturing and tailoring nanostructures [2].

Everything has started first from the classic talk entitled “*There’s Plenty of Room at the Bottom*” given by Richard P. Feynman in 1959 at Caltech [3]. He pointed out the possibility to revolutionize science and technology by controlling matter at the nanoscale (atomic) world. He mentioned that we could synthesize any substance by putting atoms the way we want; we could write all the books in the world in a cube of material one two-hundredth of an inch wide, we could have better electron microscopes, and making miniaturized superfast computers by gaining control over matter down to the atomic level.

Since then we have seen the invention of the scanning tunneling microscope (STM) by Binnig and Rohrer [4] in early 1980s. The invention of STM enabled imaging and manipulating single molecules and atoms and made the discussion of whether a single atom could be imaged coming to rest. Other important technologies like microelectronics and information technology have witnessed a remarkable improvement by implementing nanofabrication. These technologies demand the necessity of increasing the density of components in an integrated circuit in parallel with lowering the cost of fabrication. Nowadays, microprocessors with transistor gate length and dynamic random-access-memories of spacing less than 50nm are successfully been manufactured [5].

Nanotechnology is continuously striving to develop techniques and methods for controlled fabrication of functional nanostructures to fulfill the industrial and technological demands. As a result we have the possibility of producing different nanostructures with novel functionality such as semiconductor quantum dots capable of single electron tunneling and carbon nanotubes with very high electrical conductivity and mechanical strength [6,7].

Since the present thesis is devoted to various aspects of nanostructure fabrication and manipulation, the coming sections describe the principles of on-surface fabrication and engineering of various nanostructures. The thesis is based on three submitted publications which are enclosed to the thesis as separate chapters. Each publication introduces the fabrication of a specific nanostructure with a manipulation procedure for fine tuning the nanostructures. With the help of density functional theory calculations (DFT) the possible mechanisms responsible for the nanostructure formation is also proposed. Later in this chapter we address the main goals of the thesis, a glossary of the publications, and at the end we present the outline of the rest of the thesis. The present thesis and the enclosed publications aim to introduce the fabrication and manipulation means for different nanostructures on semiconducting surfaces as the crucial scientific and technological materials.

1.1 Nanofabrication

The two conventional approaches used to produce variety of nanostructures are the top-down and bottom-up techniques [8]. In this section we are introducing the general definitions of the two approaches with the common used techniques in the literature. The low energy ion beam sputtering as a top-down technique and molecular self-assembly as a bottom-up technique has been used in this thesis to fabricate the desired nanostructures. Therefore in the coming subsections the two methods are described in some detail.

1.1.1 Top-down techniques: low energy ion beam sputtering (IBS)

The top-down means fabricating a desired nanostructure by chipping away the unwanted parts. Usually the fabrication means are controlled by external parameters. The classic way to achieve this (top-down assembling) is the use of photolithography; that is using light to create the desired nanoscale patterns on the surfaces. Although, photolithography based nanofabrication is limited to the resolution of optical lenses, it is the technique being used so far to implement nanostructures in technology [8]. The dominant use of this approach is in electronics industry to produce the largest possible number of transistors in an integrated circuit following the Moor's law [9] that the number of transistors per square inch on integrated circuits had doubled every year since the integrated circuit was first invented.

Other top-down techniques such as scanning beam lithography (e.g., electron- beam and focused ion beam, FIB lithography) are used in research environments due to their high cost and difficulty in accessing. These limitations motivate introduction of a number of new unconventional techniques such as molding, stamping, embossing, printing, scanning probe lithography, and edge lithography [10,11]. Since the low energy ion beam sputtering has been used as the main top-down technique to fabricate nanoripples on $\text{TiO}_2(110)$ surface in the first enclosed publication, in the following section we are describing the technique and the theoretical attempts to describe the ion-induced nanopatterns formation.

Ion irradiation as a top-down nanofabrication method is considered as an effective mean to create and modify different nanostructures at solid surfaces [12]. Energetic ions during impact with solid surfaces loose energy. The energy loss is transferred to the surface atoms either elastically (nuclear stopping) or inelastically (electronic stopping) depending on the ion's mass and energy. Nuclear stopping is dominant for low energy ions (< 10 keV), and electronic stopping occurs for high energy ions (>100 keV) [13]. Heavy mass ions loose higher energy than lighter ones via both nuclear and electronic stopping. Ion irradiation can be applied for different purposes depending on the ion energy, low energy ions up to few keV can be used for sputtering purpose, and higher ion energies from tens of keV to a few MeV is used in ion implantation and doping experiments [12]. Sputtering a surface with low energy ions is a common technique to prepare clean and atomically flat surfaces in ultra high vacuum (UHV) environment for further growing different nanostructures. A clean and atomically flat substrate surface is prerequisite to perform different surface science techniques, such as STM, atomic force microscopy (AFM), etc.

Low energy ion bombardment, more than a routine surface cleaning tool, is also a technique to modify surfaces in a controlled way. When low energy ion beams are used to bombard materials at off-normal incidence, periodic nanopattern or ripple structures are usually develop on the surface analogous to the same effect of ripple formation when the wind blows on sand or water surface [14]. The first observation of this phenomenon was reported by Navez *et al.* [15] in 1962 when they bombarded an amorphous glass surface with Ar ion beam and found ripples with periodicity less than 100nm. They observed that the ripples orient normal to the ion beam direction for incidence angles close to normal and parallel to the ion beam direction for grazing incidence angles. The first systematic theory for description of the mechanism of pattern

formation due to ion beam irradiation on solid surfaces was proposed by Bradley and Harper (BH) in 1988 [16]. According to BH theory, the sputtering yield depends on the local surface curvature so that the regions in the bottom of trenches (valleys) erode faster than those on top of hills. Therefore, the sputtering tends to increase the surface roughness and is balanced by diffusion and smoothing effect at the surface. The competition between these two effects results in morphology formation with a characteristic periodicity that depends on the irradiation conditions.

BH theory successfully predicts the ripple wavelength and orientation in agreement with different experimental observations concerning amorphous [15] and semiconducting materials (which became amorphous in the near-surface region during sputtering) [17,18] because of isotropic diffusion of adatoms on the surface. However, it encounters some shortcomings in explaining the saturation of the ripple amplitude (amplitude increase at an exponential rate according to BH theory) and ripple rotation observed on crystalline metal surfaces due to the substrate temperature changing during sputtering. Numerous refinements of the BH theory to include different physical processes responsible for nanopatterns morphology formation on different surfaces have been introduced. The theoretical aspects of kinetic processes controlling surface evolution during sputtering are beyond the scope of this introductory section and can be found in many other literature reviews [14].

Ripple formation in the erosion regime (low energy, grazing incident angle) is the result of preferential sputtering of monatomic ascending step edges illuminated by the ion beam irradiation due to the higher sputtering yield at ascending step edges compared to flat terraces and descending step edges. The tendency of surface to reduce the sputtering effect through self arrangement in a step texture having no directional component normal to the ion beam is another factor leading to formation of nanoripples in the direction of the incident ion beam [19,20].

Crystalline metal surfaces behave in a different way that the pattern formation due to the ion sputtering cannot be described by the BH theory. On crystalline metals the adatoms produced by ion sputtering diffuse preferentially along the thermodynamically favored crystallographic directions of the substrate and are not influenced by the direction of the incident ion beam [21]. Different structures like mounds and ripples aligned with the crystallographic directions were found on different metal surfaces due to the existence of diffusion barriers known as Ehrlich-Schwoebel(ES) [22,23] barriers that can control the interlayer mass flow direction in certain

substrate temperatures. The ES effect was reported to be responsible for the pattern formation on anisotropic Cu, Ag, and other metal surfaces [24,25].

1.1.2 Bottom-up techniques: Self-Assembly

The bottom-up approach, in contrary to the top-down method which removes material to make structures, selectively ads smaller entities to create larger structures. The motivation behind the bottom-up approach is the phenomenon in nature. Nature uses bottom-up method to make the magnificent variety of ordered structures such as living cells and crystals. The definite structure and shape of naturally occurring crystals is the result of the specific interaction of the individual atoms of the matter. In living matter, the formation of complex deoxyribonucleic acid (DNA) molecules which carry the genetic codes is achieved by self-assembly of smaller organic molecules (base pairs) via intermolecular (Hydrogen bonds) interactions [26].

The term self-assembly is referred to as the spontaneous organization of two or more entities into larger structures [27]. When the interacting components are molecules, the self-assembly is termed as the molecular self-assembly and is defined as the spontaneous aggregation of individual molecules into larger structures through covalent and/or noncovalent bonding. The interactions are spontaneous and follow certain conditions imposed by the chemistry of the interacting components and the substrate electronic and thermodynamic conditions [28].

Self-assembly as a bottom-up approach is a promising strategy for nanofabrication due to its relatively simple and cheap processing. Getting a desired ordered structure only by mixing of components or ordering randomly distributed components via local interactions is very appealing for fabrication of materials with desired characteristics. Examples of nanostructures produced using this method are the block copolymer self-assembled structures [29,30], or self-assembled arrays of magnetic nanoparticles used in magnetic data storage devices [31].

We have followed the molecular self-assembly strategy to fabricate different molecular nanostructures on some semiconducting surfaces. Depending on the molecular precursor and substrate types, different kind of molecular nanostructures can be fabricated. The formation of molecular nanostructures is the result of competition between intermolecular and molecule-substrate interactions. The general principles of on-surface molecular nanostructure formation in UHV conditions and the role of intermolecular and interfacial interactions are described in the coming sections.

1.2 Principles of on-surface molecular nanostructure formation in UHV conditions

To get molecular self-assembled structures on solid surfaces, usually the molecules (building blocks) are deposited onto a flat surface and then through intermolecular (molecule-molecule) and interfacial (molecule-substrate) interactions, nanostructures form. The formation of molecular nanostructures is achieved by a subtle interplay or a competition between intermolecular and interfacial interactions [11,27,28,32]. This is a non-equilibrium phenomenon and the growth of any structure is governed by the balance between kinetics and thermodynamics at the surface [11].

Deposition of molecules in UHV conditions reduces the complexity of the assembling process because of the cleanness of the system. The ambient or liquid environments act as external molecule reservoirs, which introduce additional molecule-environment and substrate-environment interactions apart from molecule-molecule and molecule-substrate interactions [33]. Additionally in UHV systems, there is a high degree of control in preparing clean and atomically flat surfaces with low defect densities. Deposition of highly purified and defined organic molecules is also possible. The availability of various surface analysis techniques including STM and AFM provide a fabulous insight (atomic and molecular resolution) into the surface structures and are used as a sufficient tool to perform local spectroscopic measurements and manipulate the final structures. More importantly, using UHV system provides an excellent control of kinetic processes that are relevant for molecular self-assembly on surfaces. The deposition rate (or sublimation rate) of species to the surface is controlled by adjusting the evaporant temperature and the diffusivity of the adspecies can be controlled by changing the substrate temperature during or after deposition process [33,34]. Another advantages of UHV systems over solution environment is the possibility of preparing extended 1D or 2D self-organized supramolecular structures or rigid oligomers from suitable smaller precursors, that are impossible to synthesize in solution due to the solubility issues [35].

Considering aggregation of molecules into nanostructures at surfaces a main distinction has to be made between the self-assembled and the self-organized systems. The self-assembly is referred to the aggregation of the building blocks into a thermodynamically stable and favored state (equilibrium state). In contrast, a self-organized system is in a kinetically limited state far from

the equilibrium state. The difference arises from the different rates of molecular flux F and the surface diffusivity D of the adsorbates, i.e. D/F . If the flux rate is higher than the surface diffusivity of the adsorbate molecules (*small* D/F), they self-organize in a diffusion-limited state and the molecules have no chance to get to their equilibrium state. In contrast, if the flux rate of molecules is low and the diffusivity is high (*large* D/F), the molecules have enough time to self-assemble into a thermodynamically favored state [11,34]. The difference between these two states is illustrated in figure 1-1.

The formation of a thermodynamically stable structure is governed by several important energies relevant to the self-assembly processes on the surface. Upon deposition of molecules they face diffusion barriers E_d and in order to meet other molecules they must overcome the diffusion barriers. The diffusivity of the deposited molecules can be tuned by changing the substrate temperature. By increasing the substrate temperature, thermal energy is transferred to the molecules and as a result they gain sufficient kinetic energy E_{kin} to surmount the diffusion barriers and form thermodynamic equilibrium structures. We must keep in mind of course that the E_{kin} of molecules must be smaller than their binding energy E_b on the surface, otherwise they would desorb from the surface. The most crucial energy for the formation of ordered and stable assembly of molecules is the intermolecular interaction energy E_{inter} . The E_{inter} must be of sufficient strength. If the intermolecular interactions are too strong the molecules stick together very strongly (irreversibly), thus avoiding the formation of an ordered equilibrium structure. The best condition is when the intermolecular interaction energy E_{inter} is of the same order or a slightly larger than the molecular kinetic energy E_{kin} . The optimal energy profile for molecular self-assembly can be given as: $E_b > E_{inter} \geq E_{kin} > E_d$ [27,32].

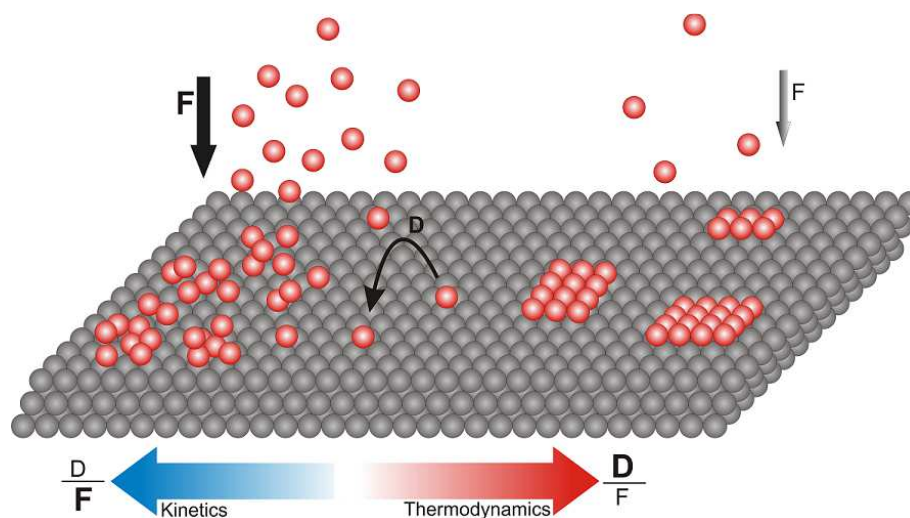


Figure 1-1 Difference between self-organization and self-assembly of adsorbates at solid surfaces (based on ref. [11]).

1.2.1 3D molecular nanostructure growth on surfaces

The organic molecule beam deposition (OMBD), thermal evaporation of organic molecules in UHV, is the common and typical method for fabrication of different nanostructures. Condensation of a substance (organic molecule beam) from the vapor phase on a surface can lead to formation of different structures ranging from 1D, 2D networks, 3D clusters, to even complete top layers [36].

In general, three growth modes can be distinguished considering the specific surface free energies of the substrate and the molecular layer as well as the interface energy: [36–38].

- 1- Layer-by-Layer (Frank-van der Merwe) mode: 2D molecular layers grow on top of each other; the molecule-substrate interaction is bigger than molecule-molecule interaction.
- 2- Island (Volmer-Weber) mode: distinct and separate 3D molecular nanocrystals (islands) form, the molecule-molecule interaction dominates the molecule-substrate interaction.
- 3- Layer-plus-Island (Stranski-Krastanov) mode: considered as the intermediate mode, one or two monolayers form (wetting layers) first, followed by 3D islands on top.

1.2.2 On-surface covalent coupling

Molecular self-assembly as a bottom up approach is considered as a promising strategy for constructing functional nanostructures on different surfaces. This approach with the help of

organic molecule synthesis has opened up a versatile research route to design a vast variety of molecular building blocks for constructing molecular nanostructures with desired functionality [27]. Typically, building blocks are deposited in UHV conditions on solid substrates and through involvement of different intermolecular and interfacial interactions, desired molecular nanostructures form. In most of physisorbed self-assembled 1D or 2D supramolecular (non-covalent) structures, building blocks aggregate via relatively weak forces, such as van der Waals, π - π stacking, hydrogen bonds, dipole-dipole, and metal-ligand interactions [27,39]. In another hand, from a technological point of view implementation of molecular nanostructures as electronic circuit elements requires high strength, thermally stable structures [35,40,41] with efficient electron transport between molecular building blocks [42].

An alternative strategy for constructing organic networks which meet the stability and good electron transport requirements is to introduce covalently interlinked structures. The growth of covalently interlinked molecular nanostructures by direct deposition of building blocks on solid surfaces (mostly metals) in UHV conditions has got a high degree of interest since last decade and has opened a versatile research avenue to construct characteristic and stable covalently bonded nanostructures. Some of the most outstanding examples of this growing field of research are given in the coming sections of the present chapter.

On-surface covalent C-C coupling has been achieved through different reactions [43], such as halogen-based covalent assembly, pyrimidine-pyrimidine coupling, homocoupling between terminal alkynes, Bergman cyclization, protecting-group-activated coupling, and carbon-metal coupling. All these covalent coupling reactions follow the concepts of on-surface condensation and radical addition [41]. The reactions usually need some sort of activation for accomplishment of the covalent coupling. Within the context of this thesis we followed the thermal triggering activation. Figure 1-2 lists the different reactions resulting in covalent assemblies on metal surfaces. Among these reactions, the halogen-based covalent reaction is considered as the most followed reaction for fabrication of extended covalently bounded molecular nanostructures on metallic surfaces. In the coming sections the state of the art of the halogen-based covalent coupling reaction and the reaction mechanism on metallic surfaces is given.

1.2.3 Halogen-based covalent reaction on different surfaces

One of the most popular reactions for on-surface covalent coupling of organic molecules in UHV conditions is the halogen-based reaction [43]. The halogen-based reaction or the radical addition reaction of halogenated monomers was first reported by Grill et al. in 2007 [44]. In their seminal work, they reported the construction of dimers, 1D covalently nanowires, and 2D covalently interlinked networks through depositing tetraphenylporphyrin (TPP) monomer building blocks with one (BrTPP), two (trans-Br₂TPP), and four bromine (Br₄TPP) substituents respectively on Au(111) surface. This work was the inspiration source for many other researches and soon after, this method has been applied on different noble metallic surfaces and a variety of covalently coupled molecular nanostructures have been developed. In general, the C-C coupling through halogen-based reaction is reported using different classes of organic halide building blocks including Porphyrin-halide [44,45], Aryl-halide [46–49], Anthrylene-halide [50,51], and Flourene-halide [52] precursors. Iodine (I) and Bromine (Br) are the two most used halogen constituents.

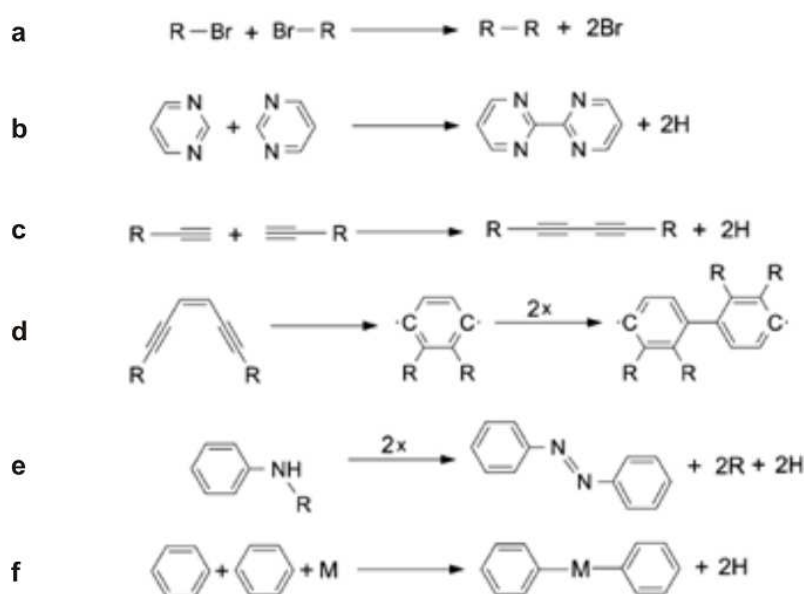


Figure 1-2 Different on-surface covalent coupling reactions. a) halogen-based coupling, b) pyrimidine-pyrimidine coupling, c) homo-coupling of terminal alkynes, d) Bergman cyclization, e) protecting-group-activated coupling, and f) carbon-metal coupling, taken from ref. [43]

The most outstanding on-surface polymerization, which is coherent with our work regarding the common used precursor and resulting in extended structures, following the strategy of the

halogen-based reaction are the works of M.Koch et al. [50] and J. Cai et al. [51]. The throughput of their work was the fabrication of atomically precise graphene nanoribbons (GNRs) obtained from 10,10'-dibromo-9,9'-bianthryl (DBBA building blocks) monomers deposited on an atomically flat Au(111) surface. Upon deposition of the DBBA precursors on hot gold substrate surface (kept at $\sim 200^\circ\text{C}$) the C-Br bonds dissociate (dehalogenation) resulting free radicals on the surface which diffuse and couple with other radicals forming polyanthrylene polymers on the surface. Then through cyclodehydrogenation process (C-C formation by releasing hydrogen at $\sim 400^\circ\text{C}$) atomically precise GNRs were obtained.

Insulators: Almost all of the covalently interlinked molecular nanostructures and on-surface polymerization reactions are carried out on metallic surfaces, since the catalytic activity of metal substrates create radicals (split-off the halogen constituent) that consequently can initiate the polymerization [41]. However, for the future technological applications (molecular nanoelectronics), it is highly desirable to have supramolecular or covalently interlinked molecular nanostructures on an electronically insulating or semiconducting substrate. Comparing formation of molecular covalent structures on insulating surfaces to metallic surfaces two main difficulties arise: Firstly, upon annealing to thermally activate the covalent coupling, molecules desorb from insulating surfaces due to their low surface energy comparing to metal surface energies [53]. Secondly, the metallic surface acts as a catalyst in Ullmann coupling reaction hence requiring lower thermal activation, while on insulating surfaces due to the lack of catalytic activity, the covalent interlinking activation step requires higher temperatures.

M. Abel et al. [54] reported the first 2D covalently interlinked organometallic monolayer on an insulating thin film. They obtained polymeric arrays by co-evaporation of Fe and 1,2,4,5-tetracyanobenzene (TCNB) in UHV conditions onto atomically clean Ag(100) surface partially covered by thin (50-100nm thick) NaCl islands. Covalent linking of organic molecules on a bulk insulator surface is important in many applications in order to decouple molecules and to prevent current leakage through the thin insulating layer to the underlying metal substrate. Kittelmann et al. [55] reported an attempt to transfer the on-surface covalent coupling of organic molecules from a thin insulating layer to a bulk insulator. They reported the covalent coupling of four different halide-substituted benzoic acid building blocks on the calcite (CaCO_3) bulk insulator. Their non contact atomic force microscopy (NC-AFM) revealed dimers, 1D and zigzag extended wires, and 2D interlinked structures depending on different halogen-based carboxylic acid

moieties they had used. The same authors [56] reported the first successful experiment of a sequential structure control on-surface covalent synthesis on calcite bulk insulator similar to the report of Grill et al. [45] on controlling on-surface polymerization by hierarchical growth on Au(111) and Au(100) metallic surfaces. They chose a molecular building block comprising three functional groups, two different halide-phenyl groups (chloro- and bromo-phenyl) for inducing site specific and sequential coupling and one carboxylic group to provide anchoring to the insulator substrate. By applying two annealing steps (570K and 610K) they induced sequential dissociation of the two different halide-phenyl bonds, as a result covalent extended zigzag and closed ring molecular nanostructures were obtained.

Semiconductors: Semiconductors are another important class of materials for on-surface polymerization, especially Silicon and Germanium because they represent the bases of the current microelectronics technology. Because the dangling bonds on the highly reactive semiconductor surfaces react strongly with the molecular building blocks, passivated semiconducting surfaces may facilitate the on-surface polymerization reaction. As far as we know, there is no successful experiment about on-surface polymerization on semiconducting surfaces reported in the literature. Berner et al. [57] have studied the adsorption of 5, 10, 15, 20-tetrakis(4-bromo-phenyl)porphyrin (H_2TBr_4PP) and 5, 10, 15, 20-tetraphenylporphyrin(H_2TPP) on both bare and hydrogen passivated Ge(001) surfaces. They showed that the hydrogen-passivation of Ge(001) is not the suitable strategy to the formation of covalently bonded molecular nanostructures. They proposed the halide-passivation route to obtain the covalent on-surface polymerization for further study of the system. Our preliminary attempts of polymerizing DBBA and DITF (diiodoterfluorene) precursors on hydrogenated Ge(001) surface were all in vain (for the molecules, Ge(001) and Ge(001):H surface models see Appendix). The passivating hydrogen atoms desorb earlier (lower temperature) than the polymerization activation temperature. Therefore, to overcome this difficulty different molecular precursors or different passivation strategies should be followed.

Titanium dioxide: Another important class of materials is the metal oxide materials [58]. Titanium dioxide (TiO_2) is considered as the prototype and model system for metal oxide materials [59]. The popularity of TiO_2 in surface science comes up from its easy processing and wide variety of applications. Therefore, understanding the on-surface processes leading to the

formation of desired molecular structures on TiO_2 surface will improve many technological branches, such as nanoelectronics, gas-and bio-sensing, solar cells and many others [60].

Different clean and atomically flat facets of rutile TiO_2 crystals can be easily prepared by ion sputtering and annealing in UHV conditions. The preparation process can make TiO_2 conductive by reduction so that unlike most of other insulating metal oxides, scanning tunneling microscopy on its surface is easily possible. Sputtering titanium dioxide surface with ions and annealing to high temperatures (700°C) introduce oxygen vacancies which in turn introduce new states within intrinsic energy band gap well below the Fermi level [61,62].

The two most studied facets of rutile TiO_2 single crystal are the (110) and (011) facets. The (110) face of the rutile titania is the most stable face that appears as (1×1) bulk truncated surface and does not undergo into any surface reconstruction at low temperatures [59]. This face is characterized by distinct bridging oxygen atoms along [001] crystallographic direction, in plane oxygen atoms and 5-fold titanium atoms [59], as shown in Appendix. The (011) face of rutile titania is the third most stable facet and undergoes into a (2×1) surface reconstruction phase [63]. It composed of double zigzag patterned oxygen rows along $[0-11]$ surface crystallographic direction protrude from the surface plane with double fold in plane oxygen atoms and slightly hidden 5-fold titanium atoms in the trenches [64,65], see Appendix. The hidden position of the 5-fold titanium atoms is the reason behind being the (011) faces of titania relatively inert surfaces for chemical reaction with the adsorbed molecules [66].

In this thesis (chapter 4, publication II), we report the first successful realization of the polymerization reaction on a semiconducting surface, namely $\text{TiO}_2(011)-(2\times 1)$ surface. The (011) face of rutile is proved to be a sufficient template for different admolecules to grow different weakly bonded 1D and 2D structures due to high diffusivity of the admolecules on this facet [67,68]. Many large polyaromatic organic molecules exhibit planar adsorption geometry with a non-covalent interaction with the aromatic board of the molecules [69]. This weak interaction does not hinder the diffusion of adsorbate molecules on the surface, which is a prerequisite for the on-surface oligomer formation.

1.2.4 Mechanism of halogen-based C-C coupling on metal surfaces

As it is stated in the previous section up to recently only metal surfaces have been used to form covalently bonded molecular structures through dehalogenation process, with the only exceptions of few works on insulators, halide-benzoic acid on Calcite [55], and our polymerization reaction of DBBA precursors on $\text{TiO}_2(011)$ surface (chapter 4, Publication II). Therefore, the only documented reaction mechanism is stated for metallic surface. Halogen-based covalent coupling on metal surfaces generally follows a two step pathway [70]: (a) dehalogenation of the molecular precursors and (b) diffusion and recombination of the resulting dehalogenated radicals. The reaction is illustrated in figure 1.3.

To date surfaces of noble transition metals (i.e., Cu, Ag, and Au) as templates, iodine (I) and bromine (Br) as halogen substituents of the molecular building blocks are mostly employed. Metal surface catalytic activity plays a crucial role to split-off the halogen constituents and trigger the polymerization reaction. Metal surfaces reduce the C-X (X=I, Br, ...) dissociation energy barrier significantly and hence lowering the on-surface dehalogenation process temperature [50]. For example, the (111) facets of noble metals reduce the dehalogenation energy barrier of bromobenzene and iodobenzene drastically, about 75% and 80% respectively comparing to the corresponding gas phase values [70]. Therefore, the metal surface acts not only as a solid physical template but also reduces the energy barriers associated with the dehalogenation process and hence lowers the temperatures at which dehalogenation takes place. It has been observed that the barrier for dissociating iodine is smaller than that of bromine as reported for different halogen-substituted molecular building blocks [45,70]. The radicals on the surface diffuse and meet other radicals and eventually couple through C-C covalent coupling. The diffusion is normally enhanced by thermal activation. The final formation of the covalently interlinked nanostructures depends strongly on the diffusivity and reaction ability (coupling rate) of the dehalogenated radicals on the surface.

If the diffusion rate of the radicals is greater than their coupling rate then the reaction is coupling limited, while if the coupling rate is greater than the radical's diffusivity then the reaction is diffusion limited. For small molecular building blocks and inert substrates the reaction of radicals is of the coupling limited nature, in contrast for more reactive and bigger precursors the reaction is diffusion limited.

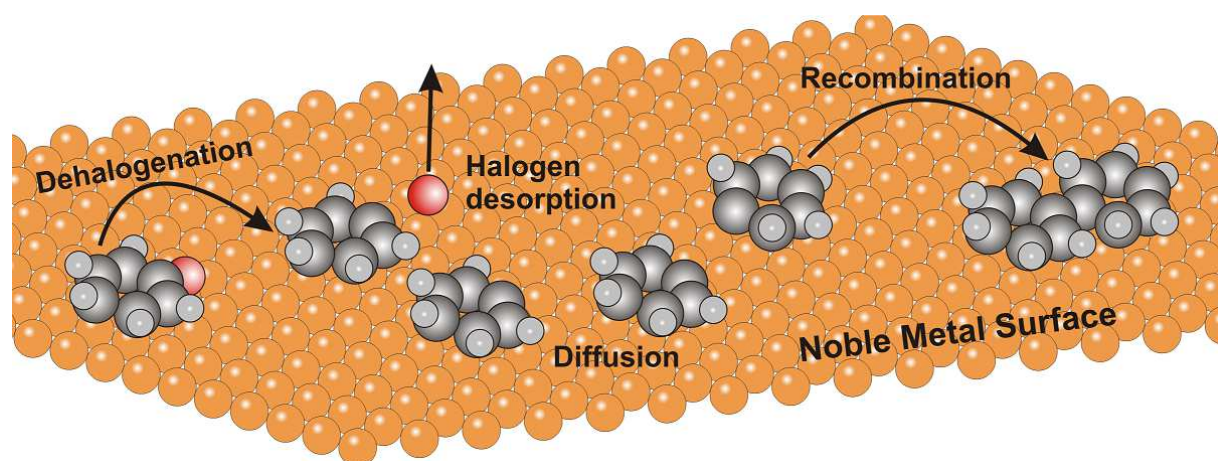


Figure 1-3 Two step mechanism of halogen-based covalent coupling on close-packed noble transition metal surfaces, two Halogen-Substituted Benzene precursors dehalogenate into Phenyls and recombine into a Biphenyl molecule. Redrawn based on Ref. [70].

The coupling limited reactions produce ordered networks while the diffusion limited reactions give non-ordered structures. For example the reaction between the cyclohexa-*m*-phenylene radicals (CHPR) on the more reactive Cu(111) surface is of diffusion-limited nature and gives unordered structures, while the reaction between the same CHPRs on the less reactive Ag(111) surface gives ordered two-dimensional networks due to the coupling-limited reactions [71].

1.3 Nanostructure Engineering

Numerous nanostructures can be fabricated by implementing different top-down and bottom-up techniques as described in the previous sections. The obtained nanostructures sometimes do not exhibit the desired uniformity and functionality and require extra manipulation by one means or another to meet the desired expectation. This problem is even more obvious when the ever smaller nanostructures and devices are required. The autonomous ordering of nano-materials is usually an irreversible process sometimes leading to non-favored structures. To overcome this unfortunate, numerous strategies have been followed to improve the current nanofabrication techniques or to introduce new unconventional ones [8,10]. In the following, three different engineering methods of changing the orientation of nanoripples on an ion-irradiated TiO₂(110) surface, decoupling 3,4,9,10-Perylene-tetracarboxylic-dianhydride (PTCDA) adsorbate molecules from Ge(001) surface, and manipulating the self-assembled PTCDA molecular nanocrystals by STM tip-assisted engineering are described and the results are given in the enclosed publications.

1.3.1 Changing the orientation of ion-induced nanoripples

The alignment of the nanopatterns produced by low energy ion beam sputtering can be controlled either by the ion beam parameters, i.e., the angle of incidence, or by the surface temperature [14]. The controllably oriented modification at the target surface may be quite useful in technological applications and may be used as a template to grow the desired metallic or molecular nanostructures such as nanowires in the grooves of the patterned surfaces [72] or to align large molecules like liquid crystals in producing higher resolution liquid crystal displays [73].

It has been shown that low energy ion beam bombardment at grazing angles is a sufficient tool to introduce nanoripples with the desired atomic steps on $\text{TiO}_2(110)$ surface. Luttrell et al. [74,75] demonstrated that low energy ion (Ar^+ , $\sim 1\text{keV}$) irradiation at grazing angles ($\sim 80^\circ$ off normal) on $\text{TiO}_2(110)$ surface at 400°C induces the formation of new directions for atomic steps that are elongated with the ion beam direction. A typical clean $\text{TiO}_2(110)$ surface exhibits step edges oriented along [001] and [1-11] surface crystallographic directions only [74]. Using this technique they were able to fabricate thermodynamically disfavored $\langle 1-10 \rangle$ steps which cannot resist the high temperature annealing in common surface preparation method. Knowing this fact it would be quite useful from a technological point of view to control the orientation of the nanoripples in a desired way. In the ion beam sputtering process, the collision of energetic ions with the surface results not only sputtering or removal of surface atoms, but also produces some surface adatoms and vacancies (defects) [21]. There are two key factors that affect the morphology evolution on ion beam sputtered crystalline metal surfaces; temperature and barriers to surface diffusion of adatoms to descend step edges known as ES energy barriers. Annealing the surface provides sufficient activation to adatoms to overcome the ES barriers. For anisotropic metal surfaces at normal ion incidence ripples evolve with an orientation governed by surface high symmetry directions. For example in the case of $\text{Ag}(110)$ [24], $\text{Cu}(110)$ [25] surfaces, at certain low temperature at normal ion incidence, ripples are elongated along the [001] high symmetry direction, while at higher temperatures the orientation switches by 90° to [1-10] and at moderate temperatures rectangular mounds reflecting the symmetry of the surface are formed. In this case the erosive action of the ion beam provides the mobile adspecies and the nanomorphology evolution is governed by the thermal activation processes at the surface.

In the publication I (chapter 3), we report the first results revealing temperature dependent orientation of nanoripples on an ion irradiated $\text{TiO}_2(110)$ surface. The study has been conducted through both STM and DFT calculations. Our results show that the orientation of the nanoripples switches by 90° with changing the substrate temperature during irradiation process quite similar to the same effect observed on the crystalline metal surfaces mentioned before. This observation suggests that the orientation switching is due to anisotropic diffusion of adspecies along the high symmetry atomic rows rather than the erosive action of the ion beam. DFT calculations revealed some interesting facts about the diffusive adspecies and corresponding hopping frequencies and diffusion energies.

1.3.2 Decoupling adsorbate molecules from the underlying surface

The scenario of nanostructure fabrication in all bottom-up strategies is based on self assembly of smaller building blocks (atoms/molecules) on clean and atomically flat substrates in UHV, ambient, or solution environments. The building blocks are deposited on the substrate surface to form nanostructures and their self assembly is governed by several atomistic processes on the surface. There are two primary parameters crucial for achieving the final desired nanostructure, namely the rate of deposition of molecules flux F , and their diffusivity on the surface D [11]. As we mentioned before the ratio D/F is the key parameter determining the evolution kinetics of nanostructures. Fortunately the rate of deposition or the flux of molecules can be highly controlled by changing the temperature of the evaporants within the Knudsen cell. In most of the self assembly experiments a low rate of evaporation at low temperatures is required to avoid molecule dissociation prior to their deposition on surfaces.

The other crucial parameter is the diffusivity of the adsorbates, the mean square distance travelled by adsorbates per unit time, on the surface. The diffusivity or diffusion coefficient D is a function of temperature [76], and can be adjusted by annealing or cooling the substrate during or after deposition process. Adjusting substrate temperature is more effective for inert insulating and noble metallic surfaces, where the molecules are physisorbed on the surface. But in order to electronically decouple molecules on more reactive metallic and semiconducting surfaces different strategies are introduced. The chemical and topological periphery of molecules can drastically change their electronic structure. The performance and reliability of a molecular nanostructure or device is strongly dependent on the successful elimination of any unwanted and

unexpected changes in the molecule electronic structure arising from surroundings [77]. Consequently, strategies to prohibit a strong coupling of the molecules and underlying substrate have to be followed.

There are several promising strategies to partially or fully eliminate the influence of the underlying substrate on the electronic structure of the molecular nanostructures on top and to tune, to some extent, the diffusivity of molecular adsorbates [77]. The first strategy is to cover a semiconducting or metallic substrate surface by an ultra-thin insulating layer such as NaCl on Cu(111) [78–80], Ag(111) [54], and Au(111) [81], or KBr on InSb(001) [82,83] and Ag(111) [84]. For the case of elemental group IV semiconductors (Ge and Si), the common way is to introduce a monolayer of hydrogen atoms to saturate the surface dangling bonds [85–88]. The semiconducting surface with saturated dangling bonds is a highly passivated surface that can electronically decouple molecules from the underlying surface and dramatically enhance molecule diffusivity on the surface as well.

In the third publication, chapter 5 in the thesis, we followed the same approach of passivating a semiconductor surfaces Ge(001) by hydrogenating and investigated the effect of the Hydrogen monolayer on the molecule-substrate interaction. Then we fabricated PTCDA molecular nanocrystals on top of the hydrogenated semiconductor surface namely Ge(001):H surface. The introduction of H-layer increased the diffusivity of the molecules and decreased the molecule-substrate interaction to such extent that eventually molecular nanocrystals in Volmer-Weber growth mode were formed on the surface. The PTCDA molecules on top of the islands resemble the herringbone structure found in the (102) plane of PTCDA bulk crystal, which indicates again that the passivation of Ge(001) surface by a hydrogen monolayer works very efficient to reduce the molecule-substrate interactions and enhances molecule-molecule interactions.

1.3.3 STM tip-induced engineering

The STM tunneling current is highly sensitive to the gap between the STM tip apex and the substrate surface, it decays exponentially with the distance and almost all stream of electrons tunnel from the last atom at the tip apex. As such, the STM tunneling current is highly localized and the tunneling direction is governed by the polarity of the bias voltage. The electrons injected from the tip are known as hot electrons because they possess energies greater than the Fermi energy of the substrate [89]. Nowadays the STM is not merely an imaging tool but is employed

as the source of hot electrons that can induce both local chemical reactions and molecular chain reactions at surfaces. It is used for manipulating single atoms and molecules on surfaces including displacement [90], dissociation and inducing chemical reactions (bond breaking and bond making) [91–93], and polymerization chain reaction at surfaces [94,95].

Positioning the individual Xenon atoms on a cold single-crystal nickel surface with atomic precision by Eigler and Schweizer [90] to write the IBM logo is a very accurate example of fine atom positioning using a STM tip.

Inducing all steps of Ullmann reaction with a STM tip by S. W. Hla [91] and coworkers contains three tip-induced manipulations, bond breaking, manipulating reactants into proximity with one another, and bond making. The Ullmann reaction steps were all induced by the tip, first the iodine was separated from iodobenzene (bond breaking) by tunneling electrons, then two resultant phenyls were brought into proximity (lateral manipulation), and finally, chemical association of the two phenyls was carried out through excitation with tunneling electrons from the tip.

We employed STM tip-assisted manipulation technique by applying voltage pulses on top of the self-assembled PTCDA nanocrystals on the hydrogen passivated Ge(001) surface. The result was the formation of a hole with some ad molecules surrounding it. With continuous scanning we were able to produce a full top-most layer. We propose that the molecules from the edges of the lower layers of the islands tend to ascend and bind to the top-most layer edge to compensate the strain stored in the molecular nanocrystal and the electric field of the STM tip seems to decrease the diffusion barrier for the molecules to join the top-most layer. The details are given in the publication III (chapter 5).

1.4 Main goals

The present thesis aims to address the fabrication and manipulation of various nanostructures on different semiconducting surfaces. Semiconductors represent the bases of many technological aspects, hence developing novel nanostructures on their surfaces and finding proper means to manipulate them will have a crucial impact on the forthcoming technologies. The main goals of the present thesis which contains three publications are summarized as follow;

- Formation of nanoripples by means of low energy ion beam sputtering at grazing incident angles on $\text{TiO}_2(110)$ surface.
 - Studying the temperature dependent orientation of the nanoripples.
 - Seeking for the proper mechanism behind the observed phenomena.
- Polymerization reaction on $\text{TiO}_2(011)-(2\times 1)$ surface.
 - Demonstration of thermally triggered on-surface C-C coupling through halogen-based reaction and looking for the optimum parameters to get the longest possible polymers of the given organic precursor on the surface.
 - Seeking for the polymerization reaction pathway on the $\text{TiO}_2(011)-(2\times 1)$ surface.
- Fabricating and manipulating PTCDA supramolecular nanocrystals on a hydrogen passivated $\text{Ge}(001)$ surface.
 - Studying the effect of a hydrogen monolayer on both decoupling the PTCDA molecules from the $\text{Ge}(001)$ surface and enhancing their diffusivity.
 - Engineering the self-assembled PTCDA nanocrystals on a hydrogen passivated $\text{Ge}(001)$ surface by means of a tip-induced manipulation technique as a top-down method.

1.5 Glossary of the enclosed publications

Three publications are attached to the present thesis as three separate chapters. Below is the glossary of the three publications.

In publication *I* (chapter 3), we present the use of high resolution STM to study the temperature dependent formation of nanoripples on $\text{TiO}_2(110)$ surfaces by low energy Ar^+ beam irradiation in UHV conditions. Ion beam of 2 keV Ar at grazing angle of 75 degrees off-normal is used for irradiation purpose and the substrate temperature was changed as $T=120\text{K}$, 300K , 620K , 720K during irradiation. As a result, very pronounced ripple structures of periodicity ~ 10 nm have been developed. It appeared that the orientation of the nanoripples switches by 90° with the change of the substrate temperature from $T=120\text{K}$ to room temperature and then to elevated temperatures during irradiation. We have described that formation of this kind of surface morphology is due to the interplay between the erosion of the monatomic ascending step edges at grazing incidence, adatoms surface diffusion along the favored crystallographic direction and at elevated temperatures, the diffusion of the excess Ti ions into the bulk of the crystal. With the help of DFT calculations applied to modeling the diffusion process on the ion irradiated

TiO₂(110) surface, the crucial surface mass transport which is responsible for forming nanoripples is dominated by the highly mobile Ti atoms diffusing as Ti(O) (adatom Oxygen assisted) species.

In publication *II* (chapter 4), we are reporting a successful on-surface polymerization on a semiconducting surface, namely TiO₂(011)-(2×1) surface. We deposited DBBA molecular precursors on a clean and atomically flat TiO₂(011)-(2×1) surface kept at room temperature in UHV conditions. STM imaging was quite difficult at RT due to the high diffusivity of the molecules as we anticipated prior to deposition. We applied two thermal activation steps to facilitate the polymerization reaction. First, we deposited molecules on the surface kept at RT then we annealed the system to 300°C. As a result some short polymers were observed on the surface. Next step which yielded the better polymerization reaction was deposition of the DBBA molecules on a hot surface (270°C), as a result different randomly distributed 1D polymers or bunches of polymers were observed on the surface. We propose that the polymerization mechanism here does not follow the same pathway as on metal surfaces. Corroborating our STM results with density functional theory (DFT) results, proposed a cooperative process of early C-C bond formation accompanied by late C-Br bond cleavage and a multistep proton assisted coupling.

In publication *III* (chapter 5), we report STM tip-assisted manipulation of PTCDA molecular nanocrystals on a hydrogen terminated Ge(001) surface. Passivating Ge(001) surface by introducing a monolayer of hydrogen atoms decouples PTCDA molecules from the surface and enhances their diffusivity. As a result, upon depositing PTCDA molecules on Ge(001):H surface, very distinct molecular 3D nanocrystals in Volmer-Weber growth mode were evolved indicating that the intermolecular interaction dominates the molecule-substrate interaction. By applying STM tip voltage pulses (injecting hot electrons) on top of the multilayered PTCDA islands, we were able to break the intermolecular electrostatic interaction and splash molecules outwards. As a result an artificial defect (hole) was produced with some admolecules surrounding it which served as a nucleation site for growing the extra structure. Then through continuous scanning and a strain driven ascending process of molecules a full top-most layer was formed with the hole remained unhealed. With this process we were able to shrink the lateral dimensions of the islands and increase the height of the islands by one monolayer.

1.6 Statement

My participation as a PhD student in the three publications was as following;

1. The nanoripple pattern formation on $\text{TiO}_2(110)-(1\times 1)$ surface:
 - Preparing and cleaning the $\text{TiO}_2(110)$ samples.
 - Performing the ion beam sputtering of the samples with controlling the desired parameters of the ion beam and the substrate.
 - Taking LEED patterns and STM images of the samples.
 - Analyzing and discussing the STM data and observed phenomena.
2. Polymerization reaction on $\text{TiO}_2(011)-(2\times 1)$ surface:
 - Discussing the motivation behind the project and designing the experiment.
 - Preparing and cleaning the $\text{TiO}_2(011)$ samples.
 - Calibrating and depositing DBBA molecules on the samples.
 - Tuning the proper substrate temperature and post deposition annealing to obtain the polymerization reaction.
 - Performing RT/STM imaging of the samples and adsorbates.
 - Analyzing and discussing the STM data.
 - Commenting and helping to write the manuscript.
3. Manipulating PTCDA nanocrystals on $\text{Ge}(001):\text{H}$ surface:
 - Discussing the motivation behind the experiment and designing the experiment.
 - Preparing and cleaning the $\text{Ge}(001)$ samples.
 - Hydrogenating the $\text{Ge}(001)$ samples to get the passivated surfaces.
 - Calibrating and depositing PTCDA molecules on the $\text{Ge}(001):\text{H}$ surface.
 - Obtaining STS/STM data and performing the tip-induced manipulation of the molecular islands.
 - Analyzing and discussing the observed phenomena.
 - Writing and commenting on the manuscript.

The DFT calculations throughout the thesis have been performed by the group of Professor Zbigniew Sojka (Dr.hab.Witold Piskorz and Dr.Filip Zasada) from the Faculty of chemistry, Jagiellonian University.

1.7 Outline

The rest of the thesis is organized as following;

In the next chapter (chapter 2) we describe the equipments and systems which have been used to perform the experiments including the UHV system and its elements (STM microscope, Ion sources, hydrogen sources, molecular evaporators, and pumping systems). The basic principles about STM operation and scanning methods are given. There is also a brief description of the sample mounting and sample cleaning procedures.

In chapter 3, publication entitled; “*Temperature-dependent orientation of self-organized nanopatterns on ion-irradiated TiO₂(110)*”, we show the first observation of the nanoripple orientation switching by 90° by a systematic change of the substrate temperature from low temperatures to room temperatures and then to higher temperatures on TiO₂(110) surface similar to the same effect observed for crystalline metallic surfaces.

In chapter 4, publication entitled; “*Polymerization of Polyanthrylene on a Titanium Dioxide (011)-(2×1) Surface*”, we present the first successful on-surface polymerization of a halogen-based organic molecule precursor DBBA on a semiconducting surface, namely TiO₂(011)-(2×1) surface. The DFT calculations for modeling the polymerization of the DBBA molecule on the TiO₂(011)-(2×1) surface as well as the possible mechanism of polymerization on this surface are given.

In chapter 5, publication entitled; “*STM tip-assisted engineering of molecular nano-structures: PTCDA islands on Ge(001):H surfaces*”, we present a tip-induced method for engineering the final morphology of PTCDA 3D molecular nanocrystals grown on Ge(001):H-(2×1) surface. A possible mechanism of the process is also given there.

In chapter 6, conclusion remarks as well as some outlooks for further investigations in the framework of the submitted works is stated.

Chapter Two

Experimental

2. Experimental

All the experiments in the present thesis have been conducted in UHV conditions and the main apparatus throughout the experimental work was the scanning tunneling microscope. Although, a brief description of the experimental procedure is given in each publication, here we would like to give a more detailed illustration of the UHV systems, equipments, the procedures of mounting and preparing the samples and molecule deposition as well as performing the STM imaging.

2.1 Ultra High Vacuum (UHV) System

Three different UHV systems have been used to carry out the experiments in this thesis; Omicron variable temperature VT-STM/AFM system, Omicron low temperature LT/STM system, and VP2 Park Scientific Instrument STM system. The systems are composed of few common interlinked chambers for preparing the samples (Prep. Chamber), STM imaging (microscope chamber), and a small entry chamber to put the samples into the UHV system (intro chamber). The difference between the systems arises from exhibiting different sample transportation systems. The LT and Park systems exhibit linear magnetic transportation systems while there is a central chamber (UFO) in the VT system which enables a radial distribution of the samples between the chambers. Most of the room temperature measurements (except ripples) were carried out in the VT-STM/AFM system. For the sake of simplicity we present in figure 2-1 only the VT-STM/AFM UHV system schematically (Schemes of the VP2 Park and LT/STM Omicron systems are shown in Appendix). It composed of five interlinked chambers, one small entry chamber to introduce samples into the UHV system, two preparation chambers; Prep. *I* chamber is known as the dirty chamber and is used to evaporate and deposit molecules on the samples. Prep. *II* chamber is used for cleaning and hydrogenating purposes, the central sample distributor, and finally the microscope chamber. In order to obtain ultra-high vacuum conditions all chambers which are separated by hand controlling valves are equipped with a series of vacuum pumps. The introduction and preparation *I* chambers are equipped with turbo-molecular pumps and other chambers are equipped with a set of ion, titanium sublimation, and turbo-molecular pumps. There is also a liquid nitrogen cryogenic trap in the microscope chamber by which a better vacuum level of an order of magnitude is obtainable. Thanks to the use of ion, turbo-molecular and titanium sublimation pumps a base pressure of about 4×10^{-10} mbar is

obtained in all chambers and filling the cryogen trap with liquid Nitrogen improves the base pressure to about $2-5 \times 10^{-11}$ mbar in the microscope chamber. In addition, the microscope chamber is equipped with a liquid nitrogen flow cryostat cooling system which enables measuring at temperatures ranging from liquid nitrogen to room temperature.

The radial distribution chamber is exclusively used to transfer samples between the chambers. It also contains a small magazine to store the sample holders. In the main preparation chamber (*Prep. II*) there is an ion gun used for sample cleaning purpose and a hydrogen cracker used for passivating germanium samples. *Prep. I* chamber is equipped with two types of molecule evaporators, one having four crucible cells (Kentax UHV equipments) separately controlled by a variable power supply unit and a standard low temperature effusion cell (Omicron, 80-400°C NTEZ) as the second one. Temperature of the cells is measured by a thermocouple of type C or K. A quartz crystal microbalance is used to control the deposition rate of molecules and the cells have a hand controlling shutter which can open or block the flow of molecules.

Within the chambers thanks to manipulators it is possible to slide and rotate samples along and to a limited extent around the axis of the manipulator (rotation). This makes it possible to select the appropriate position of the sample in the process of ion bombardment, annealing, and deposition of molecules. The sample heating is achieved either by a direct flow of current (with Omicron DH basket), or by contact thermal-radiation (with RH PREVAC basket). In the former case the sample temperature is measured using a Pyrometer (Impac IGA 140) and in the latter case it is possible to measure the temperature using a thermocouple.

In the ion-induced nanopatterning (ripples) experiment, the topography of the surfaces was imaged at room temperature by a VP2 Park Scientific Instrument STM microscope. Characterization and evaluating the optimum experimental parameters to obtain the best polyanthrylene polymerization conditions was firstly performed in Omicron VT-STM/AFM system and then in order to get high resolution STM imaging and manipulating the polymers, the Omicron LT microscope system was used. The tip-induced engineering of molecular nanostructures was carried out entirely in the VT system.

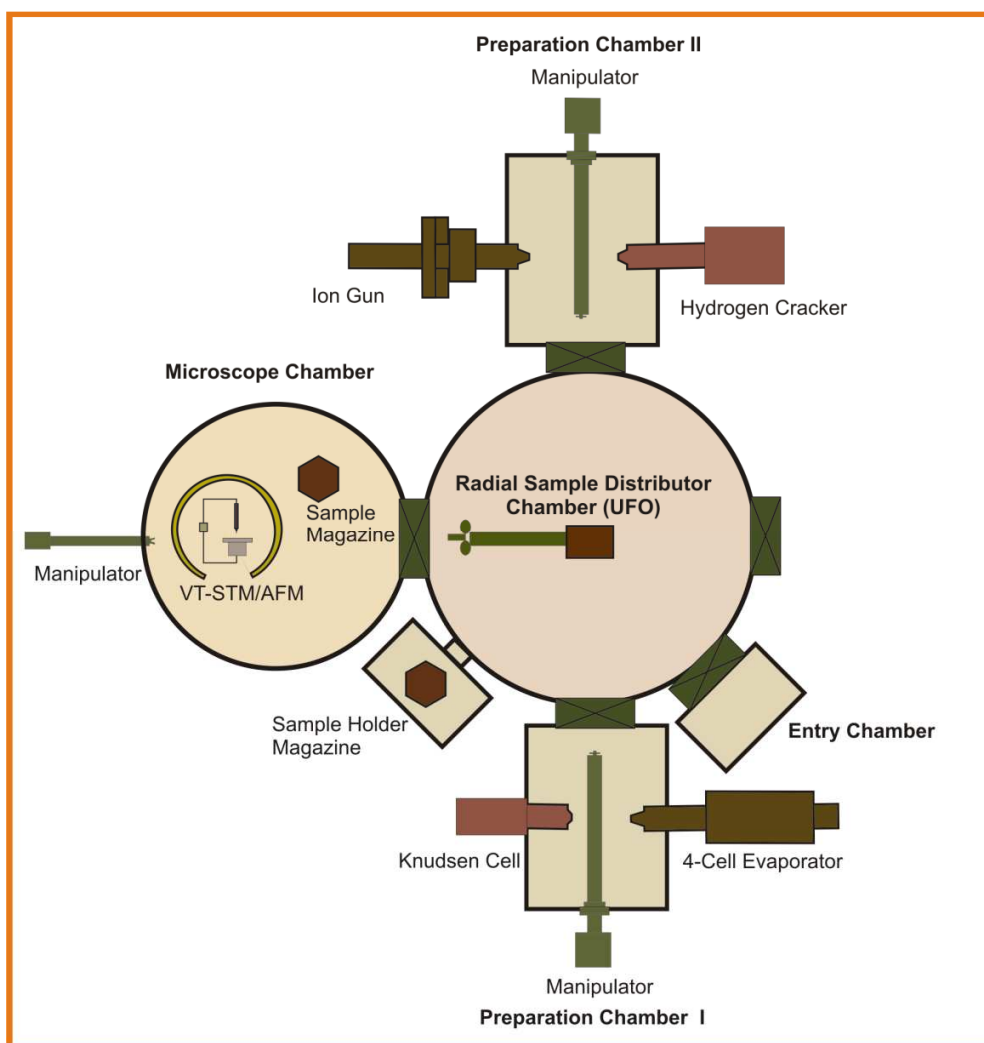


Figure 2-1 The UHV system equipped with Omicron VT-STM/AFM microscope. The system consists of 5 interlinked chambers; one small intro chamber, two sample preparation chambers, the radial distributor chamber, and the microscope chamber¹.

2.2 Scanning Tunneling Microscopy (STM)

2.2.1 STM microscope

The key instrument used in this thesis is the STM as a powerful tool for investigating conducting surfaces (metals and semiconductors) and adsorbates with atomic resolution. The scanning ability of the microscopes is determined by the piezo tubes which are installed under the scanning probe. For example the piezo tube of the Omicron VT/STM is characterized by a change in length of about $10\text{\AA}/\text{V}$. The maximum allowed voltage is about 100V, under which an

¹ This Scheme is taken with changes from the previous PhD thesis of our group, "Adsorption of Organic molecules on $\text{TiO}_2(011)$ surface" by dr.Szymon Godlewski 2011.

overall area of $1\mu\text{m}^2$ can be scanned. Figure 2-2 shows the Omicron VT-STM/AFM microscope used in this thesis. To get the highest resolution imaging a special attention is paid to ensure the proper isolation of the whole system from the electrical and mechanical vibrations of the surroundings. The STM lab is located in the basement where the floor and building vibrations are most likely negligible. The entire microscope chamber rests on three air dampers. The microscope is decoupled from the rest of the chamber using suspension springs and in addition eddy current damping ensures excellent electronic perturbation isolation. All these isolating systems provide a proper noise reduction level so that high resolution STM imaging at RT is possible.

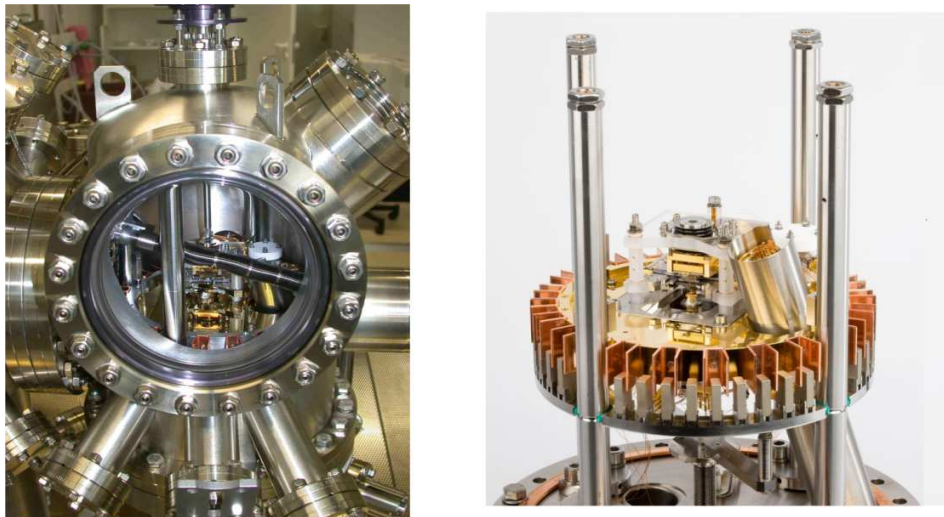


Figure 2-2 The Omicron VT STM/AFM Microscope, taken from Omicron official website www.omicron.de.

2.2.2 STM Basic Principles

The STM was invented in 1982 by two IBM employees, Gerd Binnig and Heinrich Rohrer², and soon after it became one of the most used tools in surface physics research laboratories. The impact of STM invention on the field of surface science and all other related fields was so great that its two inventors won the Noble Prize in physics in 1986.

As it is implied by its name, the STM operates basing on the quantum tunneling effect. The tunneling effect is the probability of electron's passing through a classically forbidden potential barrier. This probability depends exponentially on the barrier width. Sensing this very tiny

² G. Binnig, H. Rohrer, *Helv. Phys. Acta* 55,726(1982)

tunneling current is used for imaging surface with atomic resolution. The operation principle and structure of STM are shown in figure 2-3.

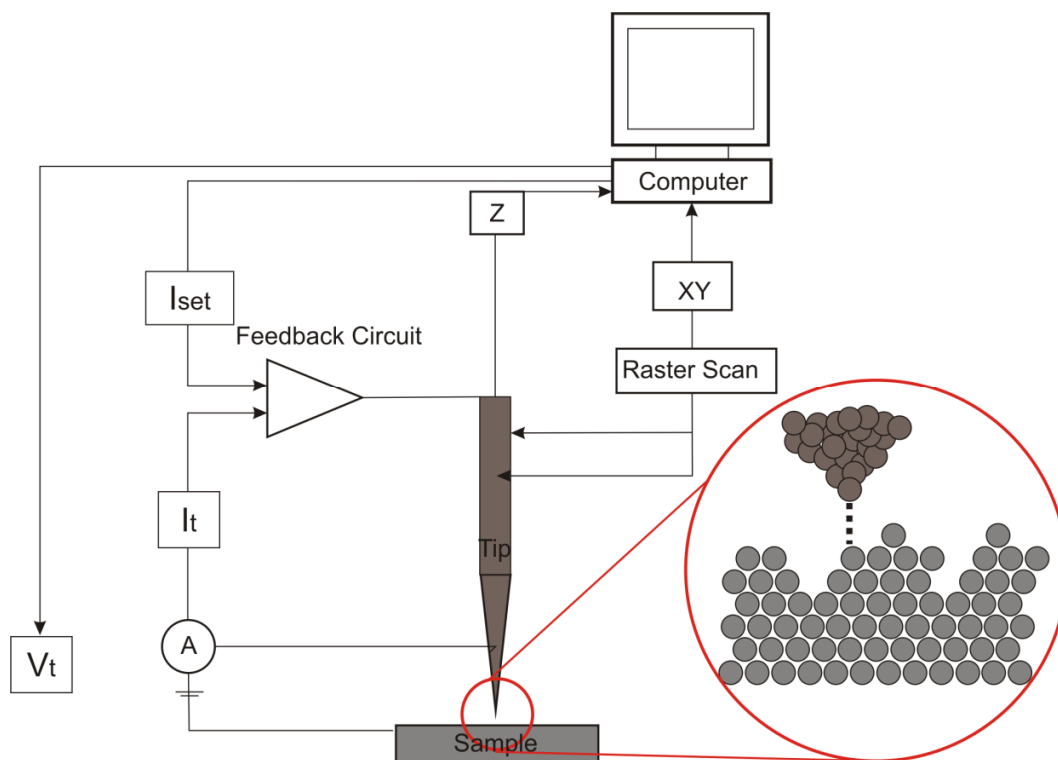


Figure 2-3 Schematic illustration of the STM operation principles.

The basic element of STM, an atomically sharp metallic tip (in our experiments chemically etched tungsten), is brought into a very close proximity to the desired conducting sample ($<10\text{\AA}$). For precise positioning of the tip in the vicinity of the sample surface piezoelectric tubes are used. These are materials that undergo a reversible type of deformation (change in length) under the influence of applied voltage. A bias voltage is applied to the tip-sample gap; as a result electrons tunnel through the gap in the tip-sample direction or vice versa depending on the polarity of the applied voltage. Classically, the height of the potential barrier between the tip and the sample is greater than the electron's energy, thus preventing current flow. However, the applied voltage makes the tip and the samples wave-functions overlap and hence increases the tunneling and current flow. The intensity of the tunneling current is typically of the order of Pico to Nano amperes and depends exponentially on the tip-sample distance, where in an increase of the gap distance by 1\AA , reduces the tunneling current by an order of magnitude.

There are two modes of operating STM. The most commonly used mode (used in this thesis too) is the constant current mode. In this mode the tip moves line by line over the sample in such a way that the measured tunneling current I_t , is compared to a preset value by a feedback circuit. It gives back a correcting voltage to the scanner piezo tube that adjusts the tip z-position in order to keep I_t constant. The x-y position of the tip as well as its corrected z-position is recorded over entire scanning area and the STM image is obtained. The STM image depends on the electronic properties (local density of states (LDOS)) of both tip and sample sides.

The other mode is the constant height mode; the system works without feedback, i.e. the z-position of the tip is kept constant. Three dimensional (topographic) images of the surface are obtained by recording the tunneling current while the tip rastering the scanning area of the sample surface.

Generally, the constant-current mode yields better resolution but the disadvantages of this mode are the noise from the feedback system. On the other hand the constant-height mode allows faster scanning.

2.3 Sample Preparation and Molecule Deposition

Rectangular Ge(001) (MTI corporation) and $\text{TiO}_2(011)\&(110)$ (MaTeck GmbH) crystals of 2mm×10mm were cleaved and mounted onto the special sample holders designed by Omicron. The structure of the holders is such that one side of the crystal is grounded through the clamping foil touching the body of the holder. The other side of the crystal is isolated from the body of the holder plates by means of ceramic bushes. With this geometry the crystal can be scanned using a probing tip. The samples were fixed using a ceramic plate screwed on top of the sample crystal. Figure 2-4 shows the mounting procedure of the samples.

Titanium dioxide samples were placed on a doped germanium or silicon crystal (wafer) of the same size as a support for the resistive heating purpose. This design is dictated by some technical aspects. First, to ensure the ability to achieve high temperatures necessary for preparation of titanium dioxide (temperature of 700 – 800°C) in a short time, since titanium dioxide is not a good electrical and thermal conductor. For this reason, silicon or germanium support crystal serves as a heater. Second, to allow reproducible measurement of sample temperature, this is crucial in the preparation of the surface. To measure the temperature of the samples during the

cleaning and direct heating processes a pyrometer is used operating in the infrared range (Impac IGA 140, 1.45 - 1.80 microns wavelength). It is the wavelengths range, at which the transmission coefficient of titanium dioxide crystal is very high. This allows measuring the temperature of the support-heater, since the radiation emitted by it is hardly absorbed by the titanium dioxide sample. For Germanium and all other types of samples the mounting system is the same with the only difference of not having the underneath supporting silicon or germanium crystal.

Two types of sample baskets used for different experimental purposes. The first one is the direct heating basket designed by Omicron, by which current passes through the sample in heating processes. This type of basket is used in different experiments, mainly during ion beam bombardment and cleaning of the samples. The second type, which is used in experiments like hydrogenating Ge(001) surface and molecular post- deposition annealing, is the resistive heating basket designed by PREVAC Company. These baskets heat the sample via resistive heating. The two types of sample baskets are shown in figure 2-5.

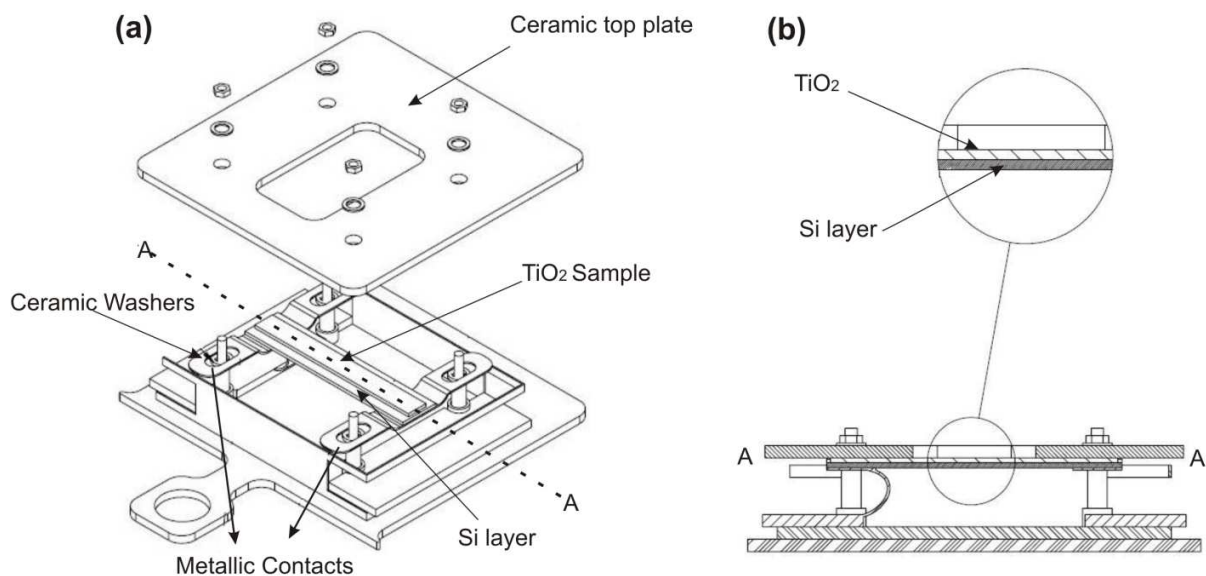


Figure 2-4 (a) Schematic representation of sample mounting, (b) Cross section view along AA line of (a) showing the Ge/Si buffer layer under the TiO₂ crystal. Schemes were made with the help of Piotr Olszowski, the lab. Technician Engineer.

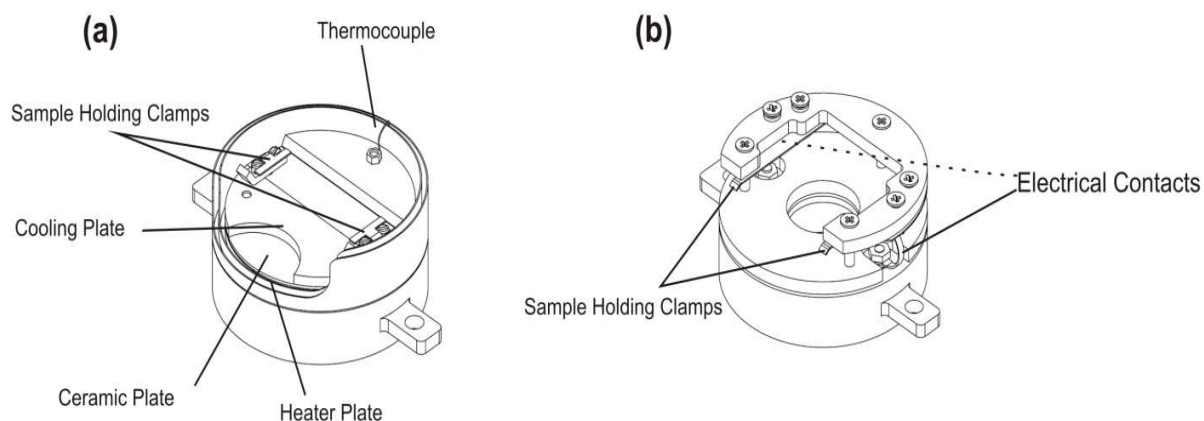


Figure 2-5 (a) The PREVAC Resistive Heating Basket (RH), (b) The OMICRON Direct Heating Basket (DH). Schemes were made with the help of Piotr Olszowski, the lab. Technician Engineer

Atomically flat Ge(001) surfaces were prepared by few cycles of simultaneous annealing of the samples at 780°C and ion beam (Vacuum Generator Ltd, CR38 ion gun) bombardment (1 KeV Ar⁺, at 45° off-normal) for 20 minutes. The ion current density was about 0.3 μA/cm². At the last two cycles the samples were held to cool down slowly at a rate of -0.1A/min to room temperature.

TiO₂ samples were prepared and cleaned also by few successive cycles of ion beam bombardment followed by direct annealing to about 780°C for 20 minutes. Then similarly at the last two cycles the samples were cooled down slowly to the room temperature. The ion beam bombarding parameters were comparable for cleaning both Ge and TiO₂ samples.

Hydrogen passivation of the germanium surfaces was carried out by exposing the surface kept at 210°C (via resistive heating) to 5×10⁻⁷ mbar molecular hydrogen pressure for about 2.5 hours. Hydrogen atoms were provided from the hot tungsten filament of a home built cracker at a distance of about 10cm from the germanium surface.

PTCDA (Sigma Aldrich, 99% purity) molecules were evaporated using the 4-Cell Evaporator (Kentax GmbH). During molecular epitaxy the Ge(001) substrate was kept at room temperature. The deposition process was performed at a rate of ~0.15 Hz/min as calibrated by quartz-crystal microbalance. DBBA molecules (St-Jean Photochemicals Inc.) were evaporated on TiO₂(011) surface using a low temperature effusion cell. The sample was kept either at room temperature or

at elevated temperature (~ 300 °C) depending on the goal of the experiment. The deposition rate was ~ 0.2 Hz/ min.

For the nanoripple formation experiment, the $\text{TiO}_2(110)$ samples were exposed to a 2 keV Ar^+ beam (Leybold-Heraeus ion source) of 1 mm^2 spot size at 75° incidence angle with respect to the surface normal. With $1 \mu\text{A}/\text{cm}^2$ ion current density the ion fluence was set between 10^{15} to 10^{17} ions/ cm^2 . The samples were mounted so that the [001] surface crystallographic direction was either parallel or normal to the direction of the ion beam projection on the surface. The crystalline quality of the sample surfaces were tested by a low energy electron diffraction-meter (LEED) which is installed in the same UHV chamber.

Chapter Three

Publication I:

Temperature-dependent orientation of self-organized nanopatterns
on ion-irradiated TiO₂(110)

Physical Review B 88, 195427(2013)

Temperature-dependent orientation of self-organized nanopatterns on ion-irradiated TiO₂(110)M. Kolmer,¹ A. A. Zebari,¹ M. Goryl,¹ F. Buatier de Mongeot,² F. Zasada,³ W. Piskorz,³ P. Pietrzyk,³ Z. Sojka,³ F. Krok,^{1,*} and M. Szymonski¹¹Research Center for Nanometer-Scale Science and Advanced Materials (NANOSAM), Faculty of Physics, Astronomy and Applied Computer Science, Jagiellonian University, Reymonta 4, 30-059 Krakow, Poland²Dipartimento di Fisica, Università di Genova, Via Dodecaneso 33, 16146 Genova, Italy³Faculty of Chemistry, Jagiellonian University, Ingardena 3, 30-060 Krakow, Poland

(Received 25 June 2013; published 25 November 2013)

Temperature-dependent self-organized formation of nanoripples on TiO₂(110) surfaces irradiated by low-energy Ar⁺ beams has been investigated by scanning tunnelling microscopy in UHV conditions. Under the experimental conditions employed (2 keV Ar⁺ and oblique incidence, 75° off-normal, $T = 120, 300, 620,$ and 720 K) on the irradiated surface the ripple structure of periodicity ~ 10 nm has developed. Interestingly, the orientation of the nanopatterns switches reversibly by 90° with the systematic change of the substrate temperature during irradiation. We have demonstrated that formation of the surface nanomorphology is determined by the interplay between the erosion of the monatomic step edges at grazing incidence, anisotropic surface diffusion along the favoured crystallographic orientation and, at elevated temperatures, the diffusion into the bulk of the excess Ti ions. As indicated by density functional theory (DFT) calculations used for modelling the diffusion processes on the ion irradiated TiO₂(110), the significant surface mass transport required to form the nanoripples is dominated by the highly mobile Ti atoms diffusing in assistance of O adatoms.

DOI: [10.1103/PhysRevB.88.195427](https://doi.org/10.1103/PhysRevB.88.195427)

PACS number(s): 61.80.Jh, 68.35.bg, 68.47.Gh, 89.75.Fb

I. INTRODUCTION

Titanium dioxide (TiO₂) is an attractive material, studied extensively over the last decades, firstly, as a model system for the whole class of metal oxides¹ and, secondly, due to its unique photocatalytic properties.² TiO₂ is widely applied in heterogeneous catalysis including hydrogen production,³ water purification,⁴ and air detoxification.⁵ In view of the controlled modification of the chemical reactivity of patterned surfaces, particularly intriguing are the results which demonstrate that the dissociation probability of simple molecules can be altered over several orders of magnitude recurring to ion beam nanopatterning of metal surfaces,⁶ since it allows to tune the density and orientation of reactive under-coordinated step and kink atoms of metal surfaces. It would be thus desirable to achieve a similar degree of morphological control by a simple self-organized process also for a more complex material like TiO₂, which is of key relevance in photocatalysis and photovoltaics. The photocatalytic performance of a TiO₂ crystal can also be enhanced by decoration of its surface with metal nanoparticles (e.g., Ag, Au, Pt, and Pd).⁷⁻¹² Indeed, the size-dependent shift in the Fermi level of the Au-TiO₂ catalysts proves the ability of gold nanoparticles to influence the energetics by improving the photoinduced charge separation.¹³ Recently, it has been shown that Au adatoms diffuse easily on TiO₂(110) surfaces and nucleate preferentially at the step edges of the substrate.¹⁴ By tailoring the surface morphology of the TiO₂ substrate, especially with respect to the density and orientation of step edges it is thus possible to improve dispersion and stability of the deposited metal particles, and tune the specific electronic properties of titanium oxide supported metal catalysts for enhancement of their photocatalytic performance and durability.

In this respect, ion beam irradiation of surfaces can lead to spontaneous formation of rich variety of nanoscale patterns with the alignment controlled either by the ion beam

parameters, i.e., the ion energy and angle of incidence, or by the crystallographic surface symmetry.¹⁵ Particularly interesting is the process of ripple pattern formation on anisotropic metal single-crystal surfaces, which remain crystalline during ion irradiation under the grazing ion incidence conditions. In this context, the (110) metal surfaces (like Ag, Cu, and Rh) show a 90° switch in the ripple orientation by changing the substrate temperature during ion irradiation.^{16,17} At grazing incidence, the final morphology of the anisotropic surface is in fact determined by the interplay of thermally activated adatom mobility along the main crystallographic directions and enhanced sputtering of the illuminated ascending step edges.¹⁸ Recently, Luttrell *et al.*¹⁹ have indeed demonstrated that also for the TiO₂(110) surfaces a grazing ion incidence irradiation at the elevated sample temperature (670 K) leads to the formation of ripple undulations elongated along the ion beam direction, due to enhanced sputtering of the illuminated ascending steps.

In this paper, high-resolution scanning tunneling microscopy (STM) is used to study temperature dependent evolution of the morphology of the ion-irradiated TiO₂(110) sample. Under these conditions, the complex hierarchy of the intra- and interlayer mass transport processes leads to a striking correspondence with the temperature dependent rotation of the nanoscale ripples previously observed on the fcc(110) metal substrates.²⁰ The result is intriguing since, contrary to common perception, ion beam irradiation of compound substrates like TiO₂(110) at room temperature does not lead to complete amorphization of the near surface layers. The resulting self-organized pattern, at room temperature, is instead aligned in registry with the high symmetry directions of the surface unit cell, implying that surface diffusion of a highly mobile adspecies is responsible for efficient mass transport. With the help of density functional theory (DFT) calculations, we demonstrate that mass transport necessary for surface restructuring is dominated by concerted diffusion of Ti ions in

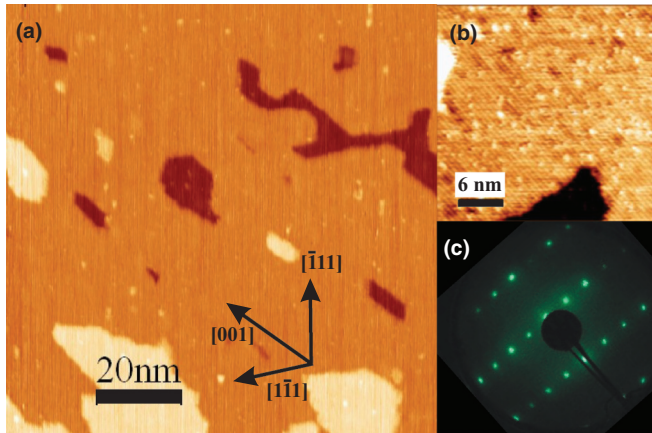


FIG. 1. (Color online) (a) STM image of the freshly prepared, clean, atomically flat $\text{TiO}_2(110)$ surface. (b) The high-resolution STM exhibiting the anisotropic structure of the surface; atomic rows along the $[001]$ crystallographic direction indicating a (1×1) reconstruction with the corresponding (c) LEED pattern ($E = 99$ eV).

assistance of O adatom [Ti(O) species] and not by diffusion of sole Ti adatoms. In this way, the crystalline order is restored on a local scale, leading to the subsequent formation of anisotropic ripples oriented along the high symmetry directions of the substrate.

II. EXPERIMENTAL

The experiments were carried out in an ultrahigh vacuum (UHV) system consisting of three interconnected chambers for sample preparation, analysis, and STM imaging. The $\text{TiO}_2(110)$ (1×1) surfaces were prepared by cycles of Ar^+ sputtering at room temperature (incident angle 60° , ion energy 1 keV) and subsequent annealing at 1050 K for 15 min. The cycles were repeated until a clear low-energy electron diffraction (LEED) pattern was observed. In Fig. 1, the STM topography of pristine $\text{TiO}_2(110)$ - (1×1) surface after such a cleaning procedure is shown. The surface exhibits atomically flat terraces with a lateral extension of tens nm, bounded by monatomic step edges oriented along $[001]$, $[-111]$, and equivalent $[1-11]$, the main crystallographic directions of the sample. The anisotropic structure of the atomically ordered terraces of the pristine surface is revealed by the high-resolution STM image and LEED pattern. The topmost surface layer is composed by protruding oxygen atomic rows, which are oriented along the $[001]$ crystallographic direction and are separated by 0.65 nm.

For the ion-beam induced restructuring, the samples were exposed to a focused beam of 2 keV Ar^+ ions having a spot size of 1 mm^2 . The beam was rastered over the entire surface area. The average ion current density was $1 \mu\text{A}/\text{cm}^2$ and the ion fluence, Φ_{ion} , was changed between 10^{15} and 10^{17} ions/ cm^2 . The incidence angle, α , of the ion beam was set at 75° with respect to the surface normal while the azimuthal orientation, i.e., the angle between the projection of the ion beam and the $[001]$ surface direction, was either 0° or 90° . The resulting surface topographies were imaged at room temperature by an STM microscope (VP2 Park Scientific Instruments) with the $U_{\text{sample}} = 1-2$ V and $I_t = 0.5$ nA.

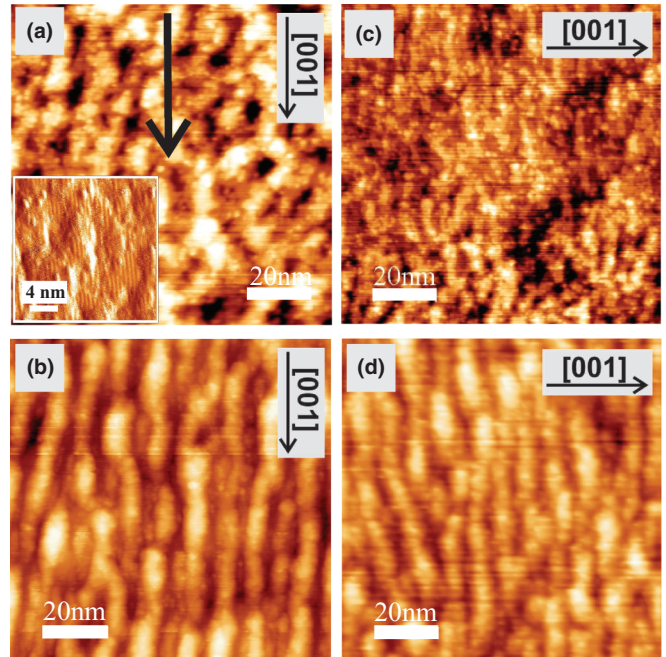


FIG. 2. (Color online) Set of STM images of Ar^+ beam modified $\text{TiO}_2(110)$ surfaces at a constant temperature of 620 K. The beam projection in (a) and (b) is directed along the $[001]$ direction of the surface unit cell, in (c) and (d) orthogonal to it. The ion fluence for (a) and (c) was 3×10^{15} ions/ cm^2 , for (b) it was 4×10^{16} ions/ cm^2 , and for (d) 1×10^{17} ions/ cm^2 ($E = 2$ keV, $\alpha = 75^\circ$). In the insert of (a) the STM current map clearly depicts evidences the local crystallinity of the bombarded surface. The black arrow is the projection of the ion beam on the irradiated surfaces.

III. STM RESULTS

The formation and evolution of ripple morphology as a function of increasing Ar ion fluence was monitored in-situ by STM imaging as shown in Fig. 2. For elevated sample temperature of 620 K (350°C) and fluencies larger than 1×10^{17} ions per cm^2 , a well defined ripple structure with a period of the order of 10 nm develops with the ridges extended along the ion beam projection, independently of the surface unit cell orientation (the atomic rows of the pristine $\text{TiO}_2(110)$ surface reconstruction are oriented along the $[001]$ direction). Another interesting feature of the patterns is that the wavelength saturates at the same value at high ion fluencies, independently on the sample crystallographic direction, indicating that the lateral range of the relaxation processes of the sputter-induced mobile defects is isotropic with respect to the surface unit cell orientation. Therefore, for such high sample temperatures, the dominant role in the pattern formation is played by the beam directed sputtering.

In Figs. 3(a)–3(d), a sequence of ion beam modified $\text{TiO}_2(110)$ topographies obtained for different sample temperatures is presented. For all images, the Ar ion beam of 2 keV energy was striking the sample at an off-normal incidence angle of 75° and perpendicularly to the initial reconstructed atomic rows, i.e., perpendicularly to the $[001]$ direction. The ion fluence was about 9×10^{16} ions/ cm^2 . The development of ripple-like nanostructures after ion irradiation is clearly visible for the whole range of the explored temperatures,

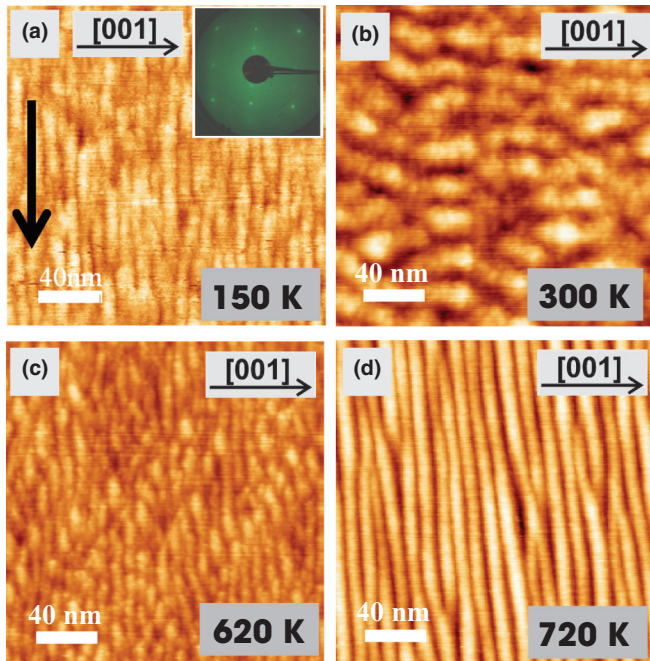


FIG. 3. (Color online) Set of STM images (size $200 \times 200 \text{ nm}^2$) of Ar^+ beam modified $\text{TiO}_2(110)$ topographies at sample temperatures of 150, 300, 620, and 720 K, respectively ($E = 2 \text{ keV}$, $\alpha = 75^\circ$, and $\Phi_{\text{ion}} = 9 \times 10^{16} \text{ ions/cm}^2$). The inset of (a): the corresponding LEED pattern ($E = 99 \text{ eV}$) of the irradiated surface. The black arrow is the projection of the ion beam on the irradiated surfaces.

spanning from 150 to 720 K. The ripple structures are locally crystalline even after irradiation at ion fluence in the range of $10^{16} \text{ ions/cm}^2$, as revealed by the sharp LEED pattern shown in the insert of Fig. 3(a). Surprisingly, the orientation of the nanopatterns presents a nonmonotonic temperature dependence. At elevated temperatures (620 and 720 K) as well as at low temperatures (150 K), the ripples are elongated along the ion beam projection, while at room temperature (RT, 300 K), the ripples change their orientation by 90° and become elongated along the orientation of the reconstructed atomic rows, i.e., perpendicularly to the ion beam direction. Furthermore, it must be stressed that both the periodicity and the morphology of the surface nanopattern formed at RT are distinctly different from those observed at lower as well as at higher sample temperatures.

In Fig. 4, we illustrate pattern formation at room temperature, as a function of the sample azimuth, i.e., when the ions strike the sample either perpendicular or parallel to the initial atomic rows, in analogy to the experiment shown in Fig. 2. In the former case the Ar^+ irradiation led to the formation of surface ripples elongated parallel to the ion beam projection independently from the sample azimuth, and beginning from the lowest ion fluencies.

In more detail, at 300 K during the initial stages of the ion irradiation along [001] [see Fig. 4(a)], small clusters are formed with size in the 5-nm range, which tend to coalesce forming anisotropic mounds (size in the 40-nm range) elongated parallel to [001]. The elongation direction coincides with the ion beam projection, and at the same time it corresponds to the high symmetry direction of the atomic

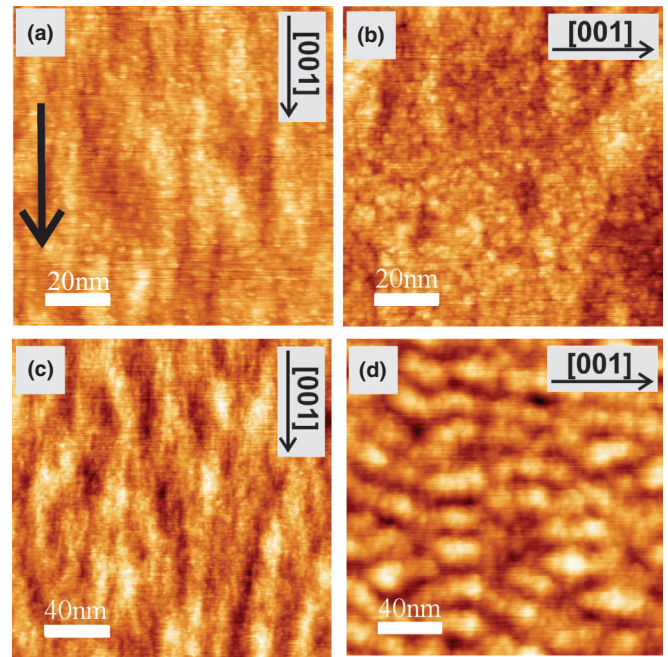


FIG. 4. (Color online) Set of STM images of Ar^+ beam modified $\text{TiO}_2(110)$ topographies at constant sample temperature of 300 K ($E = 2 \text{ keV}$, $\alpha = 75^\circ$, and ion fluence: (a) and (b) $\Phi_{\text{ion}} = 3 \times 10^{15}$, (c) 3×10^{17} , and (d) $0.9 \times 10^{17} \text{ ions/cm}^2$). The “z” scale for (a)–(c) is about 1 nm, whereas for (d) is about 2 nm. The black arrow is the projection of the ion beam on the irradiated surfaces.

row reconstructions along which faster diffusion is expected. When ion irradiation is instead performed orthogonal to the [001] orientation [see Fig. 4(b)], the elongated mounds are not formed, indicating that the erosive action of the ion beam is not responsible for the elongation of the mounds. Upon further increase of the ion fluence by two orders of magnitude, in the case of irradiation along [001], the elongation and the height of the mounds grows [see Fig. 4(c)]. At variance, when irradiation at higher ion fluencies takes place orthogonal to [001], elongated mounds are formed with the ridges rotated by 90° , i.e., perpendicular to the ion beam projection [see Fig. 4(d)]. These observations suggest that the elongation of the mounds is due to anisotropic diffusion along the high symmetry direction of the TiO_2 lattice, rather than to the erosive action of the ion beam.

In order to understand the complex morphological reorganisation which is taking place, several intermingled processes have to be taken into account. Among them the most important are: the effect of grazing ion-beam incidence on crystalline planes, the role of anisotropic surface diffusion of the mobile species produced by ion collisions on the (110) surface, possible change in composition of the multicomponent system due to preferential (nonstoichiometric) ion erosion or bulk diffusion at elevated sample temperatures. Firstly, it is well documented that ion beam irradiation of single-crystal surface under grazing incidence conditions results in ripple formation along the beam direction. Such development of ripples has been reported previously for crystalline metal substrates like $\text{Pt}(111)$,²¹ $\text{Ag}(110)$, and $\text{Cu}(110)$ surfaces,²² while more recently it has also been reported for ionic solids,

i.e., KBr(001)²³ and TiO₂(110) surfaces.²⁴ The formation mechanism leading to such morphology modifications on crystalline materials under grazing incidence is different in comparison to the case of ion incidence at more normal angles. At grazing incidence, the ripple structure results as a consequence of the higher sputtering rates of monatomic ascending step edges in comparison to the flat terraces and to the descending step edges.²⁵ Consequently, oblique irradiation results in the development of an array of grooves oriented parallel to the direction of the ion beam, with spatial periodicity increasing with the ion fluency and ion energy.²⁶ On the other hand, ion impact-induced mobile defects (adatoms, clusters, of adatoms, or vacancies) are produced as a consequence of ion collisions. Thus their subsequent thermally activated diffusion, should play a major role in determining the final surface morphology as suggested by experiments revealing ripple pattern formation on anisotropic metal surfaces both during the ion sputtering as well as in the course of homoepitaxial growth due to the occurrence of kinetic instabilities.^{16,27,28} In the case of multicomponent substrates, characterized by directional covalent bonding, the nature and the energetics of the mobile defects can be by far more complex than in metals, and for this reason molecular modelling is essential to ascertain relative importance of the various diffusion processes. In the following, we are exclusively dealing with the diffusion of adspecies generated by the ion beam thus neglecting the thermally generated species (oxygen or Ti ions) since they become relevant only at relatively high crystal temperatures $T > 1000$ K.²⁹

IV. DFT CALCULATIONS OF ADSPECIES DIFFUSION ON THE TiO₂(110) SURFACE

To rationalize the unusual temperature dependence of orientation of the surface nanopatterns, we performed DFT calculations of possible diffusion energetic barriers and the corresponding hopping frequencies for mobile adspecies (namely, Ti and O adatoms, and vacancies). The considered diffusion pathways on the TiO₂(110) surface are presented in Fig. 5.

The calculations were carried out using the VASP code³⁰ with the PW91 exchange-correlation functional,³¹ a Monkhorst-Pack grid with $3 \times 3 \times 2$ sampling mesh for bulk calculations and $2 \times 2 \times 1$ for slab calculations, as well as the cut-off energy of 380 eV. Such parameterization is well established to describe the surface properties of titania in an adequate way.^{32–36} The electronic structure of the system

was calculated in a self-consistent way (with convergence criterion set to an energy change of 10^{-5} eV), with the only constraint being the total charge neutrality of the supercell. Geometry optimization was performed until the changes in the forces acting upon the ions were smaller than 0.001 eV/Å per atom. Starting surface geometries were obtained by cleaving the solid perpendicularly to the [110] direction, and for the modeled [001] and $[1-11]$ steps were based on the geometries proposed by Luttrell *et al.*¹⁹ The nudged elastic band method (NEB)^{37,38} was used to calculate the structure of each diffusion transition state. In all calculations performed in this paper, for each diffusion pathway six to ten NEB images (including the initial and final ones) were used. However, the evolution of the resultant charge of the diffusing (and any other) adspecies along the transition trajectories was not followed explicitly.

For the transition state and starting (stable) geometries of migrating atoms, the frequency analysis was performed, and the vibrational partition function was calculated.³⁹ The Gibbs free energies were next expressed as the sum of the static DFT electronic energy and the energy of thermal contributions, $G(T) = E^{\text{DFT}} + RT + \text{ZPE} + E^{\text{osc}}(0 \rightarrow T) - T(S^{\text{osc}})$ (where ZPE is a zero-point energy and R is the gas constant). Finally, the diffusion hopping frequencies were calculated within the harmonic transition state theory.

Since it is expected that upon the ion beam irradiation the lighter oxygen atoms are preferentially sputtered,⁴⁰ giving rise to Ti-enriched surface, we first considered surface diffusion of the Ti adatoms alone. Careful inspection of possible accommodation sites of the Ti adatoms indicates that there are two such positions, namely, the “upper hollow” (UH) and the “lower hollow” (LH) position.⁴¹ In the former one, the adsorbed titanium atom is bound to the two adjacent doubly coordinated oxygen [O_(2c)] atoms and a triply coordinated oxygen [O_(3c)] atom, whereas in the latter case it is bound to two O_(3c) atoms and an O_(2c) atom, see Fig. 6. The stabilization energy of the UH sites was found to be -4.95 eV [relative to a free titanium atom in vacuum and a perfect rutile (110) surface], whereas for the lower hollow sites it was equal to -4.10 eV.

The UH-titanium can diffuse toward the closest LH position with the energy barrier of 1.14 eV (this movement is indicated by the arrow **a** in Fig. 6). The Ti adatom in the LH site can either return to the starting UH position or pursuing along the [001] channel hop into another upper hollow site (**a'** in Fig. 6). The LH \rightarrow UH transition exhibits significantly lower barrier of 0.30 eV. Obviously, such alternating hopping of the Ti adatom is responsible for its diffusion along the channel,

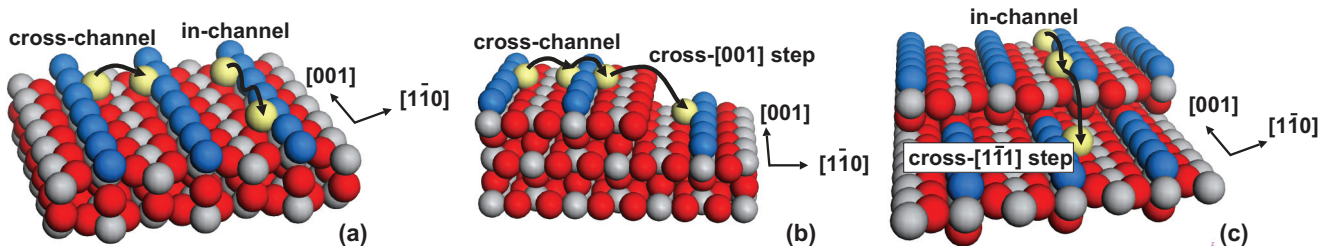


FIG. 5. (Color online) Schematic diagram representing the possible diffusion pathways on the TiO₂(110) surface: (a) intralayer “cross-channel” diffusion (across the atomic rows aligned along the [001] direction) and “in-channel” diffusion (along the [001] direction), (b) interlayer descent diffusion across the [001] step, and (c) interlayer descent diffusion across the $[1-11]$ step.

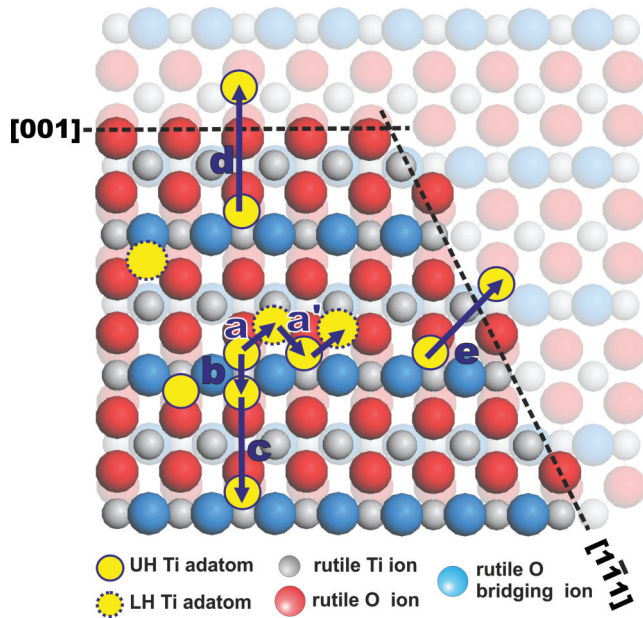


FIG. 6. (Color online) Ti adatom diffusion directions on the 110 terrace of rutile and across the [001] and [1–11] steps. (a) and (a′) “In-channel” diffusion between neighboring UH and LH sites, (c) and (d) steps responsible for “cross-channel” diffusion, (d) cross [001] step diffusion, and (e) cross [1–11] step diffusion.

and the overall energy barrier for this diffusion is determined by the highest value of the **a** and **a′** transition energy (1.14 eV). From the more stable UH position Ti can move towards the UH site located on the other side of the surface oxygen ridge (arrow **b**). Such movement has the barrier of 0.91 eV, and hence is much easier to occur. The Ti species can also diffuse into another upper hollow site located on the adjacent titanium surface row (arrow **c**). This jumping is characterized by rather high energy barrier of 2.79 eV (arising from movement of the itinerant Ti species over the positively charged pair of the surface Ti ions), which is responsible for strong inhibition of diffusion along the “cross-channel” direction. As shown in Fig. 6, crossing of the [001] step (arrow **d**) is quite similar

to the “cross-channel” diffusion. The corresponding barrier is slightly higher (3.25 eV) since Ti has to move above the pair of the less stable edge titanium ions. The last diffusion direction considered by us is crossing of the [1–11] surface step (see arrow **e** in Fig. 6), which again is akin to the already described “in-channel” diffusion sequence.

The calculated energy barriers for surface diffusion of the Ti species along the all conceivable channels (see Table I) reveal that the Ti movement alone cannot explain the considerable mass redistribution required to form the observed ripples. Likewise, the DFT modelling of surface diffusion of the O adatoms and the Ti- and O-vacancies indicated that those defects cannot explain the observed phenomena. Indeed, these calculations revealed that at low temperature (150 K) only the oxygen adatoms are able to diffuse (with the energy barrier of 0.42 eV and the hopping frequency of $2.1 \times 10^{-2} \text{ s}^{-1}$), whereas at high temperature (620 K) diffusion of the Ti adatoms is possible along both the “in-channel” and the “cross [1–11]” directions. Yet, the “cross-channel” and the “cross [001]” diffusion of the Ti species are severely hindered even at 620 K (see Table I).

To account for the efficient mass redistribution required for the formation of the observed nanostructures at moderate temperatures (300 K), participation of more involved surface diffusion pathways was found to be essential. Taking into account high mobility of the surface oxygen species (exhibiting the lowest energy barrier of 0.42 eV), we have evaluated their influence on the Ti diffusion energetics. We found that the surface Ti jumps are strongly facilitated by assistance of oxygen adatoms (displaced to surface sites during sputtering). Such assistance consist in the formation of a transient Ti-O bond in the TS geometry [see Figs. 7(a)–7(d)], which significantly lowers the activation barrier for diffusion comparing to the not-assisted Ti diffusion. This energy lowering stems from the stabilizing interactions between the oxygen and itinerant titanium adatoms. For instance, in the case of the “in-channel” diffusion (arrow **a** in Fig. 7) the resultant one step hopping process is characterized by a significantly lower energy barrier (0.71 eV), than the Ti diffusion alone. Detailed analysis of the transition geometry revealed that the Ti–O transient

TABLE I. Hopping parameters for surface diffusion of Ti and O adatoms, Ti and O vacancies, and Ti(O) species. The “O” symbol in parenthesis indicates the assistance of the O atom. We considered only the hopping frequencies exceeding the assumed threshold value of $1.0 \times 10^{-6} \text{ s}^{-1}$.

	Energy barrier, eV	Hopping frequency, s^{-1}			
		150 K	300 K	620 K	720 K
Ti in-channel	1.14	...	1.9×10^{-4}	5.6×10^4	7.6×10^5
Ti cross[1–11]	1.50	4.6×10^1	1.6×10^3
Ti cross-channel	2.79	4.9×10^{-5}
Ti cross [001]	3.25
O in-channel	0.42	2.1×10^{-2}	7.9×10^4	5.1×10^9	7.9×10^{11}
O-vacancy in-channel	1.24	1.8×10^3	3.1×10^4
Ti-vacancy in-channel	1.2×10^{-2}	1.7×10^0
Ti(O) in-channel	0.71	...	5.0×10^0	1.1×10^7	4.5×10^8
Ti(O) cross [1–11]	0.89	...	4.3×10^{-1}	3.7×10^6	2.9×10^7
Ti(O) cross-channel	2.20	3.4×10^{-3}	2.2×10^0
Ti(O) cross [001]	2.90	2.6×10^{-5}

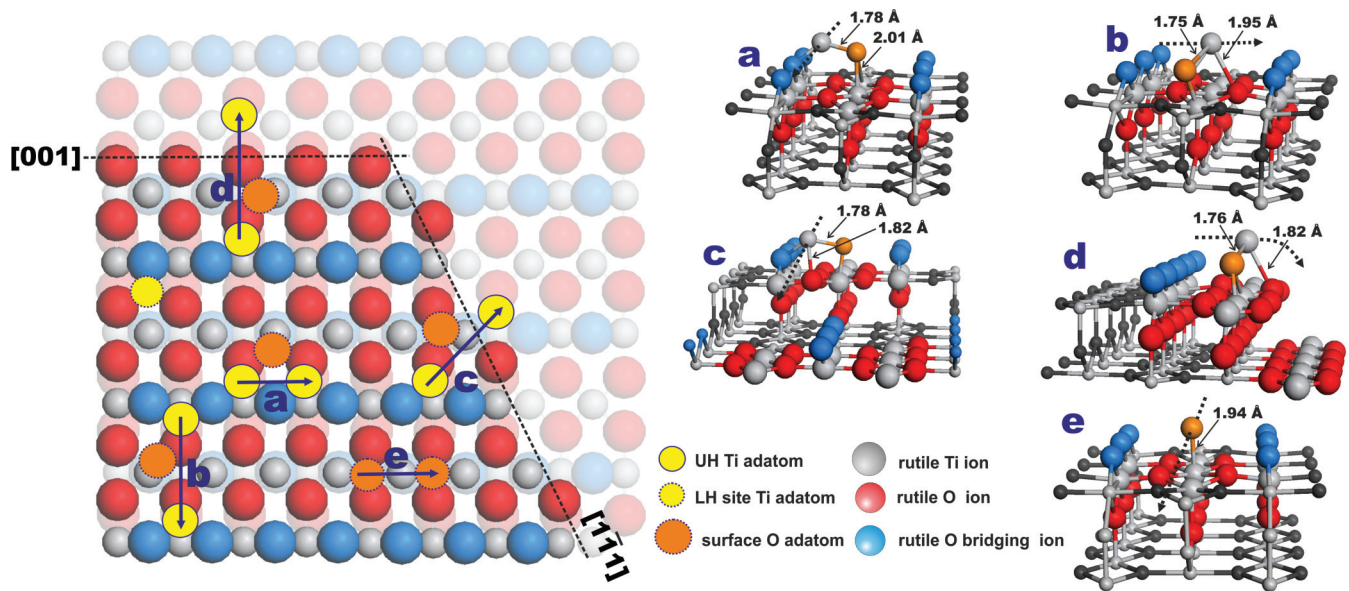


FIG. 7. (Color online) Oxygen assisted Ti adatom diffusion directions on the (110) terrace of rutile. Each arrow on the left panel has its counter pair in the right panel: (a) “in-channel” diffusion, (b) “cross-channel” diffusion, (c) cross [1–11] step diffusion, (d) cross [001] step diffusion, and (e) oxygen “in-channel” diffusion.

bond (1.78 Å) is shorter than the Ti–O distance (1.98 Å) in the starting and the ending positions of the diffusion step. Comparing those values to the Ti–O distance for the gas phase TiO dimer (1.63 and 1.54 Å for neutral and doubly positive species, respectively), we may suppose that the TS geometry can be epitomized by a loose Ti–O pair, labelled hereafter as Ti(O). Clearly, during subsequent hops the itinerant titanium can be assisted by other oxygen adatoms. This scenario holds for other diffusion pathways considered in this paper, and summarized in Fig. 7. The charge neutrality of the produced ripples is assured by association of Ti(O) with mobile oxygen adatoms, which can diffuse on their own. Of course the Ti(O) transient structure is formally net positive (2+) but for diffusion of Ti alone this charge is distinctly higher (4+), which is reflected in the resultant higher energy barriers. On the other hand, diffusion of Ti with assistance of two oxygen atoms (neutral species) being a three body process is statistically much less likely.

Analysis of the data presented in Table I reveals that concerted diffusion of the surface Ti(O) adspecies takes place at 300 K for the “in-channel” and the “cross [1–11]” modes, while it is hindered for the “cross-channel” and the “cross [001]” modes. The DFT calculations confirm that the energy barriers of the oxygen assisted Ti diffusion, Ti(O), are considerably lower and the corresponding hopping frequencies larger, comparing to the corresponding values of the sole Ti adatom hopping. These results strongly support a conjecture that indeed, a facile diffusion of the Ti(O) adspecies can be responsible for the nanoscopic morphology changes observed upon surface irradiation.

V. DISCUSSION

From the relative efficiency and the temperature hierarchy of the chosen in the present work surface diffusion processes,

we inferred that competition between the effects of the grazing incidence and the anisotropy of the different surface diffusion processes could be responsible for the formation and unusual behaviour of the nanopatterns on the TiO₂(110) surface. We can explain our observations as follows. (a) At low temperature ($T = 150$ K), the diffusion processes are inhibited (frozen) and the surface morphology development is dominated by the effect of enhanced erosion of the ascending step edges. This results in the ripple formation along the ion beam direction. (b) For the intermediate temperature ($T = 300$ K), the Ti(O) diffusion along the [001] direction becomes activated, affecting mass transport on a length scale of several tens of nanometers. The interplay of the intralayer (“in-channel”) and the interlayer (cross-[1–11] step) diffusion processes counteracts the effect of grazing incidence. Efficient mass transport of the Ti(O) down the [1–11] step heals the local sputter damage readily, decreasing considerably the effect of enhanced erosion of the illuminated ascending step edges. The competition between the enhanced ion erosion orthogonal to the illuminated [001] steps with the enhanced mass redistribution along the [001] direction results in the development of a rather anisotropic structure, as seen in Fig. 3(b). The interlayer mass transport is well activated in the in-channel direction, while it is still hampered in the cross channel pathway, resulting in a net current of mobile species, which favours their attachment at the lower edge of the [1–11] steps. Under these conditions a kinetic mounding instability can develop, leading to the formation of a periodic pattern, elongated in the fast diffusion direction.²⁷ (c) At $T = 620$ K, there is an increase in the diffusion efficiency (hopping frequency), especially, along the cross-channel direction for both the intralayer and the interlayer processes (see Table I). Moreover, as indicated by the work of Henderson,⁴² at elevated temperatures other mechanisms could be of some importance. For example, the so called “bulk-assisted reoxidation” related with the

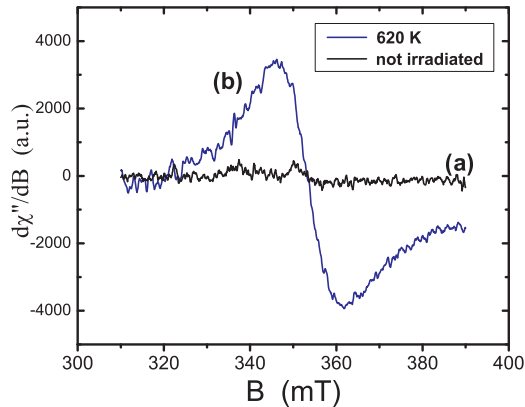


FIG. 8. (Color online) X-band EPR spectra (taken at 77 K) registered (a) on not irradiated TiO_2 and (b) TiO_2 sample irradiated with Ar^+ ion beam at temperature of 620 K. The EPR spectra were recorded with a Bruker ELEXSYS-E500 X-band spectrometer using a rectangular TE102 cavity with 100-kHz field modulation. The microwave power of 1–100 mW and the modulation amplitude of 0.3–1.0 mT were applied.

diffusion of Ti cations/O anions between the ion-reduced surface/subsurface region and the bulk crystal. At temperatures above 700 K, this is an efficient way for the restoration of the surface stoichiometry of the irradiated substrate. Indeed, as implied by our DFT calculations, for the irradiated samples at temperatures above 400 K, there is an appreciable increase of the diffusion of the excess surface Ti^{3+} , produced upon surface oxygen desorption [$2\text{O}^{2-} + 2\text{Ti}^{4+} = \text{O}_{2(\text{g})} + 2\text{Ti}^{3+}$], into the bulk. The presence of the interstitial Ti^{3+} ions in the irradiated samples at 620 K was revealed definitely by an electron paramagnetic resonance (EPR) experiment (see Fig. 8). Ion beam induced O_2 desorption and Ti diffusion into the bulk (with the rate constant of $6.3 \times 10^{-2} \text{ s}^{-1}$), independently contribute to the reduction of the density of diffusing species, thus, hindering the role of surface diffusion in the development of the ripples. They decrease significantly the net up-hill current of the mobile species along both crystallographic surface directions, and quench the kinetic mounding instability. Under these conditions the anisotropy of the pattern formation is no more dominated by the diffusion processes but rather by the enhanced sputtering orthogonal to the [001] steps. Thus the ripple pattern is now oriented along the ion beam direction. (d) Finally, at $T = 720 \text{ K}$, the ripples are very long and well ordered. The excess surface Ti easily diffuse (with the rate constant of $3.8 \times 10^0 \text{ s}^{-1}$) into the bulk, helping to re-establish the stoichiometry of the $\text{TiO}_2(110)$ surface with the well-developed step edges. Consequently, the enhanced erosion of the ascending step edges illuminated by the ion beam results in the development of the ripple structure of very high regularity and orientation along the direction of the ion beam projection.

The proposed scenario of the nanopattern formation on the $\text{TiO}_2(110)$ surface is supported by the observed difference in the wavelength of the different surface nanopatterns as depicted in Fig. 9. It independently reflects the dominant role of either (i) enhanced erosion of the ion-beam illuminated steps (at 150, 620, and 720 K) or (ii) anisotropic surface diffusion (at 300 K), in the nanopatterns formation process. In the former case, the ripple periodicity is controlled by the

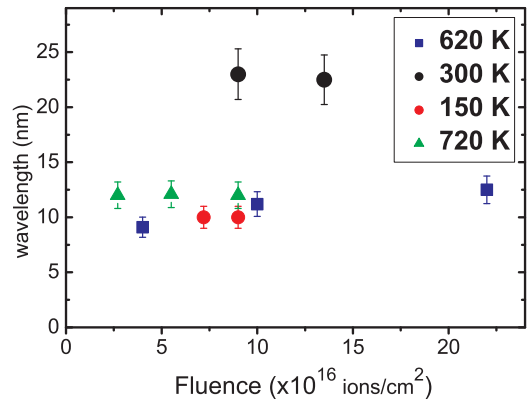


FIG. 9. (Color online) The ion beam fluence dependence of wavelength of the ripples, which developed on $\text{TiO}_2(110)$ surface under the Ar^+ irradiation with the same conditions as in Figs. 3(a)–3(d).

lateral extension of single ion impact collision cascades in the vicinity of the step edges. Furthermore, the coalescence of anisotropic collision cascade parallel to the ion projected momentum gives rise to the formation of extended ripple structures aligned along the direction of the ion beam. The similar wavelength of the ripples which developed at 150, 620, and 720 K parallel to the ion beam direction should not surprise being a reflection of the same athermal microscopic event. The situation is different at 300 K since enhanced anisotropic mass redistribution along the initial atomic rows predominates over erosion of the illuminated steps. The groove structure now develops along the [001] direction, perpendicularly to the ion beam projection, with a higher wavelength which is related to the lateral range of thermally activated diffusion processes.

To independently prove that anisotropic surface diffusion processes are involved in the formation of the anisotropic surface morphology at $T = 300 \text{ K}$, we have performed test experiments in which ion irradiation has been conducted at normal incidence. Figure 10(a) shows the $\text{TiO}_2(110)$ topography developed after irradiation of the surface with Ar^+ ions at 600 eV at normal incidence. Importantly, the surface does not evolve into a randomly rough state but, some topographic anisotropy along the [001] surface direction is

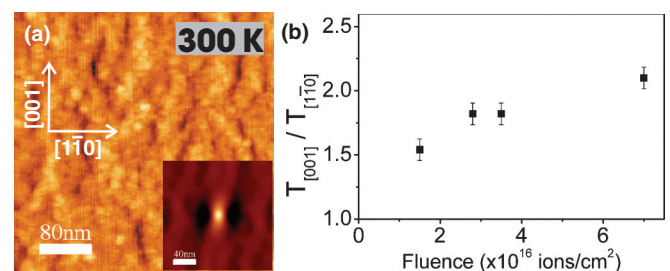


FIG. 10. (Color online) (a) STM topography (size $300 \times 300 \text{ nm}^2$) of $\text{TiO}_2(110)$ after Ar^+ bombardment at normal incidence and sample temperature of 300 K ($E = 600 \text{ eV}$ and $\Phi_{\text{ion}} = 7 \times 10^{16} \text{ ions/cm}^2$). (Inset) The corresponding 2D autocorrelation image. (b) The ratio of the autocorrelation lengths (T) along the [001] and [1–10] crystallographic direction as a function of the total ion beam fluence. The autocorrelation lengths were obtained with the height-height correlation function.⁴³

observed. This is even more clearly exhibited by the increasing ratio of the autocorrelation lengths along the [001] direction of the initial atomic rows and perpendicular to them ([1–10] direction) for increasing ion fluence [see Fig. 10(b)]. The data demonstrate that enhanced anisotropic diffusion along the favoured high symmetry crystallographic orientation takes place even at room temperature on the length scale of the order of 100 nm. This is a direct verification that under the present irradiation conditions, the local surface crystallinity is preserved, in agreement with the observation of Batzill²⁴ on the same system.

VI. CONCLUSIONS

Using STM imaging techniques, we found that nanoscale ripple patterns developed on the TiO₂(110) surfaces under the grazing ion irradiation shows a remarkable temperature-dependent reorientation. At 300 K, the groove pattern is directed perpendicularly to the ion beam direction, whereas at the other investigated temperatures (150, 620, and 720 K), well-developed ripples are aligned along the beam direction. The presented self-organized nanopatterning significantly increases the density of well defined, atomic-scale morpholog-

ical features such as step edges or kinks. This may influence not only the reactivity of TiO₂ but be also beneficial for enhanced stabilization and improved dispersion of metallic clusters on such substrates. Experimental STM, LEED, and EPR observations corroborated by DFT modelling highlight also a unique character of the anisotropic mass transport on the irradiated surfaces affected by titanium diffusion in assistance of oxygen adspecies.

ACKNOWLEDGMENTS

This work was supported by the Polish Ministry of Science and Higher Education (Project No. 777/N-WLOCHY/2010/0). F.K. acknowledges the support by the Polish National Science Centre Program No. DEC-2011/03/B/ST5/01567. F.B. acknowledges partial support from MAE in the framework of Italy-Poland bilateral project and by MSE in the framework of the operating agreement with ENEA for Research on the Electric System. The EPR experiments were carried out with the equipment purchased from the funds of Polish Innovation Economy Operational Program (POIG.02.01.00-12-023/08).

*franciszek.krok@uj.edu.pl

¹U. Diebold, *Surf. Sci. Rep.* **48**, 53 (2003).

²M. A. Henderson, *Surf. Sci. Rep.* **66**, 185 (2011).

³Z. Han, L. Xufan, F. Tongxiang, E. O. Frank, D. Jian, M. S. Erwin, Z. Diand, and G. Qixin, *Adv. Mater.* **22**, 951 (2009).

⁴W. Bahnemann, M. Muneer, and M. M. Haque, *Catal. Today* **124**, 133 (2007).

⁵C. H. Ao and S. C. Lee, *Chem. Eng. Sci.* **60**, 103 (2005).

⁶F. Buatier de Mongeot, A. Toma, A. Molle, S. Lizzit, L. Petaccia, and A. Baraldi, *Phys. Rev. Lett.* **97**, 056103 (2006).

⁷M. Haruta, N. Yamada, T. Kobayashi, and S. Ijima, *J. Catal.* **115**, 301 (1989).

⁸I. Paramasivalm, J. M. Macak, and P. Schmuki, *Electrochem. Commun.* **10**, 71 (2008).

⁹I. Bannat, K. Wessels, T. Oekermann, J. Rathousky, D. Bahnemann, and M. Wark, *Chem. Mater.* **21**, 1645 (2009).

¹⁰J. T. Carneiro, C. C. Yang, J. A. Moma, J. A. Moulijn, and G. Mul, *Catal. Lett.* **129**, 12 (2009).

¹¹M. Mrowetz, A. Villa, L. Prati, and E. Sellì, *Gold Bulletin* **40**, 154 (2007).

¹²R. Su, R. Tiruvalam, Q. He, H. Dimitratos, L. Kesavan, C. Hammond, J. A. Lopez-Sanchez, R. Bechstein, Ch. J. Kiely, G. J. Hutchings, and F. Besenbacher, *ACS Nano* **6**, 6284 (2012).

¹³V. Subramanian, E. E. Wolf, and P. V. Kamat, *J. Am. Chem. Soc.* **126**, 4943 (2004).

¹⁴D. Matthey, J. G. Wang, S. Wendt, J. Matthies, R. Schaub, E. Leagsgaard, B. Hammer, and F. Besenbacher, *Science* **315**, 1692 (2007).

¹⁵W. L. Chan and E. Chason, *J. Appl. Phys.* **101**, 121301 (2007).

¹⁶S. Rusponi, C. Boragno, and U. Valbusa, *Phys. Rev. Lett.* **78**, 2795 (1997).

¹⁷A. Molle, F. B. de Mongeot, A. Molinari, F. Xiaerding, C. Boragno, and U. Valbusa, *Phys. Rev. Lett.* **93**, 256103 (2004).

¹⁸A. Redinger, H. Hansen, U. Linke, Y. Rosandi, H. M. Urbassek, and T. Michely, *Phys. Rev. Lett.* **96**, 106103 (2006).

¹⁹T. Luttrell, W. K. Li, X. Q. Gong, and M. Batzill, *Phys. Rev. Lett.* **102**, 166103 (2009).

²⁰G. Constantini, S. Rusponi, F. Buatier de Mongeot, C. Boragno, and U. Valbusa, *J. Phys.: Condens. Matter* **13**, 5875 (2001).

²¹A. Redinger, Y. Rosandi, H. M. Urbassek, and T. Michely, *Phys. Rev. B* **77**, 195436 (2008).

²²F. Buatier de Mongeot, and U. Valbusa, *J. Phys.: Condens. Matter* **21**, 224022 (2009).

²³F. Krok, S. R. Saeed, Z. Postawa, and M. Szymonski, *Phys. Rev. B* **79**, 235432 (2009).

²⁴T. Luttrell and M. Batzill, *Phys. Rev. B* **82**, 035408 (2010).

²⁵H. Hansen, A. Redinger, S. Messlinger, G. Stoian, Y. Rosandi, H. M. Urbassek, U. Linke, and T. Michely, *Phys. Rev. B* **73**, 235414 (2006).

²⁶S. R. Saeed, O. P. Sinha, F. Krok, and M. Szymonski, *Appl. Surf. Sci.* **255**, 1766 (2008).

²⁷J. Villain, *J. Phys. I (France)* **1**, 19 (1991).

²⁸F. Buatier de Mongeot, G. Costantini, C. Boragno, and U. Valbusa, *Phys. Rev. Lett.* **84**, 2445 (2000).

²⁹K. Szot, M. Rogala, W. Speier, Z. Klusek, A. Besmehn, and R. Waser, *Nanotechnol.* **22**, 254001 (2011).

³⁰J. J. Hafner, *J. Comput. Chem.* **29**, 2046 (2008).

³¹J. P. Perdew and Y. Wang, *Phys. Rev. B* **45**, 13244 (1992).

³²J. R. B. Gomes and J. P. Prates Ramalho, *Phys. Rev. B* **71**, 235421 (2005).

³³W. F. Huang *et al.*, *J. Comput. Chem.* **32**, 1065 (2010).

³⁴Z. Helali, A. Markovits, C. Minot, A. Dhoub, and M. Abderrabba, *Chem. Phys. Lett.* **531**, 90 (2012).

- ³⁵B. Hammer, S. Wendt, and F. Besenbacher, *Top. Catal.* **53**, 423 (2010).
- ³⁶F. Zasada, W. Piskorz, S. Godlewski, J. S. Prauzner-Bechcicki, A. Tekiel, J. Budzioch, P. Cyganik, M. Szymonski, and Z. Sojka, *J. Phys. Chem. C* **115**, 4134 (2011).
- ³⁷G. Henkelman, B. P. Uberuaga, and H. Jónsson, *J. Chem. Phys.* **113**, 9901 (2000).
- ³⁸<http://theory.cm.utexas.edu/vtsttools/>.
- ³⁹W. Piskorz, F. Zasada, P. Stelmachowski, O. Diwald, A. Kotarba, and Z. Sojka, *J. Phys. Chem. C* **115**, 22451 (2011).
- ⁴⁰M. Rogala, Z. Klusek, C. Rodenbacher, R. Waser, and K. Szot, *Appl. Phys. Lett.* **102**, 131604 (2013).
- ⁴¹E. J. Sanville, L. J. Vernon, S. D. Kenny, R. Smith, Y. Moghaddam, C. Browne, and P. Mulheran, *Phys. Rev. B* **80**, 235308 (2009).
- ⁴²M. A. Henderson, *Surf. Sci.* **419**, 174 (1999).
- ⁴³GWYDDION software package, <http://gwyddion.net/>.

Chapter Four

Publication II:

Polymerization of Polyanthrylene on a Titanium Dioxide (011)-(2×1) Surface

Angew. Chem. Int. Ed. 2013, 52, 10300-10303

Polymerization of Polyanthrylene on a Titanium Dioxide (011)-(2 × 1) Surface**

Marek Kolmer, Amir A. Ahmad Zebari, Jakub S. Prauzner-Bechcicki,* Witold Piskorz, Filip Zasada, Szymon Godlewski, Bartosz Such, Zbigniew Sojka, and Marek Szymonski

One of the most challenging promises of nanotechnology is an ultimate level of control in fabrication of nanoscale structures, machines, and devices. Fine positioning of single atoms demonstrated by Eigler and Schweizer,^[1] or precise control over Ullmann reaction on Cu surface reported by Hla and co-workers,^[2] are excellent examples of achievable mastery in the field of scanning tip-induced processes. However, if larger one-dimensional and two-dimensional nanostructures are targeted, the tip-induced methods are not the most favorable: they would require tremendous amount of time for accomplishment. Thus, taking an advantage of self-assembly and thermal triggering is a very encouraging strategy among others in delivering the highest possible precision and efficiency in fabrication of large nanostructures.^[3] It has been envisaged that functionalizing individual molecular precursors (building blocks) with precisely chosen linking sites should allow for future bottom-up construction of miscellaneous molecular devices.^[3d,4] Accordingly, many research groups have recently reported successful direct on-surface formation of covalently bonded molecular structures with use of various thermally triggered chemical reactions on metallic surfaces.^[3b-d,4,5] These reports refer to formation of a wide range of structures, spanning from simple dimers to longer oligomers, or even two-dimensional molecular networks. Yet, to the best of our knowledge, the on-surface fabrication of covalently bonded molecular structures accomplished on semiconducting surfaces has not been reported.

An approach that offers direct formation of complex molecular structures in a predefined form on a desired substrate surface, by itself, is a very attractive idea from a technological point of view. A possibility to merge, in a bottom-up fashion, a substrate possessing chosen bulk and

surface properties (for example, appropriate band gap, catalytic reactivity, and so on) with specifically designed large molecular architectures (for example, networks with pores of uniform size and preferred shape) is a key advantage of the discussed method. Understanding the on-surface processes leading to the formation of such molecular objects will advance many technological branches, such as nano-electronics, gas- and bio-sensing, solar cells, and many others.

Herein, we present the on-surface polymerization on a semiconducting metal oxide surface, namely TiO₂. Molecular precursors 10,10'-dibromo-9,9'-bianthryl (DBBA, see Figure 1 A, commercially available from St-Jean Photochemicals Inc.), are deposited on a (011) face of the rutile titania (Figure 1 C) using a standard Knudsen cell. The polymerization is thermally activated, either through post- or during-deposition annealing. Formation of extended polyanthrylenes

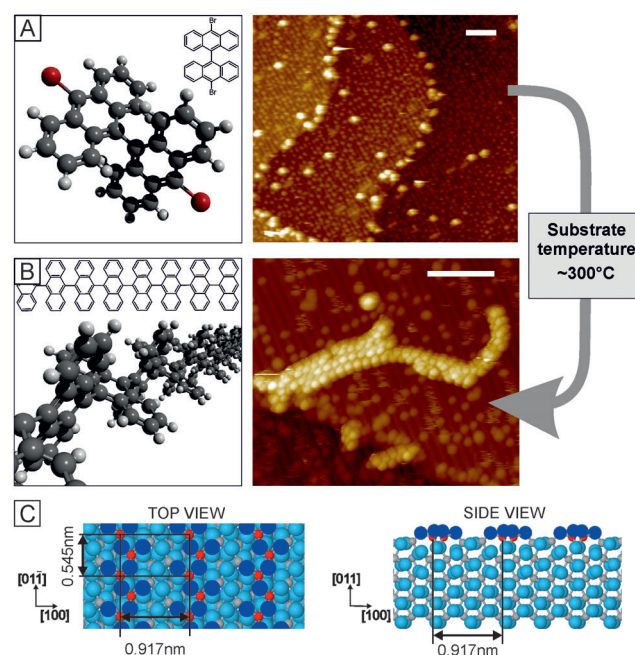


Figure 1. On-surface polymerization of DBBA molecules on a TiO₂ surface. Models and STM images (white scale bars: 5 nm) of A) DBBA monomers and B) polyanthrylenes. STM images: small bright dots on the zigzag rows are ascribed to surface hydroxyl groups.^[9] C) Model of the TiO₂(011)-(2 × 1) surface, top and side views. Oxygen atoms are marked blue (dark blue is reserved for the two-fold coordinated oxygen atoms forming the characteristic double zigzag rows, running along the [01 $\bar{1}$] crystallographic direction of the surface).^[10] Titanium atoms are marked gray; five-fold coordinated titanium atoms are shown in red.

[*] M. Kolmer, A. A. Ahmad Zebari, Dr. J. S. Prauzner-Bechcicki, Dr. S. Godlewski, Dr. B. Such, Prof. M. Szymonski Centre for Nanometer-Scale Science and Advanced Materials, NANOSAM, Faculty of Physics, Astronomy and Applied Computer Science, Jagiellonian University Reymonta 4, 30-059 Krakow (Poland) E-mail: jakub.prauzner-behcicki@uj.edu.pl

Dr. W. Piskorz, Dr. F. Zasada, Prof. Z. Sojka Faculty of Chemistry, Jagiellonian University Ingardena 3, 30-060 Krakow (Poland)

[**] We thank S. Hecht for helpful discussions. A.A.A.Z. and J.S.P.-B. thank A. Polit for technical support. This research was supported by the Polish Ministry of Science and Higher Education under Grant No. NN202 180238. Partial funding for this research has been provided by EC under Large-scale Integrating Project in FET Proactive of the 7th FP entitled "Atomic scale and single molecule logic gate technologies, AtMol".

(see Figure 1B) from DBBA molecules directly on the Au(111) surface has been reported quite recently.^[5b,6]

Oligomer formation requires substantial mobility of the adsorbed precursors. It has been shown for several molecular species studied on the (011) face of rutile that the admolecules are mobile enough to form different 1D or 2D weakly bonded structures,^[7] including formation of non-covalently bonded PTCDA molecular wires.^[8] The interaction of the polyaromatic core of PTCDA with the underlying substrate forces a planar adsorption geometry and does not impede the mobility of the admolecules. Thus, we anticipate rather high mobility of the DBBA molecules on the (011) face of rutile.

As expected, DBBA molecules deposited at low coverage on the substrate kept at room temperature are so mobile that stable scanning tunneling microscopy (STM) imaging conditions at room temperature (RT) are hardly achievable. Imaging at liquid nitrogen temperature (LNT) allows to resolve single molecules distributed on terraces and attached to step-edges (Figure 1A). There is no trace of polymeric species on the surface, suggesting that the deposited precursors still possess their halogen substituents. The polymerization reaction is triggered thermally. We annealed the sample with the molecules at 300 °C. As a result, we observed randomly distributed, short oligomers. Further annealing at the same temperature does not result in formation of more ordered or more extended structures.

Better conditions for efficient polymerization into longer chains were achieved when molecules are deposited on the substrate kept at 270 °C. During deposition we kept a low molecular flux; that is, the temperature of the evaporator was set to 135 °C to assure a submonolayer coverage and disallow a dissociation reaction in the evaporator. Monomers, dimers, and longer oligomers are obtained (Figure 2). Analysis of the STM images reveals an excellent agreement in appearance of the polymer chains between our data and the results reported for the Au(111) substrate.^[5b] Namely, along the chains there are observed protrusions appearing alternately on both sides with a periodicity of 0.86 nm, which is in line with previous observations for the DBBA polymers on the Au(111) surface, and with the periodicity of the bianthryl core,^[5b] 0.86 nm and

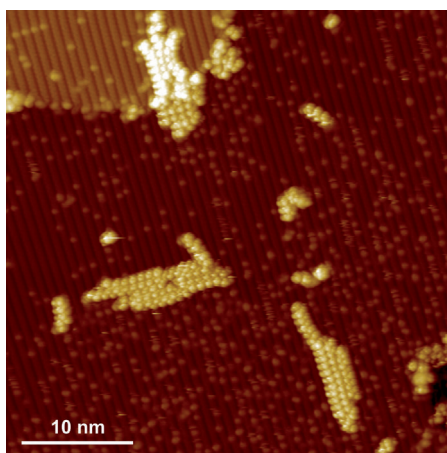


Figure 2. DBBA molecules deposited on the TiO₂(011) surface kept at 270 °C; STM imaging at LNT (10 pA, +2 V). 50 nm × 50 nm.

0.85 nm, respectively (Figure 2). The width of the polyanthrylenes expected from their structural model is about 1 nm, and as it can be inferred by comparison with the substrate periodicity (the distance between the surface reconstruction rows is about 0.92 nm; see the model in Figure 1), it is the value observed in the presented data.

Interestingly, when molecular precursors are deposited at low coverage, longer polyanthrylenes are often observed in bunches rather than as single, long entities (Figure 2, and Figure 3A). As the main building block of the oligomer is the bianthryl core, it is expected that oligomers in a bunch

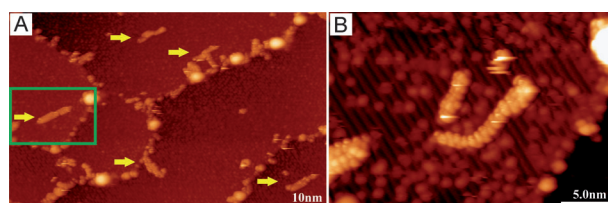


Figure 3. STM images of DBBA oligomers assembled on TiO₂(011) (imaging at LNT, 10 pA, +2 V) (A) 100 nm × 60 nm (scale bar 10 nm), longer oligomers and bunches of oligomers (marked by yellow, horizontal arrows); (B) 25 nm × 17.5 nm (scale bar 5.0 nm), enlargement of the region marked with the green rectangle in (A), showing a disintegrated bunch of polymers as a result of a tip-induced manipulation obtained by 100 pA constant current scanning conditions.

interact through the van der Waals or π -interactions. In line with such conjecture, we observed the bunches with molecular chains mostly laying parallel to each other. The interaction between oligomers is of non-covalent character, and therefore it is much weaker than the coupling that connects bianthryl monomers. Applying a tip-induced manipulation allows the oligomers to be disintegrated from a bunch, as demonstrated by two subsequent STM scans (Figure 3). As predicted for oligomers, the polyanthrylene chains survive such harsh scanning conditions, in contrast to the bunches of chains. Our result is similar to that reported by Grill et al.^[3d] In their work, porphyrin dimers were obtained by deposition of porphyrin molecules with a single Br substituent on the Au(111) surface and subsequent annealing. The heating triggered the C–Br bond cleavage, diffusion of the organic fragments, and their recombination into dimers. Eventually, the resulting porphyrin dimers were found to form clusters. Intact dimers can be easily separated from these clusters by the lateral manipulation with the STM tip. In this way, it is demonstrated that two porphyrin molecules in the dimer are bonded by a strong covalent bond in comparison to rather weak non-covalent bonds binding the clusters.^[3d]

As reported by Cai et al.,^[5b] further annealing of the polyanthrylene chains on the Au(111) surface to 400 °C leads to a cyclodehydrogenation reaction and formation of a fully aromatic system, that is, graphene nanoribbons. To test if such a reaction is feasible on the surface of titanium dioxide we decided to anneal the sample covered with oligomers. To promote formation of longer oligomers, we increased the coverage (three times longer deposition) and substrate

temperature during the deposition to 350 °C. The resulting unordered network of long molecular chains is so stable that it was possible to achieve good imaging conditions in RT STM (not shown). After further annealing of the sample at 400 °C and 450 °C (for 30 minutes at each temperature), the molecular network remained practically intact. It is concluded that up to 450 °C the cyclodehydrogenation reaction is not initialized on the TiO₂(011)-(2 × 1) surface. Additionally, it is evident that the obtained polyanthrylenes are quite robust to thermal treatment. The question whether the cyclodehydrogenation reaction leading to planarization and thus to formation of graphene nanoribbons could be thermally triggered at higher temperatures on the TiO₂(011) surface remains unanswered, and is subjected for further, on-going research.

Our experimental findings are corroborated with density functional theory (DFT) modeling of the DBBA monomer and dimer adsorbed on the TiO₂(011)-(2 × 1) surface. We used the Vienna ab initio simulations package (VASP).^[11] For reliable description of the electronic structure of rutile titanium dioxide we employed projector augmented plane wave (PAW)^[12] method for description of the electron-ion interactions, and PW91 GGA exchange-correlation functional, as parameterized by Perdew and Wang.^[13] Additionally, to account for dispersion forces that play important role in the adsorption of polycyclic molecules on the surface of rutile,^[14] we used the semi-empirical Grimme extension^[15] of the DFT method (DFT-D). The GGA/DFT-D calculations revealed a weak adsorption energy (0.11 eV per molecule) of DBBA that is dominated by the dispersion term (0.08 eV per molecule). It results from the molecule–substrate attractive interactions (−1.09 eV) counterbalanced by the ad molecule deformation (+0.98 eV). Owing to the presence of the bianthryl core in the DBBA molecule (see Figure 1), the adsorption geometry is governed by tendency to keep each anthryl as parallel to the substrate as possible. In contrast, the short C–C bond, connecting the anthryl moieties in the bianthryl core, does not let the molecule to arrive at flat geometry. Consequently, although the adsorbed molecule preserves its 90° dihedral angle between the anthryl planes, one of them is significantly deformed owing to the interaction with the protruding surface ions, thereby partly losing its aromatic character. As a result, the C–Br bond in the adsorbed DBBA is elongated ($\Delta d_{\text{C-Br}} = 0.09 \text{ \AA}$) and weakened ($\Delta BO(\text{Mayer}) = -0.16$). In the optimized geometry, the hydrogen atoms closest to the surface are 1.8 Å above the topmost ions of the substrate; additionally, the bromine atoms are 4.95 Å above the topmost ions. These results strongly suggest that no chemical interaction is expected between the molecule and the substrate. Translations along and across the zigzag rows, and rotation with respect to the surface normal, change the adsorption energy only by 2–5%. Such observations are in line with the fact that the direction-independent dispersion forces dominate the surface–molecule interactions and suggest that the monomers should be able to diffuse on the surface. Applying the same calculation for a dimer adsorbed on the (011) face gives coherent result: the dimer adsorption energy is nearly twice the monomer, namely 0.21 eV per molecule. Finally, simulations of STM images

were performed as topographs of the constant local density of states within the Tersoff–Hamann theory^[16] with additional Gaussian blurring to include tip broadening effects. As can be seen in Figure 4, there is an excellent agreement between the calculated and the measured images.

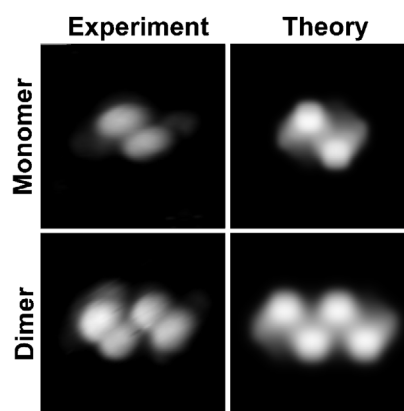


Figure 4. Comparison between experimental and theoretical STM images of DBBA monomer and dimer. Left column: in the experimental images the contrast is set to expose the molecules. The right panel: simulated images with Gaussian blurring mimicking the tip broadening of experimental images. (Both experiment and theory: 3 nm × 3 nm, 2 pA, +2 V).

For metallic surfaces and molecular precursors containing halogen atoms at linking sites, the on-surface polymerization reaction has been described as a two-step process:^[3d] 1) selective thermal C–X (X = I, Br) bond cleavage, resulting in radical/ion formation, followed by 2) radical/ion recombination, resulting in formation of oligomers. At increased substrate temperatures, there are several processes that could take place simultaneously and compete with each other, that is, cleavage of the C–X bond, diffusion of molecular precursors and radicals/ions, recombination of the radicals/ions, and desorption of smaller molecular species. Proper balance between these processes results in formation of long oligomers.^[5f]

Replacing the metal surface with titanium dioxide changes the reaction environment drastically, and thus it is rather unlikely that the on-surface polymerization will necessarily follow the same pathway. In the case of titanium dioxide surfaces, the most important issue is their distinct chemical nature and the related properties. Among several possible routes of C–C bond formation explored by DFT screening, a concerted process of early C–C bond formation accompanied by late C–Br bond cleavage and a multistep proton assisted coupling exhibited the lowest activation barriers (below 1.95 eV). The latter, being energetically most preferred and specific for oxides, is featured by proton transfer from surface hydroxyl groups to DBBA ad molecules (1.39 eV), the rather easy migration of this species on the aromatic framework (0.65–1.13 eV), and preferred attachment to the Br-bearing carbon atom. The resultant rehybridization and substantial weakening of the C–Br bond facilitates the carbon–carbon bond formation and release of Br₂ byproduct, which only requires 0.82 eV. Certainly, an exact

mechanism of oligomer formation on the titanium dioxide surface is definitely not resolved yet. Reaction details of the proposed scenario and analysis of other possible variants are the subject of on-going research.

In conclusion, we have demonstrated the feasibility of thermally triggered, on-surface polymerization on the TiO₂-(011)-(2 × 1) surface. Experimental observations were corroborated by DFT calculations and simulation of the STM images. In a broader context, the method of covalent assembly of organic building blocks on surfaces is shown to be applicable for semiconducting, photonic, or photocatalytic materials. It is expected that the reaction mechanism of DBBA polymerization on metal oxide surfaces is different from that reported for metals. Regardless of the differences in the pathways leading to covalently bonded molecular nanostructures, the discussed thermally driven on-surface polymerization appears as more universal and very promising method for constructing miscellaneous molecular devices on substrates with a suitable band gap.

Received: April 29, 2013

Revised: July 5, 2013

Published online: August 12, 2013

Keywords: nanotechnology · polymerization · rutile titanium dioxide · scanning probe microscopy · surface chemistry

-
- [1] D. M. Eigler, E. K. Schweizer, *Nature* **1990**, *344*, 524.
 [2] S. W. Hla, L. Bartels, G. Meyer, K. H. Rieder, *Phys. Rev. Lett.* **2000**, *85*, 2777.
 [3] a) S. L. Tait, *ACS Nano* **2008**, *2*, 617; b) G. Franc, A. Gourdon, *Phys. Chem. Chem. Phys.* **2011**, *13*, 14283; c) A. Gourdon, *Angew. Chem.* **2008**, *120*, 7056; *Angew. Chem. Int. Ed.* **2008**, *47*, 6950; d) L. Grill, M. Dyer, L. Lafferentz, M. Persson, M. V. Peters, S. Hecht, *Nat. Nanotechnol.* **2007**, *2*, 687.
 [4] L. Lafferentz, V. Eberhardt, C. Dri, C. Africh, G. Comelli, F. Esch, S. Hecht, L. Grill, *Nat. Chem.* **2012**, *4*, 215.
 [5] a) L. Lafferentz, F. Ample, H. Yu, S. Hecht, C. Joachim, L. Grill, *Science* **2009**, *323*, 1193; b) J. Cai, P. Ruffieux, R. Jaafar, M. Bieri, T. Braun, S. Blankenburg, M. Muoth, A. P. Seitsonen, M. Saleh, X. Feng, K. Muellen, R. Fasel, *Nature* **2010**, *466*, 470; c) R. Gutzler, H. Walch, G. Eder, S. Kloft, W. M. Heckl, M. Lackinger, *Chem. Commun.* **2009**, 4456; d) J. A. Lipton-Duffin, O. Ivasenko, D. F. Perepichka, F. Rosei, *Small* **2009**, *5*, 592; e) M. In't Veld, P. Iavicoli, S. Haq, D. B. Amabilino, R. Raval, *Chem. Commun.* **2008**, 1536; f) M. Bieri, M.-T. Nguyen, O. Groening, J. Cai, M. Treier, K. Ait-Mansour, P. Ruffieux, C. A. Pignedoli, D. Passerone, M. Kastler, K. Muellen, R. Fasel, *J. Am. Chem. Soc.* **2010**, *132*, 16669; g) M. Treier, N. V. Richardson, R. Fasel, *J. Am. Chem. Soc.* **2008**, *130*, 14054; h) N. A. A. Zwaneveld, R. Pawlak, M. Abel, D. Catalin, D. Gigmes, D. Bertin, L. Porte, *J. Am. Chem. Soc.* **2008**, *130*, 6678; i) S. Boz, M. Stohr, U. Soydaner, M. Mayor, *Angew. Chem.* **2009**, *121*, 3225; *Angew. Chem. Int. Ed.* **2009**, *48*, 3179.
 [6] M. Koch, F. Ample, C. Joachim, L. Grill, *Nat. Nanotechnol.* **2012**, *7*, 713.
 [7] a) S. Godlewski, A. Tekiel, J. S. Prauzner-Bechcicki, J. Budzioch, A. Gourdon, M. Szymonski, *J. Chem. Phys.* **2011**, *134*, 224701; b) S. Godlewski, J. S. Prauzner-Bechcicki, J. Budzioch, L. Walczak, I. G. Stara, I. Stary, P. Sehnal, M. Szymonski, *Surf. Sci.* **2012**, *606*, 1600.
 [8] A. Tekiel, S. Godlewski, J. Budzioch, M. Szymonski, *Nanotechnology* **2008**, *19*, 495304.
 [9] J. G. Tao, Q. Cuan, X. Q. Gong, M. Batzill, *J. Phys. Chem. C* **2012**, *116*, 20438.
 [10] a) X. Q. Gong, N. Khorshidi, A. Stierle, V. Vonk, C. Ellinger, H. Dosch, H. Z. Cheng, A. Selloni, Y. B. He, O. Dulub, U. Diebold, *Surf. Sci.* **2009**, *603*, 138; b) X. Torrelles, G. Cabailh, R. Lindsay, O. Bikondoa, J. Roy, J. Zegenhagen, G. Teobaldi, W. A. Hofer, G. Thornton, *Phys. Rev. Lett.* **2008**, *101*, 185501.
 [11] J. Hafner, *J. Comput. Chem.* **2008**, *29*, 2044.
 [12] a) P. E. Blöchl, *Phys. Rev. B* **1994**, *50*, 17953; b) G. Kresse, D. Joubert, *Phys. Rev. B* **1999**, *59*, 1758.
 [13] J. P. Perdew, Y. Wang, *Phys. Rev. B* **1992**, *45*, 13244.
 [14] S. Godlewski, A. Tekiel, W. Piskorz, F. Zasada, J. S. Prauzner-Bechcicki, Z. Sojka, M. Szymonski, *ACS Nano* **2012**, *6*, 8536.
 [15] a) S. Grimme, *J. Comput. Chem.* **2006**, *27*, 1787; b) S. Grimme, *J. Comput. Chem.* **2004**, *25*, 1463.
 [16] J. Tersoff, D. R. Hamann, *Phys. Rev. B* **1985**, *31*, 805.
-

Chapter Five

Publication III:

STM tip-assisted engineering of molecular nano-structures:
PTCDA islands on Ge(001):H surfaces

Beilstein J. Nanotechnol. 2013, 4, 927-932.

STM tip-assisted engineering of molecular nanostructures: PTCDA islands on Ge(001):H surfaces

Amir A. Ahmad Zebari, Marek Kolmer and Jakub S. Prauzner-Bechcicki*

Full Research Paper

Open Access

Address:

Research Centre for Nanometer-scale Science and Advanced Materials (NANOSAM), Institute of Physics, Jagiellonian University, Reymonta 4, 30-059 Krakow, Poland

Email:

Jakub S. Prauzner-Bechcicki* - jakub.prauzner-behcicki@uj.edu.pl

* Corresponding author

Keywords:

molecular nanostructures; scanning tunneling microscopy; tip-induced processes

Beilstein J. Nanotechnol. **2013**, *4*, 927–932.

doi:10.3762/bjnano.4.104

Received: 10 October 2013

Accepted: 10 December 2013

Published: 18 December 2013

This article is part of the Thematic Series "Advanced atomic force microscopy techniques II".

Guest Editors: T. Glatzel and T. Schimmel

© 2013 Ahmad Zebari et al; licensee Beilstein-Institut.

License and terms: see end of document.

Abstract

Islands composed of perylene-3,4,9,10-tetracarboxylic dianhydride (PTCDA) molecules are grown on a hydrogen passivated Ge(001):H surface. The islands are studied with room temperature scanning tunneling microscopy and spectroscopy. The spontaneous and tip-induced formation of the top-most layer of the island is presented. Assistance of the scanning probe seems to be one of the factors that facilitate and speed the process of formation of the top-most layer.

Introduction

On-surface engineering of molecular nanostructures is one of the key elements for many forthcoming technologies. A wide range of possibilities is explored to search for an efficient, precise and cheap strategy for the fabrication of various organic nanostructures. Recently, there has been an increasing interest in the field of molecular self-assembly-based processes as a means of organic nanostructure formation [1-3]. As such, self-assembly allows for obtaining nanowires, two dimensional lattices, molecular islands, and molecular mono- and multi-layers with a high yield. The resulting structures are often stable and almost perfect. The implementation of bottom-up self-assembly-based methods in an industrial process may require, however, the reshaping and tailoring of the structure with

precise top-down methods to obtain the desired shape and properties. Scanning tip induced processes may serve as such a step to adjust the final form of the molecular nanostructure.

The design and formation of a molecular device is a key element of its successful operation. However, the desired properties of the device may be severely hampered by its environment, e.g., dangling bonds of a semiconducting substrate surface or electrical contact with a metallic substrate. There have been developed several strategies to minimize or even eliminate the influence of the underlying substrate on a molecular nanostructure on-top of it [4]. From an industrial perspective, a very promising approach is to cover the chosen substrate

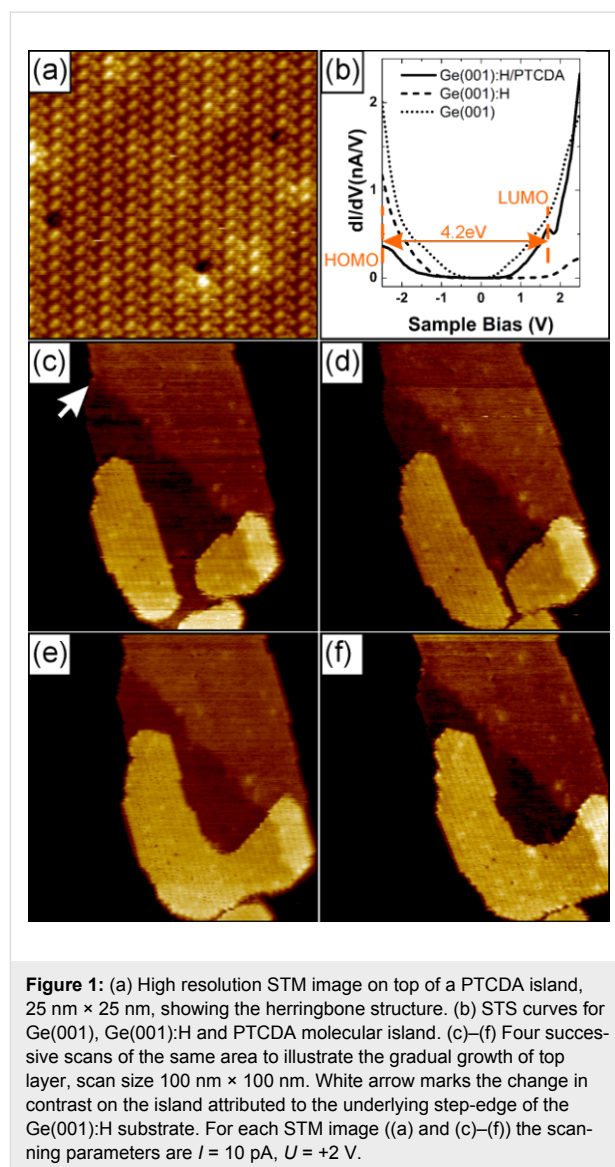
by an additional ultra-thin buffer layer, i.e., either a few monolayers of an insulator (e.g., NaCl on metal surfaces [5-13] or KBr on InSb [14,15]) or even a single layer of an atomic or molecular species (e.g., passivation of Si or Ge surfaces [16-19]). Such an extremely thin interlayer not only electronically decouples on-top adsorbed molecular species, but additionally may dramatically enhance the mobility of the molecules and increase their chances to self-assemble and form molecular nanocrystals [9-11,20]. For the purpose of the present study it is very convenient to focus on the hydrogen passivation of Si and Ge surfaces. It has been shown in case of Si(001) [17], Si(111) [18] and Ge(001) [19] surfaces that such a passivating layer electronically decouples the molecule from the substrate and increases their mobility.

In this article, high-resolution scanning tunneling microscope (STM) measurements of self-assembled perylene-3,4,9,10-tetracarboxylic dianhydride (PTCDA) molecular islands on a hydrogen passivated germanium surface, Ge(001):H, are presented. The application of bias voltage pulses in STM allows for the modification of the islands. We found that the presence of a scanning tip of the tunneling microscope facilitates and speeds the formation of a new full top-layer of the island.

Results and Discussion

Due to the presence of a passivating hydrogen layer on the Ge(001) surface, molecule–substrate interactions are significantly weakened and molecules are extremely mobile. The imaging of a single molecule at room temperature is impossible. At the high coverage, however, the accumulation of the PTCDA molecules is dominated by molecule–molecule interactions and molecular islands are formed. The islands grow in the Volmer–Weber mode. The density of the islands is $2.5 \times 10^9 \text{ cm}^{-2}$ for coverage of 0.7 ML. Approximately 60% of the islands exhibit a strip-like hexagonal shape with two long edges and four short ones. It is noteworthy that molecular islands quite often extend in one direction over 100 nm and more, traversing several substrate terraces without any influence to their structure. It is possible to achieve high-resolution images on top of the islands in rt STM (see Figure 1a). These images show that the islands have crystalline character, and the top-most layer closely resembles the herringbone structure found for the (102) plane of PTCDA bulk crystal [21,22]. Similar arrangements have been reported for the Si(001):H/PTCDA system [20]. Most of the islands have a height of 2.1 nm, what corresponds to 6 molecular layers.

Insight into the electronic structure of the studied system is obtained by rt STS measurements (see Figure 1b). For a bare germanium surface a band gap of $\approx 0.2 \text{ eV}$ is obtained, in fair agreement with literature data [23-25]. A hydrogen passivated



surface exhibit a band gap of $\approx 0.85 \text{ eV}$, similarly to a recently reported value obtained from low temperature measurements [25]. The energy gap between the highest occupied molecular orbital (HOMO) and the lowest unoccupied molecular orbital (LUMO) of a PTCDA island on Ge(001):H is measured as 4.2 eV. The latter value corresponds well with results reported for thick films ($>5 \text{ nm}$) [26-29]. The electronic properties of the PTCDA islands are very different from the underlying passivated germanium, and there are no other features in the bias window from -2.5 V to 1.7 V (corresponding to the semiconducting energy gap of PTCDA molecules) of the STS curves. This means that the electronic structure of PTCDA is unperturbed by the electronic properties of the underlying substrate.

Figure 1c–f show a set of four consecutive scans of the same area on top of the PTCDA island. The change of the contrast in

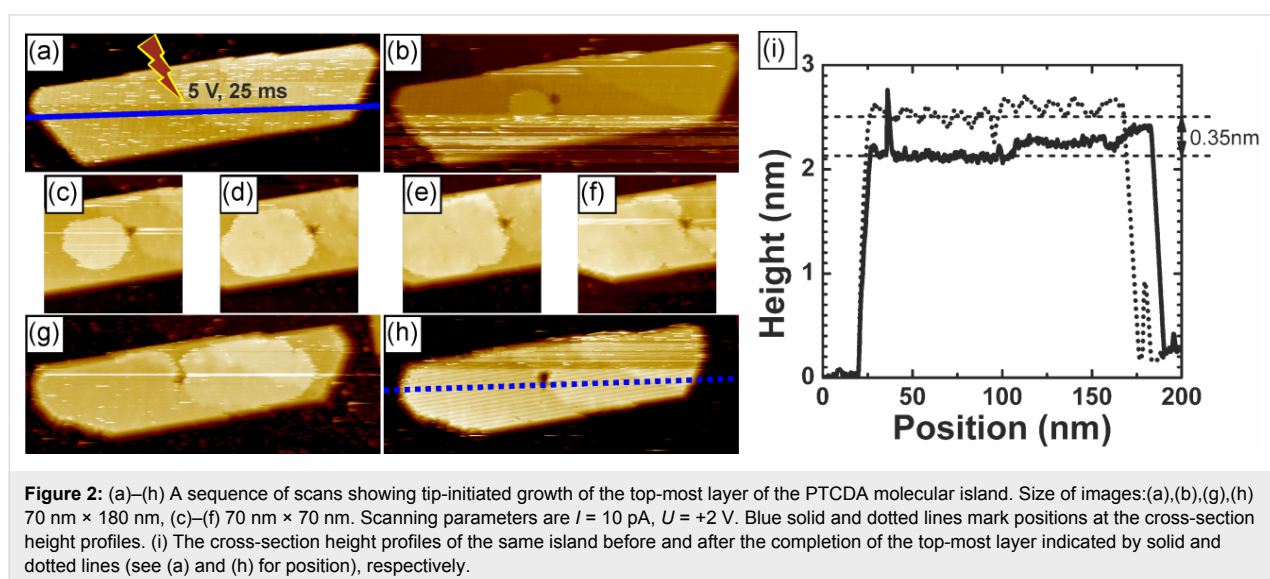
the middle of each of the scans (see white arrow in Figure 1c) originates from the step-edge of the underlying Ge(001):H surface. It may serve as a reference point for the observed evolution of the top-most layer. Every scan took 9 minutes (taking one image from the top to the bottom includes forward and backward scans). In the first scan from the set (Figure 1c) one can see that the starting structure of the top-most layer of the molecular island was composed of separate features, each of which has a height of one monolayer. On a subsequent scan (Figure 1d) one can observe a gradual growth of these features, eventually leading to their coalescence into one object (Figure 1e) that continues to gradually grow (Figure 1f). Typically, the morphology of PTCDA islands are stable during a STM/STS characterization. We assume that the presented evolution of the top-most molecular layer was probably unintentionally induced during a “cleaning” procedure of the scanning probe, i.e., by application of high voltage pulses.

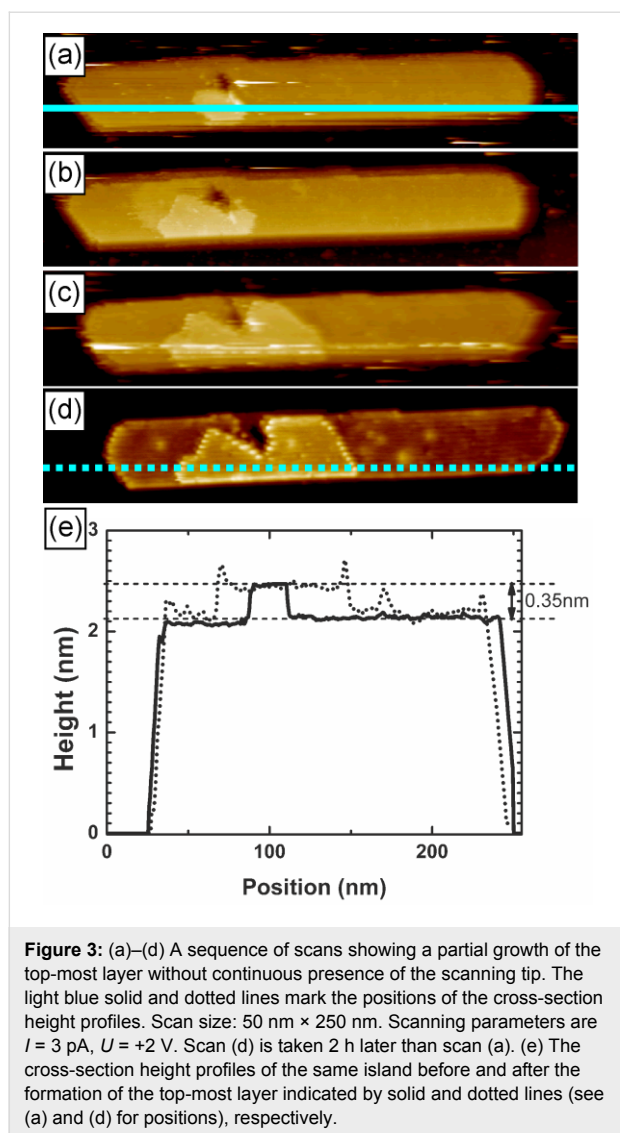
To investigate the initiation of growth of the top-most layer of an island by well-defined conditions we applied a bias voltage pulse of 5 V for 25 ms in the middle of the island (Figure 2a). As a consequence we observed a hole at the position of the pulse, and ad-molecules gathered around (Figure 2b). Consecutive scans (Figure 2c–h) show a gradual growth of the top-most layer. In the course of time a new full top layer is formed with the pulse-made hole remaining unhealed. The speed of the growth of the top-most layer is approximately $124 \text{ nm}^2/\text{min}$.

The edges of the hole play the role of nucleation sites for the created layer. Energy barriers at the rim of the hole, i.e., Ehrlich–Schwoebel barriers, are too high to be crossed by diffusing molecules at rt, even in the presence of the field created by the scanning tip, and the molecules prefer to diffuse

laterally within the same layer instead of moving downward to fill in the hole [30]. The height of the island changes by 0.35 nm, as can be inferred from a comparison of the cross-section profiles of the island before and after the top-most layer was formed (Figure 2i). The observed change in the height corresponds well to the distance between molecular planes in the [102] direction of the PTCDA bulk molecular crystal [20]. The edges of lower laying molecular sheets are a plausible source of molecules for the newly formed top-most layer. The edges observed on the scans are quite often fuzzy and change their shape during the manipulation (Figure 2). Moreover, after the adlayer formation the island considerably decreased its lateral dimension (Figure 2i).

In both discussed examples the island was continuously scanned during formation of the top-most layer. To shed some light on the role of the scanning tip in the process we performed a follow-up experiment. We applied a bias voltage pulse on top of an island (7 V, 25 ms). In Figure 3a we present the image of the island immediately after the pulse. Then, we retracted the tip for 10 minutes. After that time only a small increase in the size of the newly formed top-most layer was observed (Figure 3b). Thereafter, we retracted the tip again, this time for 20 minutes. Similarly, only a slight change in the size of the new adlayer was recorded (Figure 3c). We decided to retract the tip once more, for 30 minutes. And again, a minor change in the size was observed. In Figure 3d we present the image of the top-most layer of the island 130 minutes after the pulse. The total time elapsed from the pulse includes 60 min when tip was retracted and 70 min spent on scanning. From the inspection of the cross-section height profiles in Figure 3e it is clear that there was only a single-layer-height structure formed on the top of the island that did not exceed over the whole island. The overall





average speed of growth of the observed structure in this case is approximately $13 \text{ nm}^2/\text{min}$.

Most probably, the three dimensional mesa-like shape of the PTCDA crystalline nanoislands grown on Ge(001):H surface results from an efficient ascending interlayer transport. The configuration of molecules in a layer is determined, to some extent, by strain in the layer. Roughly speaking, the less strained a layer is the more relaxed molecules are in it. Yet, the amount of stress encountered by the molecules in the layer depends on the distance from the island–substrate interface. Thus, the further away from the interface the layer is, the less strain it experiences [31]. Consequently, binding energies on the edges of lower lying layers are smaller than binding energies on the edges of higher lying layers. Therefore, molecules attached to the edges of lower lying layers prefer to ascend and attach to more favorable sites on higher lying layers. Due to the applied

bias voltage pulses we created new edges on the top-most layer offering convenient adsorption sites with high binding energies. Thus, we expect that an ascending interlayer transport is responsible for the newly grown top-most layer. The presence of the scanning tip seems to enhance that kind of process. Most probably, the presence of the electric field generated by a biased STM probe efficiently decreases the corresponding energy barriers for an ascending interlayer molecular transport. Hence, a continuous scanning of the island after pulsing allows for formation of the top-most layer roughly one order of magnitude faster than has been observed for intermittent scanning (compare results presented in Figure 2 and Figure 3). We would like to stress that this result is of qualitative character only, as many different parameters (e.g., tip composition/geometry, current set-point, bias voltages, sample temperature, etc.) may play a role in setting the final growth rate.

It is rather expected that in our experiment the scanning probe is coated with molecular material. One could then argue that the direct deposition from the tip should also significantly contribute to the observed growth of the top-most layer. However, if such a mechanism was the main source of the material it would usually lead to unstable imaging conditions. On the contrary, we observe growth of the top-most layer without disturbances typically associated with scanning tip modifications. Additionally, the direct deposition from the tip would not necessarily result in changes in the lateral dimensions of the islands, which is seen in each of the analyzed events of the growth (see for example cross-section height profiles in Figures 2i and 3e).

Conclusion

We presented a rt STM/STS study of PTCDA crystalline nanoislands on a Ge(001):H surface. The high-resolution measurements revealed that the top-most layer has a structure closely resembling the herringbone structure found for the (102) plane of PTCDA bulk crystal. Spectroscopic data showed no influence of the substrate on the electronic properties of the islands. The crystalline nanostructures can be easily modified by the scanning probe, and the presence of the tip seems to be one of the factors that facilitate and speed formation of the top-most layer of the island. This feature may be a suitable supplementary step for self-assembly-based methods to fine-tune the final form of the molecular nanostructures of interest.

Experimental

The experiments were carried out in a multi-chamber ultra-high vacuum system equipped with variable temperature STM (Omicron GmbH). The base pressure in the system was in the low 10^{-10} mbar range, with the exception of the microscope chamber where the pressure was $4\text{--}5 \times 10^{-11}$ mbar. Atomically

flat Ge(001) surfaces were prepared by a few cycles of simultaneous annealing of the samples at 780 °C (as measured by infrared pyrometer) and ion beam bombardment (1 keV Ar⁺, at 45° off-normal) for 20 minutes. The ion current density was approximately 0.3 μA/cm². The samples were held to slowly cool down to room temperature at a rate of 0.1 A/min. To obtain a passivated surface the Ge(001) samples were exposed to hydrogen atoms provided by a homebuilt hydrogen cracker. The partial hydrogen pressure in the chamber was kept at 4–5 × 10⁻⁷ mbar for 2.5 hours, and the sample was kept at 200 °C. The PTCDA molecules were deposited with the use of a standard effusion cell (Kentax GmbH) at 310 °C on the sample, which was kept at room temperature. The molecular flux was controlled by a quartz-microbalance. STM measurements were carried out in constant current mode at room temperature (rt) by means of electrochemically etched tungsten tips as probes. Scanning tunneling spectroscopy (STS) measurements were carried out at rt. The STS data were averaged over 2500 curves taken from a grid covering a 10 × 10 nm² surface area. The differential tunneling conductance (dI/dV) as a function of the sample bias *V* was obtained numerically from the *I*–*V* curves.

Acknowledgements

The authors are grateful to Prof. M. Szymonski for his helpful advice and encouragement. The authors acknowledge helpful comments by S. Godlewski on the experimental procedures. This work was supported by a grant from Switzerland through the Swiss Contribution to the enlarged European Union (Joint Polish-Swiss Research Program) no PSPB-085/2010 “Molecular assemblies on semiconductors and insulating surfaces” (<http://www.molsurf.eu>).

References

- Otero, R.; Gallego, J. M.; Vázquez de Parga, A. L.; Martin, N.; Miranda, R. *Adv. Mater.* **2011**, *23*, 5148–5176. doi:10.1002/adma.201102022
- Palma, C.-A.; Cecchini, M.; Samori, P. *Chem. Soc. Rev.* **2012**, *41*, 3713–3730. doi:10.1039/c2cs15302e
- Tait, S. L. *ACS Nano* **2008**, *2*, 617–621. doi:10.1021/nn800207w
- Prauzner-Bechcicki, J. S.; Godlewski, S.; Szymonski, M. *Phys. Status Solidi A* **2012**, *209*, 603–613. doi:10.1002/pssa.201127623
- Gross, L.; Moll, N.; Mohn, F.; Curioni, A.; Meyer, G.; Hanke, F.; Persson, M. *Phys. Rev. Lett.* **2011**, *107*, 086101. doi:10.1103/PhysRevLett.107.086101
- Repp, J.; Meyer, G.; Stojković, S. M.; Gourdon, A.; Joachim, C. *Phys. Rev. Lett.* **2005**, *94*, 026803. doi:10.1103/PhysRevLett.94.026803
- Liljeroth, P.; Repp, J.; Meyer, G. *Science* **2007**, *317*, 1203–1206. doi:10.1126/science.1144366
- Abel, M.; Clair, S.; Ourdjini, O.; Mossayan, M.; Porte, L. *J. Am. Chem. Soc.* **2011**, *133*, 1203–1205. doi:10.1021/ja108628r
- Wang, Y.; Kröger, J.; Berndt, R.; Tang, H. *J. Am. Chem. Soc.* **2010**, *132*, 12546–12547. doi:10.1021/ja105110d
- Bombis, C.; Kalashnyk, N.; Xu, W.; Lægsgaard, E.; Besenbacher, F.; Linderoth, T. R. *Small* **2009**, *5*, 2177–2182. doi:10.1002/smll.200900301
- Rossel, F.; Pivetta, M.; Patthey, F.; Čavar, E.; Seitsonen, A. P.; Schneider, W.-D. *Phys. Rev. B* **2011**, *84*, 075426. doi:10.1103/PhysRevB.84.075426
- Bombis, C.; Ample, F.; Lafferentz, L.; Yu, H.; Hecht, S.; Joachim, C.; Grill, L. *Angew. Chem., Int. Ed.* **2009**, *48*, 9966–9970. doi:10.1002/anie.200904645
- Ramoino, L.; von Arx, M.; Schintke, S.; Baratoff, A.; Güntherodt, H. J.; Jung, T. A. *Chem. Phys. Lett.* **2006**, *417*, 22–27. doi:10.1016/j.cplett.2005.10.006
- Such, B.; Goryl, G.; Godlewski, S.; Kolodziej, J. J.; Szymonski, M. *Nanotechnology* **2008**, *19*, 475705. doi:10.1088/0957-4484/19/47/475705
- Godlewski, S.; Goryl, G.; Kolodziej, J. J.; Szymonski, M. *Appl. Surf. Sci.* **2010**, *256*, 3746–3752. doi:10.1016/j.apsusc.2010.01.018
- Mayne, A. J.; Riedel, D.; Comtet, G.; Dujardin, G. *Prog. Surf. Sci.* **2006**, *81*, 1–51. doi:10.1016/j.progsurf.2006.01.001
- Bellec, A.; Ample, F.; Riedel, D.; Dujardin, G.; Joachim, C. *Nano Lett.* **2009**, *9*, 144–147. doi:10.1021/nl802688g
- Gruyters, M.; Pingel, T.; Gopakumar, T. G.; Néel, N.; Schütt, C.; Köhler, F.; Herges, R.; Berndt, R. *J. Phys. Chem. C* **2012**, *116*, 20882–20886. doi:10.1021/jp3058433
- Godlewski, S.; Kolmer, M.; Kawai, H.; Such, B.; Zuzak, R.; Saeys, M.; de Mendoza, P.; Echavarren, A. M.; Joachim, C.; Szymonski, M. *ACS Nano* **2013**, *7*, 10105–10111. doi:10.1021/nn404254y
- Vaurette, F.; Nys, J. P.; Grandidier, B.; Priester, C.; Stievenard, D. *Phys. Rev. B* **2007**, *75*, 235435. doi:10.1103/PhysRevB.75.235435
- Ogawa, T.; Kuwamoto, K.; Isoda, S.; Kobayashi, T.; Karl, N. *Acta Crystallogr., Sect. B* **1999**, *55*, 123–130. doi:10.1107/S0108768198009872
- Forrest, S. R. *Chem. Rev.* **1997**, *97*, 1793–1896. doi:10.1021/cr941014o
- Radny, M. W.; Shah, G. A.; Schofield, S. R.; Smith, P. V.; Curson, N. J. *Phys. Rev. Lett.* **2008**, *100*, 246807. doi:10.1103/PhysRevLett.100.246807
- Nakatsuji, K.; Takagi, Y.; Komori, F.; Kusunohara, H.; Ishii, A. *Phys. Rev. B* **2005**, *72*, 241308. doi:10.1103/PhysRevB.72.241308
- Kolmer, M.; Godlewski, S.; Kawai, H.; Such, B.; Krok, F.; Saeys, M.; Joachim, C.; Szymonski, M. *Phys. Rev. B* **2012**, *86*, 125307. doi:10.1103/PhysRevB.86.125307
- Tautz, F. S. *Prog. Surf. Sci.* **2007**, *82*, 479–520. doi:10.1016/j.progsurf.2007.09.001
- Hill, I. G.; Kahn, A.; Soos, Z. G.; Pascal, R. A., Jr. *Chem. Phys. Lett.* **2000**, *327*, 181–188. doi:10.1016/S0009-2614(00)00882-4
- Tsiper, E. V.; Soos, Z. G.; Gao, W.; Kahn, A. *Chem. Phys. Lett.* **2002**, *360*, 47–52. doi:10.1016/S0009-2614(02)00774-1
- Zahn, D. R. T.; Gavrilă, G. N.; Gorgoi, M. *Chem. Phys.* **2006**, *325*, 99–112. doi:10.1016/j.chemphys.2006.02.003
- Yim, S.; Kim, K.-i.; Jones, T. S. *J. Phys. Chem. C* **2007**, *111*, 10993–10997. doi:10.1021/jp0715272
- Zhong, D. Y.; Hirtz, M.; Wang, W. C.; Dou, R. F.; Chi, L. F.; Fuchs, H. *Phys. Rev. B* **2008**, *77*, 113404. doi:10.1103/PhysRevB.77.113404

License and Terms

This is an Open Access article under the terms of the Creative Commons Attribution License (<http://creativecommons.org/licenses/by/2.0>), which permits unrestricted use, distribution, and reproduction in any medium, provided the original work is properly cited.

The license is subject to the *Beilstein Journal of Nanotechnology* terms and conditions: (<http://www.beilstein-journals.org/bjnano>)

The definitive version of this article is the electronic one which can be found at:
[doi:10.3762/bjnano.4.104](https://doi.org/10.3762/bjnano.4.104)

Chapter Six

Conclusions and Outlooks

6. Conclusions and Outlooks

According to the results of the submitted papers in the present thesis the conclusions in the framework of each publication are as followings;

Formation of nanoripples by means of low energy ion beam sputtering at grazing incident angles on TiO₂(110) surface

- **Studying the temperature dependent orientation of the nanoripples,**
 - The developed nanoripples on the TiO₂(110) surface under the grazing ion irradiation (75° off-normal) and low energy ion beam (Ar⁺, 2keV), show a remarkable temperature-dependent orientation quite similar to the same phenomena observed for the crystalline metallic surfaces.
 - At 300K (RT), the ripples are directed perpendicular to the ion beam direction along the surface high symmetry crystallographic directions.
 - At lower and higher temperatures (T=120, 620, and 720K), the grooves are elongated in the ion beam direction.
 - The ion irradiated TiO₂(110) surface retain its crystalinity up to the $\Phi_{ion} = 9 \times 10^{16}$ ions/cm² fluencies as revealed by LEED patterns.
- **Seeking for the proper mechanism behind the observed phenomena**
 - Performing DFT calculations highlighted that a rather fluent diffusion of titanium atoms in assistance of oxygen adspecies Ti(O) plays the crucial role in the mass transport process and is responsible for determining the nanopattern orientation. At room temperature the rather easy Ti(O) diffusion counterbalances the erosive effect of the ion beam resulting the formation of a periodic pattern elongated in the fast diffusion direction normal to the ion beam. At low temperatures the diffusion processes are frozen and the nanoripple formation is dominated by the erosive action of the ion beam as a result the ripples orient along the ion beam direction. At elevated temperatures desorption of oxygen and Ti diffusion into the bulk reduces the role of surface diffusion in ripple formation, hence the pattern formation is dominated by the enhanced sputtering of the ascending steps by the incident ion

beam. As a result we obtained long and well ordered nanoripples elongated in the ion beam direction.

For further investigation of the given system we propose the study of the effect of the mass of the incident ion beam, i.e., using different inert gases like Krypton and Xenon with different atomic weights on the nanopattern formation is of great interest. It is also desirable to verify the role of the nanoripples on orienting the adsorbate organic molecules and metallic nanoparticles on the $\text{TiO}_2(110)$ surface.

Polymerization reaction on $\text{TiO}_2(011)-(2\times 1)$ Surface

- **Demonstration of thermally triggered on-surface C-C coupling through halogen-based reaction**
 - The on-surface covalent coupling of halogen-based organic molecular precursors is feasible on $\text{TiO}_2(011)$ surface for the DBBA molecular precursors.
 - DBBA molecules bear on their halogen constituents when deposited at RT as the STM imaging was not possible but at liquid nitrogen (LN) temperatures. Post-deposition annealing to 300°C results in randomly distributed short oligomers on the surface.
 - Long single or bunches of polymers were obtained when molecules were deposited on hot sample (270°C). In polymers, the moieties are strongly linked via covalent bonding while, within bunch polymers, interact via van der Waals or π -interactions and can be easily separated using STM tip induced manipulation.
- **Seeking for the polymerization reaction pathway on the $\text{TiO}_2(011)-(2\times 1)$ surface**
 - Due to the distinct chemical properties of titanium dioxide it is very unlikely that the polymerization reaction pathway on its surface will be the same as on metals. It is quite hard to make any distinction based on STM images only, thus corroborating the STM data with DFT calculations is highly required. With the help of DFT calculations a hypothesis has been proposed that the important role in the polymerization reaction is played by the surface hydroxyl groups which serve as the proton reservoir for the reaction and a concerted multistep proton assisted process of early C-C bond formation accompanied by the late C-Br cleavage acquires the minimum activation barrier.

In order to generalize this hypothesis many open questions have to be answered and many further experiments have to be conducted. The first important question is to verify whether it works for different types of halogen-based molecular precursors with different halogen constituents. Also the products of the reaction must be identified through proper spectroscopy measurements like mass spectroscopy. It also should be verified that if the products of the reaction remain on the surface or just escape to the vacuum. And the last but not the least, the role of the oxidation/reduction state of the surface in the reaction should be verified.

Fabricating and manipulating PTCDA supramolecular nanocrystals on Ge(001):H surface

- **Studying the effect of a hydrogen monolayer on decoupling and diffusivity enhancement of PTCDA molecules on Ge(001) surface**
 - Hydrogen termination of Ge(001) surface decouples PTCDA molecules electronically from the surface very efficiently, no features relevant to the surface electronic states have been observed in the LUMO-HOMO molecular energy gap region in the STS curves and enhances their diffusivity dramatically.
 - Upon depositing PTCDA molecules on Ge(001):H, very distinct 3D supramolecular nanocrystals in the Volmer-Weber growth mode have been observed indicating weak molecule-substrate interaction. High resolution STM imaging of the top-most layer of the islands revealed the herringbone structure found for the (102) plane of PTCDA bulk crystal indicating again weak molecule-substrate and stronger molecule-molecule interactions.
- **Engineering the self-assembled PTCDA nanocrystals on a hydrogen passivated Ge(001) surface by means of a tip-assisted manipulation technique**
 - A new top-most layer could be produced by injecting hot electrons to the top of the molecular islands through STM tip voltage pulses (5-7V, 25ms). As a result a hole is produced in the position of the voltage pulse with some admolecules surrounding it. This hole acts as a nucleation site for further growing of the top-most layer.
 - A strain driven upward diffusion of molecules is proposed to be the mechanism of the top most layer formation. Molecules from the edges of the lower layers (close to the substrate surface) of the molecular crystals tend to ascend to the higher layers to compensate the strain stored in the molecular crystal from the substrate surface. As a

result the lateral dimensions of the molecular islands shrink and a top-most layer is produced with continues tip presence.

- The electric field of the scanning tip seems to reduce the ascending potential barrier for the molecules and hence accelerates the growth of the top-most layer. The presence of the scanning tip seems to be necessary for the formation of a full top-most layer.

This tip-induced manipulation process may be a sufficient complementary action to fine tailoring the final morphology of the molecular nanostructures of interest for many technological applications.

7. Appendices

7.1. Molecules and Surfaces

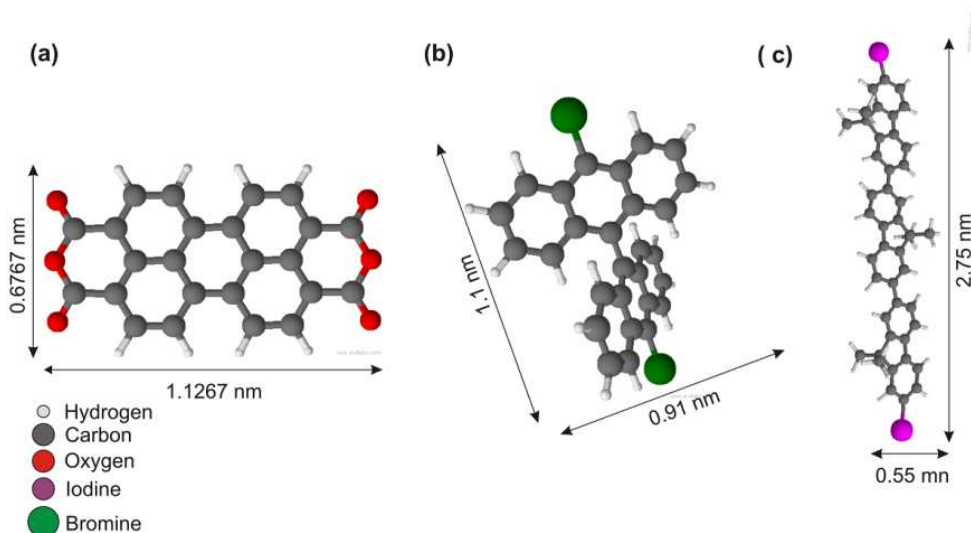


Figure 7-1 The organic molecules mentioned in the experiments of the present thesis. (a) 3, 4, 9, 10 perylene tetracarboxylic dianhydride (PTCDA), (b) 10,10'-dibromo-9,9'-bianthryl (DBBA), and (c) Diiodoterfluorene (DITF). The dimensions are given in the ChemSketch software.

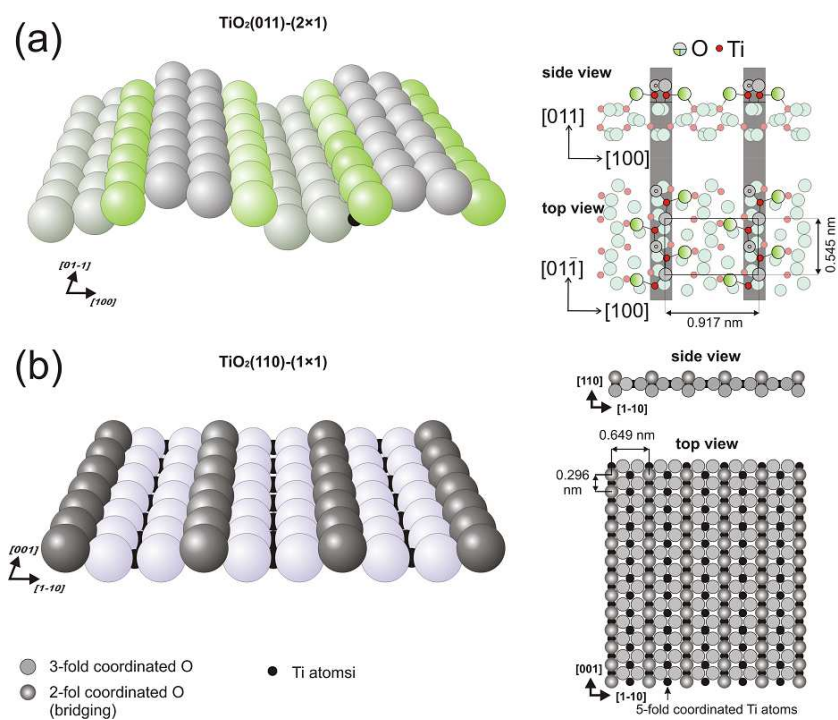


Figure 7-2 Different facets of rutile titania; perspective, top and side views (a) $\text{TiO}_2(011)-(2 \times 1)$ surface, (b) $\text{TiO}_2(110)-(1 \times 1)$ surface.

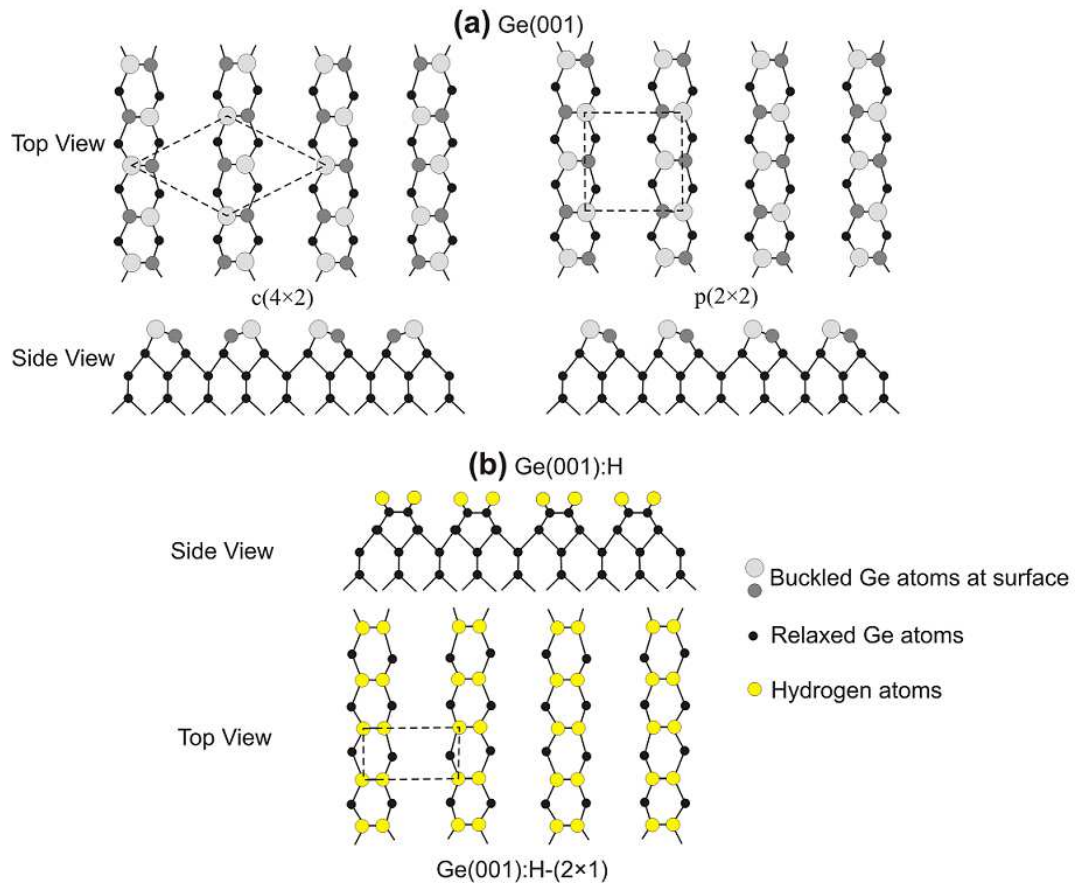


Figure 7-3 (a) The $c(4\times 2)$ and $p(2\times 2)$ Ge(001) reconstructions, (b) Hydrogen-passivated Ge(001) surface showing the (2×1) reconstruction.

7.2 Omicron LT and VP2 Park UHV Systems

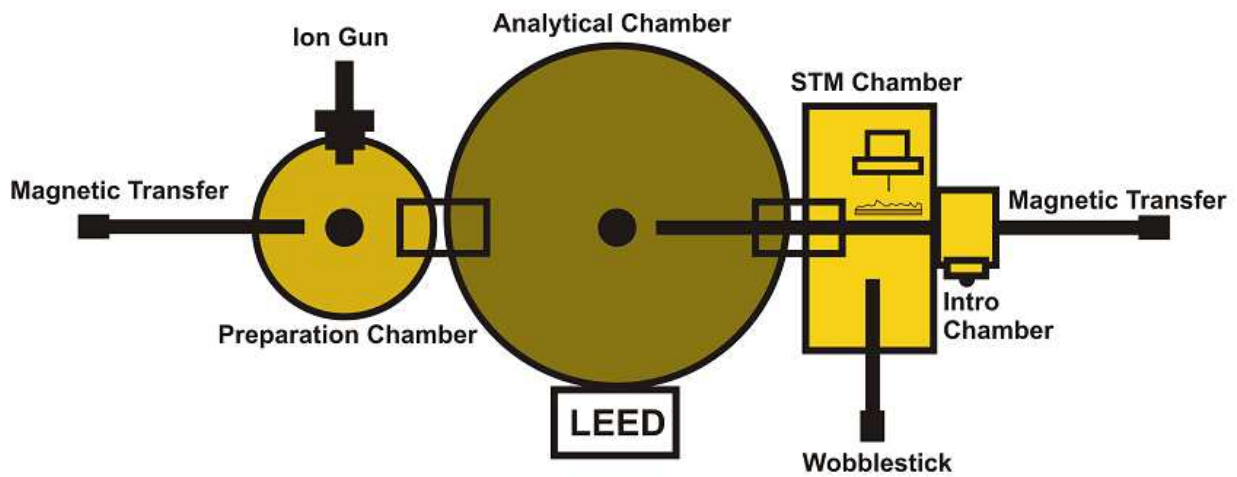


Figure 7 -4 The VP2 Park Scientific Instrument STM microscope system with the UHV chambers and equipments. The formation of nanoripples on $\text{TiO}_2(110)$ surface was carried out in this system. The system has linear magnetic transfer system of samples.

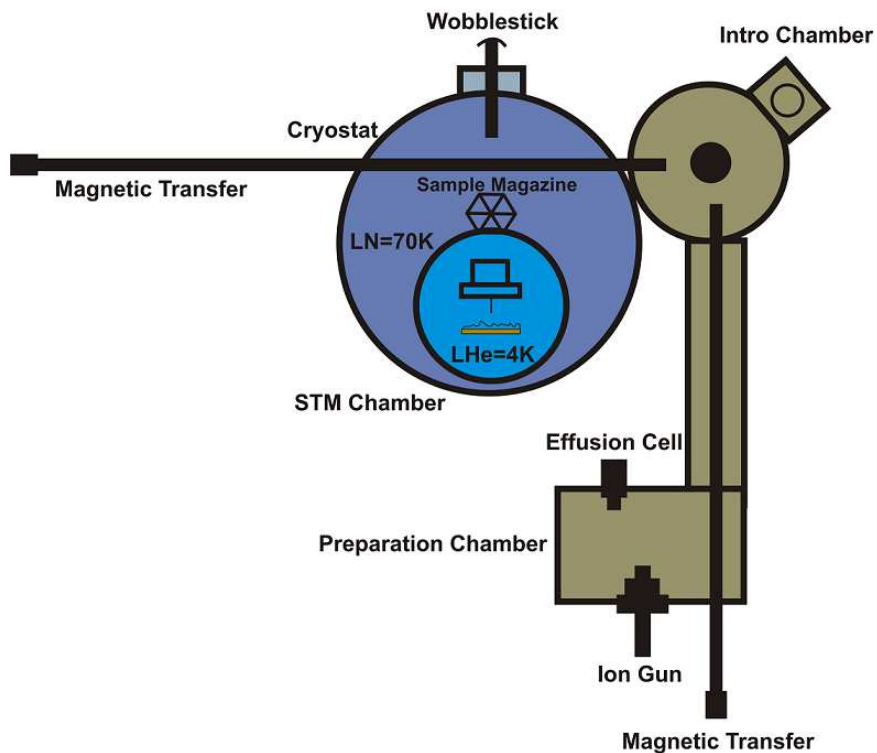


Figure 7-5 The Omicron LT system. The system exhibits a cryostat having outer cylinder filled with liquid nitrogen and the inner cylinder filled with liquid helium enabling a low temperature of 4K. The system has linear magnetic transfer system for sample transferring between the chambers.

8. Bibliography

- [1] J. Ramsden, *Essentials of Nanotechnology* (Ventus 2009 Jeremy Ramsden & Publishing ApS, 2009).
- [2] S. M. Lindsay, *Introduction to Nanoscience* (Oxford University Press Inc., New York, 2010).
- [3] R.P.Feynman, Eng. Sci. Mag. Caltec Inst. Technol. **23**, 22 (1960).
- [4] G. Binning, H. Rohrer, C. Gerber, and E. Weibel, Phys. Rev. Lett. **49**, 57 (1982).
- [5] W. Nawrocki and Y. M. Shukrinow, Metrol. Meas. Syst. **XIX**, 481 (2012).
- [6] C. Dekker, Phys. Today 22 (1999).
- [7] M. Kasfner, Phys. Today 24 (1993).
- [8] A. Biswas, I. S. Bayer, A. S. Biris, T. Wang, E. Dervishi, and F. Faupel, Adv. Colloid Interface Sci. **170**, 2 (2012).
- [9] G. Moore, Electronics **38**, (1965).
- [10] B. D. Gates, Q. Xu, M. Stewart, D. Ryan, C. G. Willson, and G. M. Whitesides, Chem. Rev. **105**, 1171 (2005).
- [11] J. V Barth, G. Costantini, and K. Kern, Nature **437**, 671 (2005).
- [12] D. Avasthi and J. Pivin, Curr. Sci. **98**, 780 (2010).
- [13] D. K. Avasthi, Hyperfine Interact. **160**, 95 (2005).
- [14] W. L. Chan and E. Chason, J. Appl. Phys. **101**, 121301 (2007).
- [15] D. C. M.Navez, C. Sella, Compt. Rend. J. Phys. Acad.Sci., Paris **254**, 240 (1962).
- [16] R. M. Bradley, J. Vac. Sci. Technol. A Vacuum, Surfaces, Film. **6**, 2390 (1988).
- [17] B. Ziberi, M. Cornejo, F. Frost, and B. Rauschenbach, J. Phys. Condens. Matter **21**, 224003 (2009).
- [18] T. Kumar, A. Kumar, N. P. Lalla, S. Hooda, S. Ojha, S. Verma, and D. Kanjilal, Appl. Surf. Sci. **283**, 417 (2013).
- [19] A. Redinger, Y. Rosandi, H. Urbassek, and T. Michely, Phys. Rev. B **77**, 195436 (2008).
- [20] T. Luttrell, W.-K. Li, X.-Q. Gong, and M. Batzill, Phys. Rev. Lett. **102**, 166103 (2009).
- [21] F. Buatier de Mongeot and U. Valbusa, J. Phys. Condens. Matter **21**, 224022 (2009).
- [22] R. L. Schwoebel, J. Appl. Phys. **40**, 614 (1969).

Bibliography

- [23] G. Ehrlich, *J. Chem. Phys.* **44**, 1039 (1966).
- [24] C. B. and U. V. G Constantini, S Rusponi, F Buatier de Mongeot, *J. Phys. Condens. Matter* **13**, 5875 (2001).
- [25] S. Rusponi, G. Costantini, C. Boragno, and U. Valbusa, *Phys. Rev. Lett.* **81**, 4184 (1998).
- [26] E. Ban and C. R. Picu, *Biomacromolecules* **15**, 143 (2014).
- [27] K. S. Mali and S. De Feyter, *Philos. Trans. A. Math. Phys. Eng. Sci.* **371**, 20120304 (2013).
- [28] R. Otero, J. M. Gallego, A. L. V. de Parga, N. Martín, and R. Miranda, *Adv. Mater.* **23**, 5148 (2011).
- [29] I. Hamley, *Nanotechnology* **14**, R39 (2003).
- [30] J. Y. Cheng, C. A. Ross, E. L. Thomas, H. I. Smith, and G. J. Vancso, *Appl. Phys. Lett.* **81**, 3657 (2002).
- [31] Q. Dai, J. Frommer, D. Berman, K. Virwani, B. Davis, J. Y. Cheng, and A. Nelson, *Langmuir* **29**, 7472 (2013).
- [32] A. Kühnle, *Curr. Opin. Colloid Interface Sci.* **14**, 157 (2009).
- [33] S. L. Tait, *ACS Nano* **2**, 617 (2008).
- [34] S. Weigelt, C. Bombis, C. Busse, M. M. Knudsen, K. V Gothelf, E. Laegsgaard, F. Besenbacher, and T. R. Linderoth, *ACS Nano* **2**, 651 (2008).
- [35] A. Gourdon, *Angew. Chem. Int. Ed. Engl.* **47**, 6950 (2008).
- [36] S. Kowarik, A Gerlach, and F. Schreiber, *J. Phys. Condens. Matter* **20**, 184005 (2008).
- [37] G. Gilmer, H. Huang, and C. Roland, *Comput. Mater. Sci.* **12**, 354 (1998).
- [38] S. Chambers, *Surf. Sci. Rep.* **39**, 105 (2000).
- [39] J. Lehn, *Angew. Chem. Int. Ed. Engl.* **27**, 89 (1988).
- [40] A. P. Côté, A. I. Benin, N. W. Ockwig, M. O’Keeffe, A. J. Matzger, and O. M. Yaghi, *Science* **310**, 1166 (2005).
- [41] M. Lackinger and W. M. Heckl, *J. Phys. D. Appl. Phys.* **44**, 464011 (2011).
- [42] A. Nitzan and M. A Ratner, *Science* **300**, 1384 (2003).
- [43] J. Björk and F. Hanke, *Chemistry* **20**, 928 (2014).
- [44] L. Grill, M. Dyer, L. Lafferentz, M. Persson, M. V Peters, and S. Hecht, *Nat. Nanotechnol.* **2**, 687 (2007).
- [45] L. Lafferentz, V. Eberhardt, C. Dri, C. Africh, G. Comelli, F. Esch, S. Hecht, and L. Grill, *Nat. Chem.* **4**, 215 (2012).

Bibliography

- [46] M. Bieri, M. Treier, J. Cai, K. Ait-Mansour, P. Ruffieux, O. Gröning, P. Gröning, M. Kastler, R. Rieger, X. Feng, K. Müllen, and R. Fasel, *Chem. Commun. (Camb)*. 6919 (2009).
- [47] J. A. Lipton-Duffin, J. A. Miwa, M. Kondratenko, F. Cicoira, B. G. Sumpter, V. Meunier, D. F. Perepichka, and F. Rosei, *Proc. Natl. Acad. Sci. U. S. A.* **107**, 11200 (2010).
- [48] R. Gutzler, H. Walch, G. Eder, S. Kloft, W. M. Heckl, and M. Lackinger, *Chem. Commun. (Camb)*. 4456 (2009).
- [49] J. A. Lipton-Duffin, O. Ivasenko, D. F. Perepichka, and F. Rosei, *Small* **5**, 592 (2009).
- [50] J. Cai, P. Ruffieux, R. Jaafar, M. Bieri, T. Braun, S. Blankenburg, M. Muoth, A. P. Seitsonen, M. Saleh, X. Feng, K. Müllen, and R. Fasel, *Nature* **466**, 470 (2010).
- [51] M. Koch, F. Ample, C. Joachim, and L. Grill, *Nat. Nanotechnol.* **7**, 713 (2012).
- [52] L. Lafferentz, F. Ample, H. Yu, S. Hecht, C. Joachim, and L. Grill, *Science* **323**, 1193 (2009).
- [53] P. Rahe, R. Lindner, M. Kittelmann, M. Nimmrich, and A. Kühnle, *Phys. Chem. Chem. Phys.* **14**, 6544 (2012).
- [54] M. Abel, S. Clair, O. Ourdjini, M. Mossoyan, and L. Porte, *J. Am. Chem. Soc.* **133**, 1203 (2011).
- [55] M. Kittelmann, P. Rahe, M. Nimmrich, C. M. Hauke, A. Gourdon, and A. Kühnle, *ACS Nano* **5**, 8420 (2011).
- [56] M. Kittelmann, M. Nimmrich, R. Lindner, A. Gourdon, and A. Kühnle, *ACS Nano* **7**, 5614 (2013).
- [57] N. C. Berner, Y. N. Sergeeva, N. N. Sergeeva, M. O. Senge, A. A. Cafolla, and I. T. McGovern, *Phys. Status Solidi(C)* **9**, 1404 (2012).
- [58] M. A. Barteau, *Chem. Rev.* **96**, 1413 (1996).
- [59] U. Diebold, *Surf. Sci. Rep.* **48**, 53 (2003).
- [60] X. Chen and S. S. Mao, *Chem. Rev.* **107**, 2891 (2007).
- [61] A. G. Thomas and K. L. Syres, *Chem. Soc. Rev.* **41**, 4207 (2012).
- [62] A. Thomas, W. Flavell, A. Mallick, A. Kumarasinghe, D. Tsoutsou, N. Khan, C. Chatwin, S. Rayner, G. Smith, R. Stockbauer, S. Warren, T. Johal, S. Patel, D. Holland, A. Taleb, and F. Wiame, *Phys. Rev. B* **75**, 035105 (2007).
- [63] M. Ramamoorthy, D. Vanderbilt, and R. King-Smith, *Phys. Rev. B* **49**, 16721 (1994).
- [64] X. Torrelles, G. Cabailh, R. Lindsay, O. Bikondoa, J. Roy, J. Zegenhagen, G. Teobaldi, W. Hofer, and G. Thornton, *Phys. Rev. Lett.* **101**, 185501 (2008).
- [65] X.-Q. Gong, N. Khorshidi, A. Stierle, V. Vonk, C. Ellinger, H. Dosch, H. Cheng, A. Selloni, Y. He, O. Dulub, and U. Diebold, *Surf. Sci.* **603**, 138 (2009).
- [66] J. M. R. Muir and H. Idriss, *Surf. Sci.* **607**, 187 (2013).

Bibliography

- [67] S. Godlewski, A. Tekiel, J. S. Prauzner-Bechcicki, J. Budzioch, A. Gourdon, and M. Szymonski, *J. Chem. Phys.* **134**, 224701 (2011).
- [68] A. Tekiel, S. Godlewski, J. Budzioch, and M. Szymonski, *Nanotechnology* **19**, 495304 (2008).
- [69] S. Godlewski and M. Szymonski, *Int. J. Mol. Sci.* **14**, 2946 (2013).
- [70] J. Björk, F. Hanke, and S. Stafström, *J. Am. Chem. Soc.* **135**, 5768 (2013).
- [71] M. Bieri, M.-T. Nguyen, O. Gröning, J. Cai, M. Treier, K. Ait-Mansour, P. Ruffieux, C. A. Pignedoli, D. Passerone, M. Kastler, K. Müllen, and R. Fasel, *J. Am. Chem. Soc.* **132**, 16669 (2010).
- [72] A. Toma, D. Chiappe, D. Massabò, C. Boragno, and F. Buatier de Mongeot, *Appl. Phys. Lett.* **93**, 163104 (2008).
- [73] P. Chaudhari, J. Lacey, J. Doyle, E. Galligan, S. C. Lien, A. Callegari, G. Hougham, N. D. Lang, P. S. Andry, R. John, K. H. Yang, M. Lu, C. Cai, J. Speidell, S. Purushothaman, J. Ritsko, M. Samant, J. Stöhr, Y. Nakagawa, Y. Katoh, Y. Saitoh, K. Sakai, H. Satoh, S. Odahara, H. Nakano, J. Nakagaki, and Y. Shiota, *Nature* **411**, 56 (2001).
- [74] T. Luttrell, W.-K. Li, X.-Q. Gong, and M. Batzill, *Phys. Rev. Lett.* **102**, 166103 (2009).
- [75] T. Luttrell and M. Batzill, *Phys. Rev. B* **82**, 035408 (2010).
- [76] J. Barth, *Surf. Sci. Rep.* **40**, 75 (2000).
- [77] J. S. Prauzner-Bechcicki, S. Godlewski, and M. Szymonski, *Phys. Status Solidi(A)* **209**, 603 (2012).
- [78] H. Karacuban, S. Koch, M. Fendrich, T. Wagner, and R. Möller, *Nanotechnology* **22**, 295305 (2011).
- [79] L. Gross, N. Moll, F. Mohn, A. Curioni, G. Meyer, F. Hanke, and M. Persson, *Phys. Rev. Lett.* **107**, 086101 (2011).
- [80] J. Repp, G. Meyer, S. Stojković, A. Gourdon, and C. Joachim, *Phys. Rev. Lett.* **94**, 026803 (2005).
- [81] Y. Wang, J. Kröger, R. Berndt, and H. Tang, *J. Am. Chem. Soc.* **132**, 12546 (2010).
- [82] B. Such, G. Goryl, S. Godlewski, J. J. Kolodziej, and M. Szymonski, *Nanotechnology* **19**, 475705 (2008).
- [83] S. Godlewski, G. Goryl, J. J. Kolodziej, and M. Szymonski, *Appl. Surf. Sci.* **256**, 3746 (2010).
- [84] C. Loppacher, U. Zerweck, L. M. Eng, S. Gemming, G. Seifert, C. Olbrich, K. Morawetz, and M. Schreiber, *Nanotechnology* **17**, 1568 (2006).
- [85] A. J. Mayne, D. Riedel, G. Comtet, and G. Dujardin, *Prog. Surf. Sci.* **81**, 1 (2006).
- [86] A. Bellec, F. Ample, D. Riedel, G. Dujardin, and C. Joachim, *Nano Lett.* **9**, 144 (2009).
- [87] M. Gruyters, T. Pingel, T. G. Gopakumar, N. Néel, C. Schütt, F. Köhler, R. Herges, and R. Berndt, *J. Phys. Chem. C* **116**, 20882 (2012).

Bibliography

- [88] S. Godlewski, M. Kolmer, H. Kawai, B. Such, R. Zuzak, M. Saeys, P. de Mendoza, A. M. Echavarren, C. Joachim, and M. Szymonski, *ACS Nano* **7**, 10105 (2013).
- [89] J. M. MacLeod, J. Lipton-Duffin, C. Fu, and F. Rosei, *ACS Nano* **3**, 3347 (2009).
- [90] D.M. Eigler and E.K. Schweizer, *Nature* **344**, 524 (1990).
- [91] S. Hla, L. Bartels, G. Meyer, and K. Rieder, *Phys. Rev. Lett.* **85**, 2777 (2000).
- [92] P. Maksymovych, D. Dougherty, X.-Y. Zhu, and J. Yates, *Phys. Rev. Lett.* **99**, 016101 (2007).
- [93] L. Chen, H. Li, and A. T. S. Wee, *ACS Nano* **3**, 3684 (2009).
- [94] Y. Okawa and M. Aono, *Nature* **409**, 683 (2001).
- [95] Y. Okawa and M. Aono, *J. Chem. Phys.* **115**, 2317 (2001).